REVISED: DECEMBER 1978
AUTHOR: S. S. MANSON

NONFERROUS ALLOYS

	Ni
15	Co
10	Cr
5.5	Al
4.7	Ti
3	Mo
0.95	V

IN-100

1. GENERAL

This nickel-base alloy, containing large additions of aluminum and titanium, achieves very high strength at elevated temperature. It has thus received considerable attention for application in components of high performance jet engines such as turbine blades, vanes and nozzles, and even integral turbine wheels.

Because of the large quantities of strengthening elements included in the composition, the alloy is not hot worked, and is therefore used in the as-cast condition. Recently, however, there has been considerable development of a powder metallurgy product which permits working of the alloy. At high temperatures the powder-consolidated product becomes superplastic, thus opening many possibilities in fabrication-to-shape of wrought complex components.

Also, because of the high content of gamma prime precipitate that constitutes one of the strengthening components of the alloy, the equilibrium solution temperature approaches the solidus, so the material is usually used in the as-cast condition, without heat treatment. However, it is subjected to heat treatment during the deposition of protective coatings. The powder metallurgy product is heat treated to achieve desirable properties.

The low oxidation and corrosion resistance of the alloy at the high temperatures where the strength of the alloy is most advantageously used, introduces the need for protective systems. A large number of coating types have been studied, and most have been found to provide sufficient protection to extend the useful life of the alloy, commensurate with its strength.

Exposure to high temperature and stress for long periods of time may also result in embrittlement due to precipitation of sigma phase. The alloy has been extensively studied to determine how to avoid such embrittlement. Maintaining a low content of aluminum plus titanium has been found effective, and the most recent specifications require bounds in the titanium content (in accordance with electron vacancy density calculations) to insure that no deleterious precipitates develop. Because of the interest in its potential use in advanced jet engine components, the alloy (especially the powder product) has also been extensively studied in relation to its fatigue characteristics, particularly fatigue crack growth during cyclic loading.

1.01 Commercial Designation
IN-100

1.02 Alternate Designations
(17)p 122, (18)p 36, Austenal 100, AMS 5397 IN-100, Udimet IN-100, Haynes Alloy IN-100, All-vac IN-100, Vertex IN-100.

1.021 Special designations of modifications of basic compositions to achieve freedom from sigma phase proneness.
International Nickel Co., -INCO 731X
General Electric Co., -Rene' 100

1.03 Specifications
AMS5397. Investment cast
G.E. (original spec.) C50T77A.
G.E. (Rene' 100 modification) C50T77C.

1.031 G.E. Spec. C50T77C specifies that the electron vacancy number $\overline{Nv}$ be calculated by the Pha Comp concept, using the procedure of Woodyatt - Sims - Beattie (15). A maximum value of 2.47 is allowed for each heat.

1.032 AMS 5397 specifies minimum values as follows:
F_{tu} - 115 ksi
F_{ty} - 95 ksi
e(percent in 1 in or 4D)-5 percent

1.033 AMS 5397 Spec. for creep rupture test at 1800F, 29 ksi, rupture time minimum of 23 hrs, and elongation, (in 4D) after rupture shall be 4 percent minimum.

1.04 Composition
Table 1.04

1.05 Heat Treatment (see also 3.023)

1.051 Commonly used in as-cast condition with no further heat treatment.

1.052 Heating for 2 - 4 hr at 1900 to 2000F can re-solution sigma phase precipitated by creep exposure at lower temperature, and also makes alloy more resistant to sigma phase precipitation upon subsequent exposure to long-time creep conditions at lower temperatures (12).

1.053 Coating applications may expose alloy to temperatures 1600 - 2000F for periods up to 25 hrs (10, p. 9). INCO recommends that if the coating is to be diffused at 1900-1950F, the alloy should receive a preliminary high temperature solutioning at 2100-2150F, followed by aging at 1500-1600F. This should provide the alloy with a capability of maintaining a consistently high level of mechanical properties.

1.054 For the powder metallurgy product, Pratt and Whitney Aircraft (Ref. 19, p 6) recommends solutioning at 2050F, stabilization at 1600 and 1800F, and precipitation hardening at 1200 and 1400F. Typical heat treatment used (see Table 3.023) 2215F, 4 hrs + 2000F, 4 hrs + 1550F, 16 hrs.

1.06 Hardness

1.061 AMS specifies Hardness RC 30-44 or equivalent.

1.062 Effect of temperature on hardness, Fig. 1.062

1.063 Effect of test temperature on Brinell Hardness, as determined by mutual indentation, for air melted and cast alloy and for vacuum melted and cast alloy, Fig. 1.063.

1.07 Forms and Conditions Available
Investment Castings
Gatorized (Trade Mark, Pratt & Whitney Aircraft for creep-formed powder product hydrostatically pressed at elevated temperature) turbine disks and other shapes.

1.08 Melting and Casting Practice
Vacuum melted and cast

1.09 Special Considerations

1.091 Because of the low chromium content, as well as the presence of Vanadium, oxidation resistance is not adequate at the high temperatures where the strength of the alloy assumes special advantage. The problem is usually overcome by the use of aluminum or aluminum-base coatings. Many of these are proprietary, and the compositions as well as heat-treatments are not revealed. Information provided by the coating producers show beneficial effects of coatings as protection against oxidation and sulfidation, and improvement of thermal shock resistance. These benefits are apparently obtained without impairing the tensile and creep properties at high temperature, (5)(6)(7)(10)(41) to (45).

1.092 The high hardener content of the alloy makes it particularly prone to the precipitation of embrittling phases, such as sigma, upon prolonged exposure to high temperature, especially if stress is simultaneously applied. Special compositions, low in titanium content have been found advantageous for avoiding such embrittlement. The International Nickel Company, original developers of IN 100, has developed a modification designated as IN 731X, (13) and the General Electric Company has developed Rene' 100 for this purpose, (13). Both use Pha Comp techniques (wherein electron vacancy of the remaining matrix after the major hardening precipitates have formed, is used as a basis for the determination of whether sigma will form). Every heat requires a separate computation to determine sigma-proneness because of the large variations permitted in the chemistry of individual heats; however, in general, the revised composition limits with lower titanium contents, are usually sigma-free within the specified limits of the other elements. The tendency toward sigma-proneness was first reported in reference (11) to be a result of exposure to high temperatures for long times, expecially at stress. Reference (14) demonstrates more extensively the effects of exposure to temperature, and simultaneous exposure

	Ni
15	Co
10	Cr
5.5	Al
4.7	Ti
3	Mo
0.95	V

IN-100

to stress and temperature. Reference (12) reveals that life in creep-rupture at 1500F could be reduced by factors as high as 4 to 8 when sigma phase precipitates as compared to extrapolated values for sigma free material. It was also shown in reference (12) that sigma formed at 1650F could be solutioned at 1900 - 2000F, in 2 - 4 hrs and that a 2000F, 2 hour heat treatment delayed sigma formation. This heat treatment was observed to delay sigma formation whether applied to an as-cast bar or whether applied to a bar previously exposed to 1650F, containing sigma. This observation points to the possibility of beneficial effects of heat treatment, in contrast to the normally used as-cast structure. It also points to the possibility of removing creep damage by re-heat treatment for this alloy. The question of sigma phase precipitation has been extensively studied (Ref. 22 to 24), and effect on properties determined in detail.

1.093 The alloy in the powder metallurgy form has been extensively studied (Refs. (19)(20)(33)(34)(35)(36) both in regard to mechanical properties of fabricated products and especially in regard to crack growth.

1.094 High pressure hydrogen reduces tensile ductility, particularly at RT (see Table 3.03171).

2. PHYSICAL AND CHEMICAL PROPERTIES

2.01 Thermal Properties

2.011 Melting range 2305 - 2435F (3), p 7.

2.012 Phase changes. Structure consists of intragranular as well as eutectic or primary $Ni_3(Al, Ti)$, Ti(C, N) and M_2B, also possibly perovskite carbide within $Ni_3(Al, Ti)$ islands. On aging precipitation of perovskite-like phase (Ni_3 (Al, Ti)C) occurs at 1400F, and continues at 1600F where, after about 100 hr, an acicular sigma phase also begins to nucleate at grain and phase boundaries. The formation of sigma phase appears to be promoted by stress to 1800F. In the absence of stress, solution of Ti(C, N) and Ni_3 (Al, Ti)C and the resultant precipitation of $M_{23}C_6$ are the main structural changes at 1800F, (11). The tendency toward the formation of sigma phase can be eliminated by keeping the electron vacancy number $\overline{Nv}$ below 2.47.

2.0120 Effect of aging time and temperature on minor phase concentration, Fig. 2.0120.

2.0121 Effect of exposure for 5000 hours at various temperatures on minor phase concentration, Fig. 2.0121.

2.0122 Transformation to sigma phase for as-cast and forged alloy for two levels of electron vacancy concentration, Fig. 2.0122.

2.0123 Time-temperature relation for the onset of sigma phase precipitation for medium and high electron vacancy concentration ($\overline{Nv}$) compositions, and in fine or coarse grain size structure, Fig. 2.0123.

2.013 Thermal conductivity, Fig. 2.013.

2.014 Coefficient of thermal expansion, Fig. 2.014.

2.015 Specific heat, Fig. 2.015

2.016 Thermal diffusivity.

2.02 Other Physical Properties

2.021 Density 0.280 lb per cu in, 7.75 gm per cu cm (4) p 2

2.022 Electrical Properties
143.0 microhm - cm at RT (4, p 2)

2.023 Magnetic Properties

2.03 Chemical Properties

2.031 Because of the lower chromium content of this alloy compared to other high temperature, high strength nickel base alloys, oxidation resistance is somewhat reduced. However, since it retains strength at high temperature, its intended use range is above that of many other nickel base alloys. Thus, where an oxidizing or sulfidizing environment is present as in turbojet applications, a protective coating is usually applied. Common coatings are of the aluminum and aluminum base types. These can substantially improve the sulfidation resistance, oxidation resistance and thermal shock characteristics. While only limited data are available at present, it appears that these coatings do not reduce the creep rupture strength, rupture elongation, or room temperature fatigue strength of the as-cast alloy. The oxidation characteristics in a high velocity gas stream containing oxygen is very complex, particularly if steady load and thermal shock cycles are superimposed. Depending on temperature, a weight gain or weight loss may occur under the same velocity conditions, (see Figure 2.034). An uncoated material may first gain weight and subsequently lose weight in the same test, due to the fact that heavy build-up of oxide (weight gain) may be followed by spalling (weight loss), as shown in Figure 2.035. Coating may reduce oxidation and thus prevent spalling, as also shown in Figure 2.035. Surface effects may also be important, Figure 2.036. At present the process is regarded as too complex to be predictable from thermodynamic principles. This complexity is the result of the interplay among heterogeneous oxide growth, oxide interactions, oxide vaporization, and spalling, especially in the presence of creep strain and cyclic plastic strain due to thermal shock (6) p 3. Caution is advised against extrapolating behavior from one set of conditions to another. Rather, it is suggested that tests be conducted under conditions closely simulating operation.

2.032 Summary of main stages of oxidation, Figure 2.032.

2.033 Typical plot of weight gain versus time in static oxidation Figure 2.033.

2.034 Dynamic oxidation tests at 1600 and 1800F indicating complexity of process. Weight gain occurs at 1600F, loss at 2000F, Figure 2.034.

2.035 Cyclic oxidation behavior with and without protective aluminum base diffusion coating, Figure 2.035.

2.0312 Platinum-Aluminum coatings.

2.03121 Typical weight change pattern for coated alloy cycled for one hour intervals at 2000F, followed by cooling to RT in 3 minutes. Figure shows data for Pt-Al alloy, with summary of results for several other alloys, Fig. 2.03121

2.0313 Corrosion.

2.03131 Effect of corrosive environment on weight change in bare and coated condition, Table 2.03131.

2.03132 Relative corrosion of various superalloys for two fuels of different sulfur content and two salt/air ratio contents, Fig. 2.03132.

2.03133 Correlation showing that low corrosion resistance of alloy is related to its low chromium content, Fig. 2.03133.

2.03134 Correlation showing that the low threshold temperature for corrosion is principally related to its low chromium content, Fig. 2.03134.

2.03135 Corrosion (as measured by depth of attack) for alloy in 700 FPS velocity gas jet using low sulfur fuel (JP4) with 4ppm and 8 ppm sea salt in inlet air, Fig. 2.03135.

2.03136 Corrosion (as measured by depth of attack) for alloy in 700 FPS velocity gas jet using high sulfur fuel (JP-4R) with 4 ppm and 8 ppm sea salt in inlet air, Fig. 2.03136.

2.03137 Hot corrosion resistance of thinwall alloy with two proprietary coatings in 1900F cyclic temperature test, Table 2.03137.

2.03138 Comparison of hot-corrosion behavior in a marine turbine simulator with other nickel - and cobalt-base alloys, Fig. 2.03138.

2.036 Dynamic oxidation at 1800F of alloy in two conditions of surface finish. Rougher surface promotes more rapid oxidation, Fig. 2.036.

2.037 Slurry coatings.

2.0371 Cyclic furnace oxidation in 20 hour cycles at 2000F of FeAl + Fe-Cr-Al aluminized slurry of average composition Fe-25Cr-Al, and comparison with oxidation of alloy protected by cladding of Fe-25Cr-4Al-1Y, Fig. 2.0371.

2.0372 Cyclic furnace oxidation in 20 hour cycles at 2000F of NiAl slurry coated alloy with comparison to oxidation of commercial conversion coating, Fig. 2.0372.

2.0373 Oxidation of NiAl aluminized slurry coating in Mach 1 jet at 2000F, with comparison to commercial aluminide coating, Fig. 2.0373.

2.038 Metallided coatings.

2.0381 High gas velocity oxidation and thermal fatigue cracking at 1900F of alloy coated by an electrolytic fused salt process

	Ni
15	Co
10	Cr
5.5	Al
4.7	Ti
3	Mo
0.95	V

IN-100

(metallided). and comparison with oxidation of bare alloy and pack aluminum coated alloy, Fig. 2.0381.

2.0382 High velocity oxidation and thermal fatigue cracking at 2000F of alloy coated by an electrolytic fused salt process (metallided), and comparison with bare alloy and pack aluminum coated alloy, Fig. 2.0382.

2.0383 Static oxidation at 2000 and 2100F of alloy coated by electrolytic fused salt process (metalliding), Fig. 2.0383.

2.0384 Comparison of static oxidation with oxidation in high velocity jet (Mach 1) at 2100F for metallided coating, Fig. 2.0384.

2.039 Claddings

2.0391 Effect of cladding thickness on cyclic oxidation of Fe-25Cr-4Al-1Y clad alloy at 1900 and 2000F, Fig. 2.0391.

2.0392 Effect of cladding thickness on cyclic oxidation of Ni-20Cr-4Al-1.2Si clad alloy at 1900 and 2000F, Fig. 2.0392.

2.0393 Effect of cladding thickness on cyclic oxidation of Ni-30Cr-1.4Si at 1900 and 2000F, Fig. 2.0393.

2.0310 Vapor deposited coatings.

2.03101 Weight change and thermal fatigue cracking tendencies of alloy with vapor deposited CoCrAlY coating, and comparison with performance of alloy coated by commercial pack aluminide process, Fig. 2.03101.

2.0311 Embedded alumina particle coatings.

2.03111 Weight change and thermal fatigue cracking tendencies of alloy with EAPA (embedded alumina-particle aluminide) subjected to 1 hour cycles at 2000F in Mach 1 jet burner, and comparison with performance of bare alloy and other types of coatings, Fig. 2.03111.

2.04 Nuclear Properties

3. MECHANICAL PROPERTIES

3.01 Specified Mechanical Properties
See 1.032 and 1.033.

3.02 Mechanical Properties at Room Temperature
See also 3.03.

3.021 Room temperature tensile properties of as cast alloy in three levels of electron vacancy concentration, and at two levels of grain size, Table 3.021.

3.022 Mechanical properties at room temperature of forged alloy in three conditions of proneness to sigma phase precipitation. Properties shown after normal heat treatment and after heat treatment followed by exposure to elevated temperature, Table 3.022.

3.023 Effect of thermal exposure subsequent to heat treatment on room temperature tensile properties for forged alloy with three levels of Al + Ti content (electron vacancy concentration, $\bar{N}v$, relating to propensity toward sigma formation), Table 3.023.

3.024 Effect of exposure at 1550F for 250 hour and for 2500 hour on room temperature tensile properties of alloy with Al-Ti composition varied to achieve 3 levels of electron vacancy concentration, $\bar{N}v$, Fig. 3.024.

3.025 Room temperature tensile properties and hardness of powder metallurgy product prepared from powders of various compositions and grain size and consolidated by several processes, Table 3.025.

3.026 Tensile properties of superplastically formed pancake forging used in fatigue crack growth studies, Table 3.026.

3.027 Comparison of tensile properties of alloy with Ni-20Cr-4Al-1.2Si cladding alloy before and after oxidation, Fig. 3.027.

3.028 Stress strain curves. See Fig. 3.03111

3.029 Impact

3.0291 Unnotched charpy impact strength at room temperature after hold for 500 or 1000 hours at elevated temperature, Fig. 3.0291.

3.03 Mechanical Properties at Various Temperatures

3.031 Tension

3.0311 Stress strain curves

3.03111 Stress-strain curves for as cast alloy at rooom and elevated temperatures, Fig. 3.03111

3.03112 Stress-strain curves for JoCoated alloy at room and elevated temperatures, Fig. 3.03111.

3.0312 Tensile properties

3.03121 Effect of test temperature on mechanical properties as cited by alloy developer, Fig. 3.03121.

3.03122 Tensile properties of as cast bar at room and elevated temperatures, Fig. 3.03122.

3.03123 Tensile properties of JoCoated bar at room and elevated temperatures, Fig. 3.03123.

3.0313 Heat treatment effects

3.03131 Effect of several solution heat treatments on the tensile properties at 1300F, Table 3.03131.

3.0314 Coating and coating repair effects.

3.03141 Tensile properties at room and elevated temperatures of thinwall alloy coated with two proprietary coatings, Table 3.03141.

3.03142 Effect of coating, high temperature exposure, and several repair processes on tensile and yield strength at 1800F compared to as cast uncoated base material, Fig. 3.03142

3.03143 Effect of coating, high temperature exposure, and several repair processes on elongation at 1800F compared to as cast uncoated base material, Fig. 3.03143.

3.0315 Powder metallurgy product.

3.03151 Effect of reduction practice and heat treatment on the tensile properties at RT and 1200F of powder metallurgy alloy, Table 3.03151.

3.03152 Tensile properties of specimen from powder alloy pancake at RT and 1300F, with comparison to Pratt & Whitney specifications for alloy, Fig. 3.03152.

3.03153 Flow characteristics in the range at low strain rates and temperatures where superplasticity can be achieved, Fig. 3.03153.

3.03154 Relation between stress and high deformation rate at 1900 to 2100F for alloy directly extruded from powder, Fig. 3.03154.

3.03155 High strain rate effect on elongation at fracture at 1900 to 2100F for alloy directly extruded from powder, Fig. 3.03155.

3.03156 Superplasticity exhibited by powder metallurgy alloy, Fig. 3.03156.

3.0317 High pressure gas effects.

3.03171 Tensile properties at RT and 1250F in 5000 psig helium and hydrogen, Table 3.03171.

3.032 Compression

3.0321 Effect of test temperature on compression yield strength for air melted and cast alloy and for vacuum melted and cast alloy, Fig. 3.0321.

3.033 Impact

3.0331 Effect of temperature on Charpy V impact energy, Fig. 3.0331.

3.034 Bending

3.035 Torsion and shear

3.036 Bearing

3.037 Stress concentration. (see also 3.05)

3.0371 Notch properties

3.0372 Fracture toughness

3.038 Combined properties

3.04 Creep and creep rupture properties. (see also 3.054)

3.041 Creep curves at various temperatures.

3.0411 Creep curves of as cast alloy at 1562F, Fig. 3.0411.

3.0412 Creep curves for JoCoated alloy at 1562F, Fig. 3.0412.

3.0413 Creep curves of as cast alloy at 1697F, Fig. 3.0413.

3.0414 Creep curves for JoCoated alloy at 1697F, Fig. 3.0414.

3.0415 Creep curves of as cast alloy at 1832F, Fig. 3.0415.

3.0416 Creep curves for JoCoated alloy at 1832F, Fig. 3.0416.

3.0417 Alloy developer's suggested design curves for creep strain and creep rupture at 1350F, Fig. 3.0417.

3.0418 Alloy developer's suggested design curves for creep strain and creep rupture at 1500F, Fig. 3.0418.

3.0419 Alloy developer's suggested design curves for creep strain and creep rupture at 1700F, Fig. 3.0419.

3.04110 Alloy developer's suggested design curves for creep strain and creep rupture at 1800F, Fig. 3.04110.

3.04111 Alloy developer's suggested design curves for creep strain and creep rupture at 1900F, Fig. 3.04111.

3.04112 Minimum creep rate curves for temperatures from 1350 to 1900F, Fig. 3.04112.

3.042 Creep of superplastically formed product.

3.0421 Creep and creep rupture properties of superplastically formed pancake forging used in fatigue crack growth

	Ni
15	Co
10	Cr
5.5	Al
4.7	Ti
3	Mo
0.95	V

IN-100

studies, Table 3.0421.

3.043 Relation of creep to creep rupture.

3.0431 Relation among start of third stage creep, time to 1% creep, and rupture time for as cast alloy, Fig. 3.0431.

3.0432 Relation among time of third stage creep, time to 1% creep, and rupture time for JoCoated alloy, Fig. 3.0432.

3.044 Effects of repair coatings on creep and creep rupture.

3.0441 Creep and rupture properties of alloy after repair of oxidation and mechanical damage effects, Fig. 3.0441.

3.045 Creep rupture, general.

3.0451 Typical creep rupture properties in life range from 10 to 10,000 hours at temperatures from 1300 to 2000F, Fig. 3.0451.

3.0452 Creep rupture curves for as cast alloy at 1562F, 1697F, and 1832F, Fig. 3.0452.

3.0453 Creep rupture data for as cast alloy as determined by developer, Fig. 3.0453.

3.046 Creep rupture, heat treatment effects.

3.0461 Effect of several solution heat treatments on the creep-rupture life at 1800F, 29 ksi, Table 3.0461.

3.047 Creep rupture, coating effects.

3.0471 Effect of coating on creep rupture properties at stresses and temperatures yielding creep rupture lives in the range of 50 to 200 hours, Table 3.0471 .

3.0472 Creep rupture curves for JoCoated alloy at 1562F, 1697F and 1832F, Fig. 3.0472.

3.0473 Correlation between ductility and rupture time at 1562F, 1697F, and 1832F for JoCoated alloy, Fig. 3.0473.

3.0474 Creep rupture lives and elongations at 1450F and 1800F for thinwall alloy coated with two proprietary coatings, Table 3.0474.

3.048 Creep rupture, sigma phase instability effects.

3.0481 Beneficial effects on creep rupture behavior achieved by avoiding sigma phase precipitation, Table 3.0481.

3.0482 Creep rupture properties of forged alloy in three conditions of proneness to sigma phase precipitation, Table 3.0482.

3.0483 Creep rupture curves for fine grain alloy of composition sufficiently low in Al and Ti to avoid sigma precipitation, Fig. 3.0483.

3.0484 Creep rupture curves at 40ksi for alloy in three levels of electron vacancy concentration achieved by additions of Al-Ti to a single heat, tested in as cast condition or after exposure at 1550F for 250 and 2500 hours, Fig. 3.0484.

3.0485 Creep rupture curves for fine grain alloys of low, medium and high electron vacancy concentration (Nv), representing progressively increasing tendency toward sigma phase precipitation. Curves show that strong tendency for sigma precipitation results in reduction of creep rupture strengths, Fig. 3.0485.

3.049 Creep rupture, powder metallurgy product.

3.0491 Creep rupture properties in very short time range at 1900 to 2100F for extruded alloy prepared from two lots of powder, Fig. 3.0491.

3.0492 Creep rupture curves at 1800F for cast alloy of various grain sizes and for alloy extruded from powders, Fig. 3.0492.

3.0410 Creep rupture in special environments.

3.04101 Creep rupture of alloy in helium, hydrogen, and hydrogen/water vapor at 1250F and 5000 psig pressure, Fig. 3.04101.

3.05 Fatigue properties

3.051 Mechanically induced fatigue

3.0511 Effect of aluminum base coating on rotating bending fatigue properties at room temperature, Table 3.0511.

3.0512 Low cycle fatigue characteristics of smooth hollow specimen with one-inch gage length of uniform cross section at temperatures from 1000 to 2000F in strain-controlled cycling, Fig. 3.0512.

3.0513 Low cycle fatigue characteristics at 1700F of hollow specimen with two sets of diagonal holes, Fig. 3.0513.

3.0514 Strainrange partitioning life relationships for cast alloy at 1700F, Fig. 3.0514

3.0515 Axial fatigue at 1650F of simulated hollow airfoils coated with proprietary coatings, Fig. 3.0515.

3.052 Thermally induced fatigue

3.0521 Thermal shock fatigue characteristics of airfoil shape with and without aluminum base coating, Table 3.0521.

3.0522 Thermal fatigue resistance of square plate rapidly heated and cooled at periphery of central hole, and comparison with thermal fatigue resistance of other commonly used cast alloys, Fig. 3.0522.

3.0523 Thermal fatigue crack initiation of as cast or directionally solidified alloy with and without JoCoat tested in alternate fluidized beds at 1990 and 600F, Fig. 3.0523.

3.0524 Thermal fatigue crack initiation of as cast or directionally solidified alloy with and without JoCoat tested in alternate fluidized beds at two sets of temperatures, Fig. 3.0524.

3.0525 Effect of cycle time on thermal fatigue cracking of coated and uncoated wedges alternately immersed in fluidized beds at 600 and 1990F, Fig. 3.0525.

3.0526 Effect of maximum cycle temperature on thermal fatigue cracking of coated and uncoated airfoils simulating turbine blades subjected to Mach 1 gas flow followed by rapid air jet cooling, Fig. 3.0526.

3.0527 Relation between crack growth rate and resistance to initial cracking in thermal cycling, Fig. 3.0527.

3.0528 Thermal fatigue of thinwall alloy with two proprietary coatings subjected to 10.5 ksi tensile mean stress and to temperature cycling from 2050F, Table 3.0528.

3.0529 Correlation of time to initiate thermal cracking with weight gain slope parameter for alloy coated in various ways, Fig. 3.0529.

3.053 Mechanical loading of powder metallurgy product.

3.0531 Stress range variation during low cycle fatigue tests at 1200F of powder metallurgy bars prepared by Pratt & Whitney Aircraft Gatorizing$_{TM}$process, Fig. 3.0531.

3.0532 Low cycle fatigue at 1200F of powder metallurgy bars prepared by Pratt and Whitney Gatorizing$_{TM}$process. Data points represent cycles to complete fracture, Fig. 3.0532

3.0533 Low cycle fatigue at 1200F of powder metallurgy bars prepared by Pratt and Whitney Aircraft Gatorizing$_{TM}$ process. Data points represent cycles to 5 percent load drop, Fig. 3.0533.

3.0534 Low cycle fatigue at 1200F of specimen from powder metallurgy compressor disk, Fig. 3.0534.

3.054 Crack growth in steady loading or continuous cycling.

3.0541 Basic crack growth curves at RT, 1200F and 1350F for constant amplitude loading of WOL specimen, Fig. 3.0541.

3.0542 Effect of net section stress on crack growth rate at 1200F, Fig. 3.0542.

3.0543 Effect of temperature and specimen thickness on sustained load crack propagation rate, Fig. 3.0543.

3.0544 Effect of specimen thickness on crack growth rate at RT, Fig. 3.0544

3.0545 Effect of frequency on crack growth rate in continuous cycling at 1200F, Fig. 3.0545.

3.0546 Effect of temperature on crack growth rate at 10cpm, R = 0.1, Fig. 3.0546.

3.0547 Effect of stress ratio on crack growth rate at 1200F, 10cpm, Fig. 3.0547.

3.0548 Effect of stress ratio on crack growth rate at 1200F, 20cps, Fig. 3.0548.

3.0549 Effect of specimen thickness on crack growth rate at 1200F, continuous cycling at 10cpm, Fig. 3.0549.

3.055 Crack growth-overload effects.

3.0551 Crack growth at 1200F under continuous cycling and with 50 percent overload every 5, 20, or 40 cycles, Fig. 3.0551.

3.0552 Crack growth at 1200F under continuous cycling and with 25 percent or 50 percent overloads every 21 cycles, Fig. 3.0552.

3.0553 Crack growth at 1200F under sustained load and with 25 percent or 50 percent overloads every 2 minutes, Fig. 3.0553.

3.056 Crack growth-dwell periods.

3.0561 Effect of net section stress on crack growth rate for 2 minute dwell at peak stress at 1200F, Fig. 3.0561.

3.0562 Effect of specimen thickness on crack growth rate at 1200F, Two minute dwell at max load, 10cpm during variable stress period, Fig. 3.0562.

Effect of dwell time at peak stress on crack growth rate at 1200F, R = 0.1, Fig. 3.0563.

3.0564 Crack growth at 1350F under continuous cycling, or with 25 and 50 percent overload, or with 2 minute dwell at the

	50 percent overload condition, Fig. 3.0564.
3.0565	Interaction of low cycle fatigue with dwell periods at max load for tests at 1200F, R = 0.1, Fig. 3.0565.
3.0566	Interaction of low cycle fatigue with dwell periods at max load for tests at 1350F, R = 0.1, Fig. 3.0566.
3.057	Crack growth-delay effects due to overloads.
3.0571	Delay cycles prior to resumption of basic crack growth after single cycle of overload. Baseline Kmax = 23.2 ksi $\sqrt{in}$, Fig. 3.0571.
3.0572	Delay cycles prior to resumption of basic crack growth after single cycle of overload. Baseline Kmax = 35.2 ksi $\sqrt{in}$, Fig. 3.0572.
3.058	Helium and hydrogen effects at high pressure.
3.0581	Low cycle fatigue at 1250F in high pressure hydrogen and helium, Fig. 3.0581.
3.0582	High cycle axial fatigue in high pressure hydrogen and helium at 1250F, Fig. 3.0582.
3.05141	Inelastic strain range vs. low-cycle fatigue life for each partioned strain range component for as-cast thinwall tubing at 1700F. Fig. 3.05141.
3.05142	Strainrange partioning life relationships at 1652F and 1832F for as-cast aluminum-coated alloy, Fig. 3.05142.
3.05143	Inelastic strainrange vs. low-cycle fatigue life for each partitioned strainrange component at 1400F. Specimens from creep-formed (Gatorized$_{T3I}$) turbine disk, Fig. 3.05143.
3.05144	Total strain range vs. low-cycle fatigue life at 1200F of powder metallurgy bars prepared by Pratt & Whitney Gatorizing$_{T3I}$ process and tested under rapid strain cycling, tensile stress-hold, and tensile strain-hold, Fig. 3.05144.
3.05145	Inelastic strainrange vs. low cycle fatigue life at 1200F of powder metallurgy bars prepared by Pratt and Whitney Gatorizing$_{T3I}$ process and tested under rapid strain cycling, tensile stress-hold, and tensile strain-hold, Fig. 3.05145.
3.06	Elastic properties
3.061	Poisson's ratio, 0.298
3.062	Dynamic modulus of elasticity, Fig. 3.062.
3.063	Modulus of rigidity
4.0	FABRICATION
4.1	Strength of shaped parts
4.11	Mechanical properties from RT to 1300F of specimens from the 10-12th stage compressor of F100/F401 engine, Fig. 4.11.
4.12	Room temperature tensile strength of fir tree simulating turbine blade attachment, Table 4.12.
4.13	Creep rupture at 1400F of fir tree simulating turbine blade attachment, Fig. 4.13.
4.14	Fatigue at RT under combined static and vibratory stress of turbine blade fir tree fastening, Table 4.14.
4.2	Welding and joining
4.21	Weldments
4.211	Room temperature tensile strength of weldment to Waspaloy, Table 4.211.
4.212	Creep rupture at 1400F of electron beam weldment to Waspaloy, Table 4.212.
4.213	Fatigue at RT under combined static and vibratory stress of electron beam weldment to Waspaloy, Table 4.213.
4.22	Brazed joints
4.221	Room temperature tensile strength of brazed attachment to Waspaloy, Table 4.221.
4.222	Fatigue at RT under combined static and vibratory stress of brazed joint simulating turbine blade fastening to Waspaloy, Table 4.222.
4.23	TLP bonding
4.231	Tensile properties at 1400F for TLP bond between cast alloy and wrought Udimet 700, Table 4.231.

	Ni
15	Co
10	Cr
5.5	Al
4.7	Ti
3	Mo
0.95	V

IN-100

	Ni
15	Co
10	Cr
5.5	Al
4.7	Ti
3	Mo
0.95	V

IN-100

Alloy	Ni-15Co-10Cr-5.5Al-4.7Ti-3Mo-0.95V					
Condition	As Cast					
Source	Original Inco spec. (1960-1965) also GE spec C50T 77A		New Inco spec. also AMS5397		GE Rene' 100 spec C50T77C	
	Percent		Percent		Percent	
	Min	Max	Min	Max	Min	Max
Cobalt	13	17	13	17	14	16
Chromium	8	11	8	11	9	10
Aluminum	5	6	5	6	5.3	5.7
Titanium	4.5	5.5	4.5	5.0	4.0	4.4
Aluminum + Titanium	-	-	10	11	-	-
Molybdenum	2	4	2	4	2.7	3.3
Iron	0	1	0	1	0	1
Vanadium	.7	1.2	.7	1.2	.9	1.1
Boron	.01	.02	.01	.02	.01	.02
Carbon	.15	.20	.15	.20	.15	.20
Manganese	-	-	-	.10	-	-
Sulfur	-	-	-	.015	-	-
Silicon	-	-	-	.15	-	-
Nickel	Balance		Balance		Balance	

TABLE 1.04 COMPOSITION

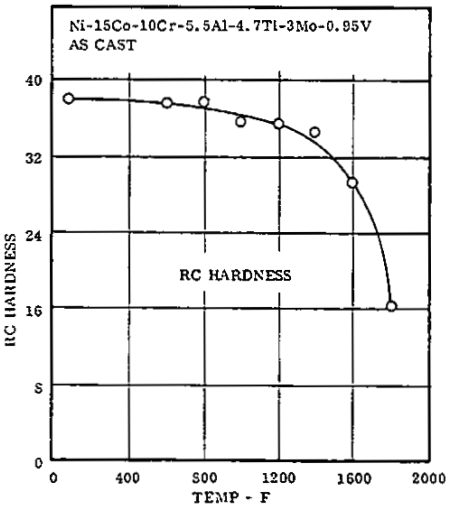

FIG. 1.062 EFFECT OF TEMPERATURE ON HARDNESS
(4, p. 11)

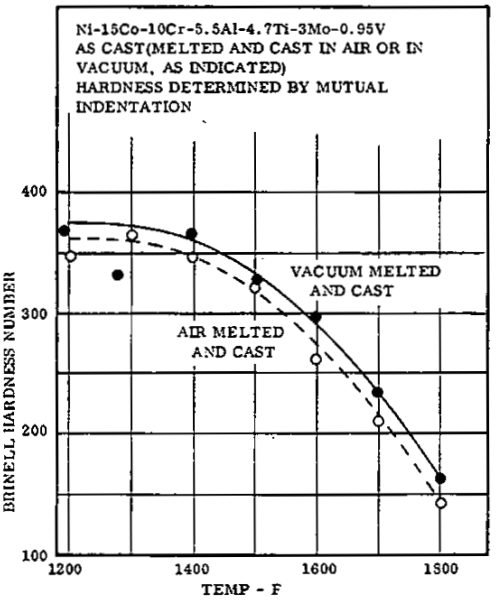

FIG. 1.063 EFFECT OF TEST TEMPERATURE ON BRINELL HARDNESS, AS DETERMINED BY MUTUAL INDENTATION, FOR AIR MELTED AND CAST ALLOY AND FOR VACUUM MELTED AND CAST ALLOY
(32, FIGS. 1,2)

	Ni
15	Co
10	Cr
5.5	Al
4.7	Ti
3	Mo
0.95	V

IN-100

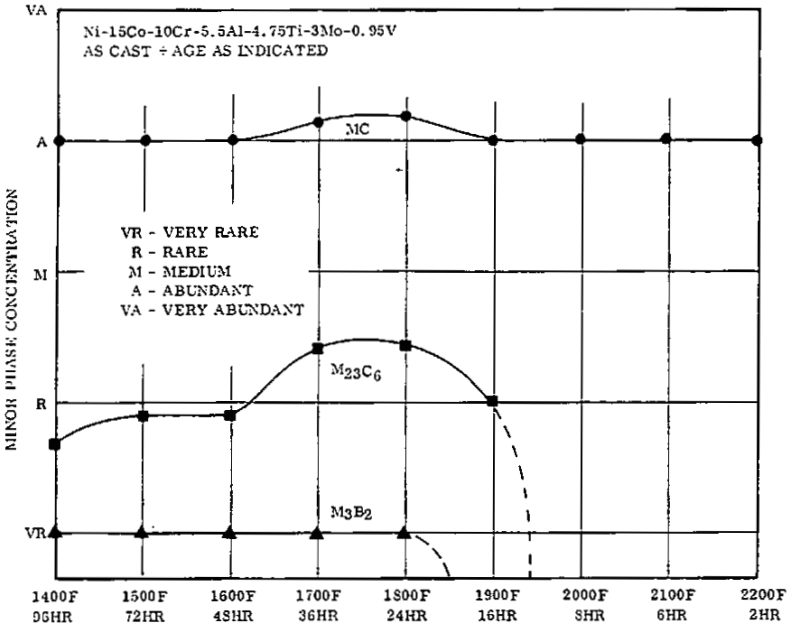

FIG. 2.0120 EFFECT OF AGING TIME AND TEMPERATURE ON MINOR PHASE CONCENTRATION (2, FIG. 1)

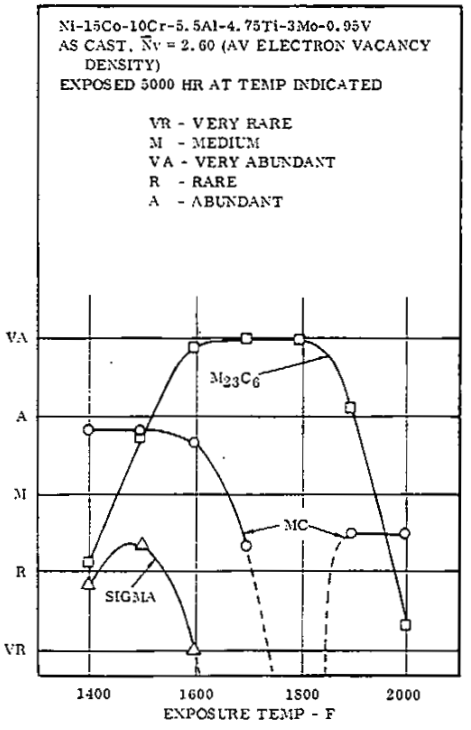

FIG. 2.0121 EFFECT OF EXPOSURE FOR 5000 HR AT VARIOUS TEMPERATURES ON MINOR PHASE CONCENTRATION (21, pp. 82, 84)

	Ni
15	Co
10	Cr
5.5	Al
4.7	Ti
3	Mo
0.95	V

IN-100

Ni-15Co-10Cr-5.5Al-4.75Ti-3Mo-0.95V (NOMINAL)
ACTUAL COMPOSITION FOR 2 LEVELS OF $\bar{N}v$
MED $\bar{N}v$ (2.49):Ni-13.3Co-10.14Cr-5.5Al-4.29Ti-3.55Mo-0.96V
HIGH $\bar{N}v$ (2.65):Ni-13.3Co-10.12Cr-5.6Al-4.69Ti-3.51Mo-0.97V
ALL ALLOYS MADE FROM SAME MASTER HEAT. ADDITIONS OF Al AND Ti MADE DURING CASTING TO ACHIEVE DESIRED LEVEL OF ELECTRON VACANCY CONCENTRATION ($\bar{N}v$)
TESTED AS CAST OR FORGED TO PANCAKE IN FOLLOWING STEPS:
1. EXTRUSION AT 2050F FROM 5 IN DIA INGOT TO 3 1/8 IN STEEL PIPE
2. FLATTENED AT 2050F TO 1 3/4 IN DIA PANCAKE
3. FLATTENED AT 2050F TO 1 IN DIA PANCAKE
4. FLATTENED AT 2050F TO 5/8 IN DIA PANCAKE

TEST SPECIMEN 1/4 IN DIA BAR x 1 1/4 IN GAGE LENGTH EXPOSED WITHOUT STRESS FOR TIMES AND TEMP SHOWN

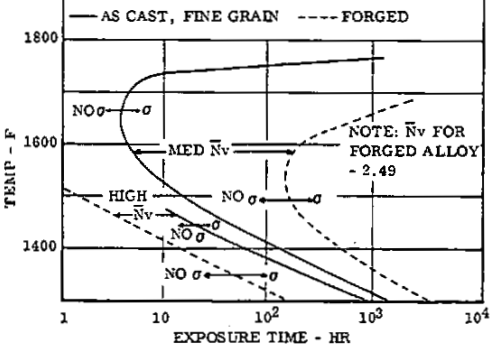

FIG. 2.0122 TRANSFORMATION TO SIGMA PHASE FOR AS CAST AND FORGED ALLOY FOR TWO LEVELS OF ELECTRON VACANCY CONCENTRATION (22,pp.14,19,23)

Ni-15Co-10Cr-5.5Al-4.7Ti-3Mo-0.95V(NOMINAL)
ACTUAL COMPOSITION FOR TWO LEVELS OF $\bar{N}v$
MEDIUM $\bar{N}v$(2.49): Ni-13.3Co-10.14Cr-5.5Al-4.29Ti-3.55Mo-0.96V
HIGH $\bar{N}v$(2.65): Ni-13.3Co-10.12Cr-5.6Al-4.69Ti-3.51Mo-0.97V
ALL ALLOYS MADE FROM SAME MASTER HEAT. ADDITIONS OF Al&Ti MADE DURING CASTING TO ACHIEVE DESIRED LEVEL OF ELECTRON VACANCY CONCENTRATION $\bar{N}v$
COARSE GRAIN ALLOYS PREPARED BY NORMAL INVESTMENT CASTING PROCEDURES; FINE GRAIN ALLOYS PREPARED BY MOLD INNOCULATION
TEST SPECIMEN 1/4 IN DIA x 1 1/4 IN GAGE LENGTH
EXPOSED WITHOUT STRESS FOR TIMES AND TEMPERATURES INDICATED

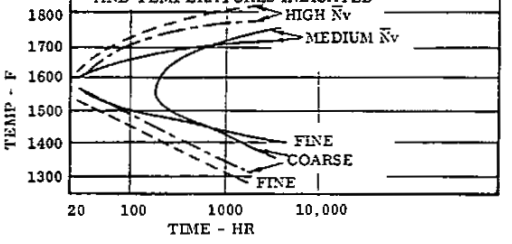

FIG. 2.0123 TIME-TEMPERATURE RELATION FOR THE ONSET OF SIGMA PHASE PRECIPITATION FOR MEDIUM AND HIGH ELECTRON VACANCY ($\bar{N}v$) COMPOSITIONS, AND IN FINE AND COARSE GRAIN SIZE STRUCTURE. (23,pp. 3,7,8)

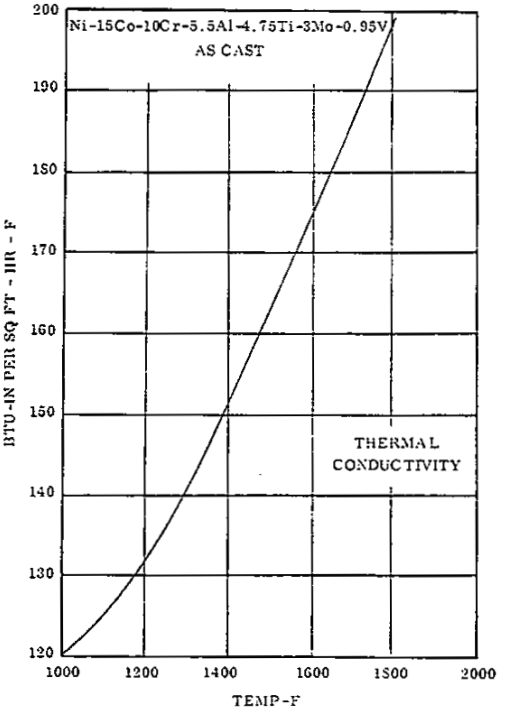

FIG. 2.013 THERMAL CONDUCTIVITY (11p.C-15)

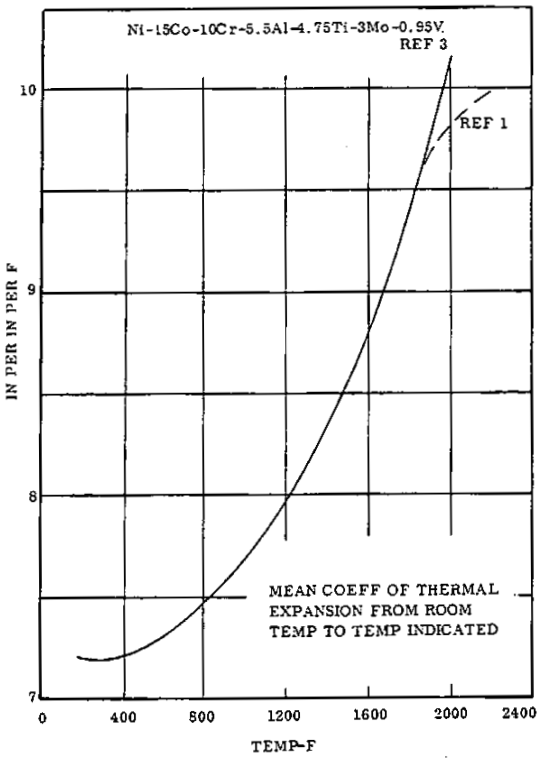

FIG. 2.014 COEFFICIENT OF THERMAL EXPANSION
(1,p.C-14)(3,p.10)

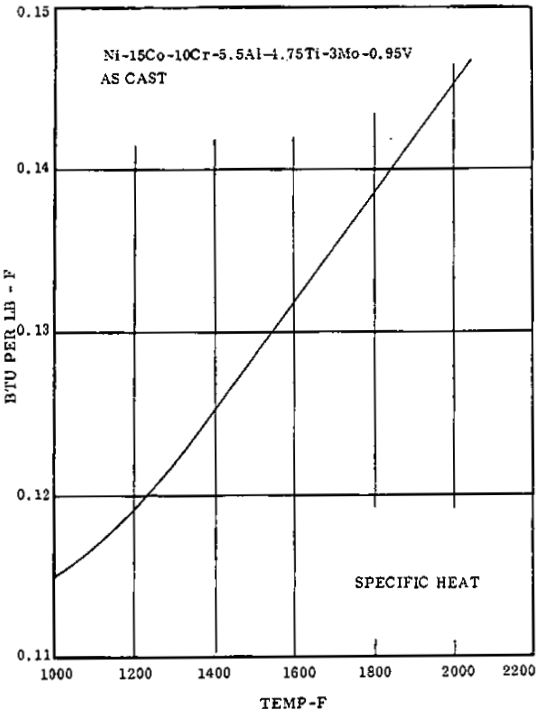

FIG. 2.015 SPECIFIC HEAT (1) p.C-15

	Ni
15	Co
10	Cr
5.5	Al
4.7	Ti
3	Mo
0.95	V

IN-100

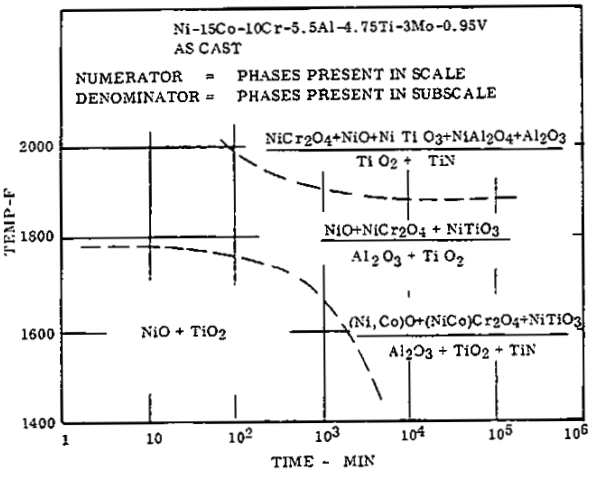

FIG. 2.032 SUMMARY OF MAIN STAGES OF OXIDATION (6)p.98

	Ni
15	Co
10	Cr
5.5	Al
4.7	Ti
3	Mo
0.95	V

IN-100

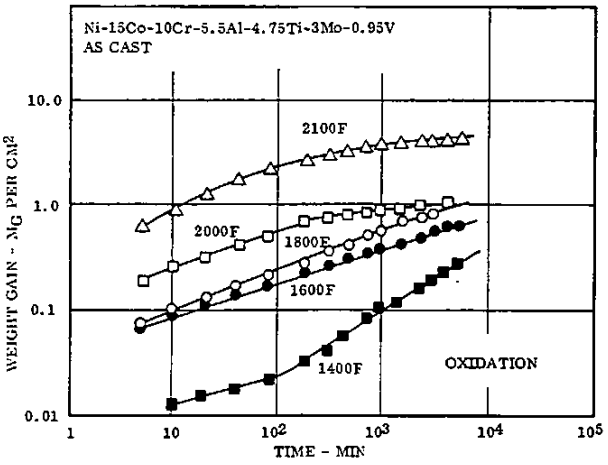

FIG. 2.033 TYPICAL PLOT OF WEIGHT GAIN VS TIME IN STATIC OXIDATION (6, p. 38)

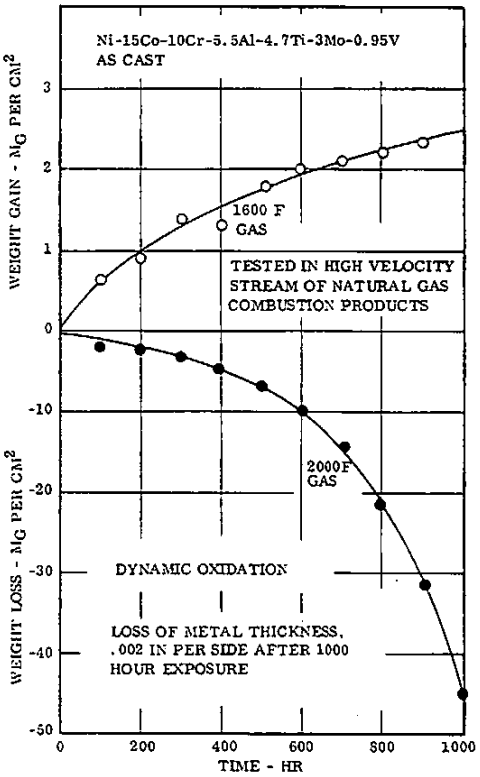

FIG. 2.034 DYNAMIC OXIDATION TESTS AT 1600F AND 1800F INDICATING COMPLEXITY OF PROCESS. WEIGHT GAIN OCCURS AT 1600F, LOSS AT 2000 F (6, pp.131, 132)

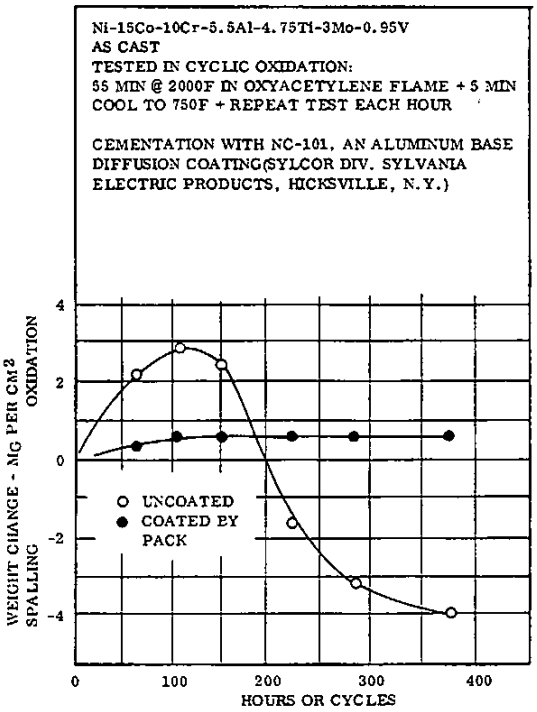

FIG. 2.035 CYCLIC OXIDATION BEHAVIOR WITH AND WITHOUT PROTECTIVE ALUMINUN BASE DIFFUSION COATING (7, pp. 33)(8)(9)

	Ni
15	Co
10	Cr
5.5	Al
4.7	Ti
3	Mo
0.95	V

IN-100

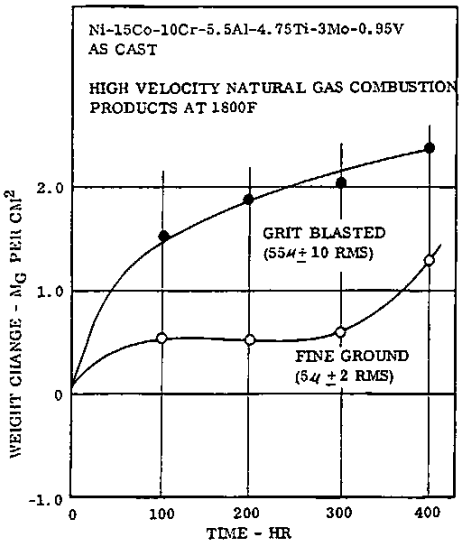

FIG. 2.036 DYNAMIC OXIDATION AT 1800F OF ALLOY IN TWO CONDITIONS OF SURFACE FINISH. ROUGHER SURFACE PROMOTES MORE RAPID OXIDATION (6, p. 162)

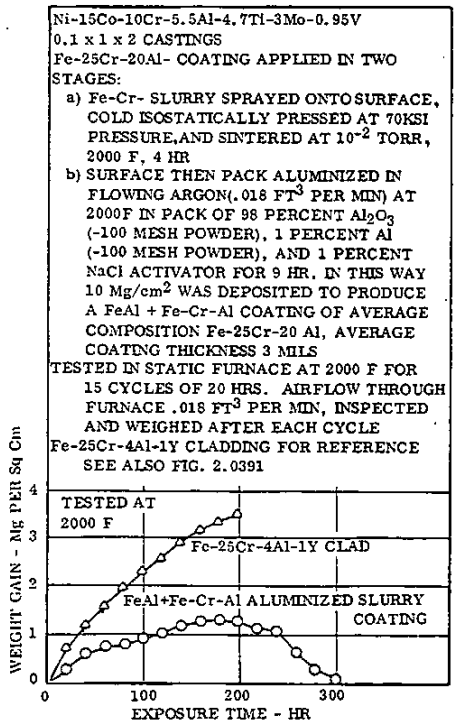

FIG. 2.0371 CYCLIC FURNACE OXIDATION IN 20 HR CYCLES AT 2000 F OF FeAl+Fe-Cr-Al ALUMINIZED SLURRY OF AVERAGE COMPOSITION Fe-25Cr-Al, AND COMPARISON WITH OXIDATION OF ALLOY PROTECTED BY CLADDING OF Fe-25Cr-4Al-1Y (41, pp. 3,4,18)

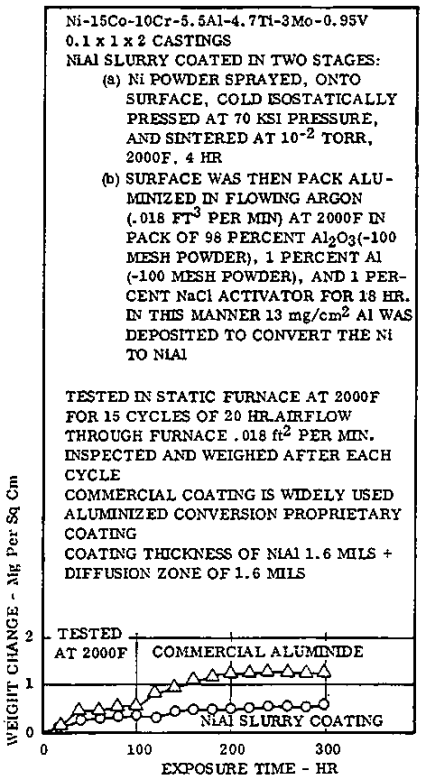

FIG. 2.0372 CYCLIC FURNACE OXIDATION IN 20 HR CYCLES AT 2000F OF NiAl SLURRY COATED ALLOY WITH COMPARISON TO OXIDATION OF COMMERCIAL CONVERSION COATING (41, pp. 3,4,14)

	Ni
15	Co
10	Cr
5.5	Al
4.7	Ti
3	Mo
0.95	V

IN-100

Ni-15Co-10Cr-5.5Al-4.7Ti-3Mo-0.95V
SIMULATED AIRFOIL SPECIMEN, SEE FIG. 2.03111
COATED WITH NiAl SLURRY COATING APPLIED IN TWO STAGES:

a) Ni POWDER SPRAYED ONTO SURFACE, COLD ISOSTATICALLY PRESSED AT 70 KSI PRESSURE AND SINTERED AT 10^{-2} TORR, 2000 F, 4 HR

b) SURFACE THEN PACK ALUMINIZED IN FLOWING ARGON (.018 FT^3 PER MIN) AT 2000F IN PACK OF 98 PERCENT Al_2O_3(-100 MESH POWDER),1 PERCENT Al (-100 MESH POWDER), AND 1 PERCENT NaCl ACTIVATOR FOR 18 HR. IN THIS MANNER 13 Mg PER Cm^2 Al WAS DEPOSITED TO CONVERT Ni TO Ni Al. AVERAGE COATING THICKNESS 1.6 MILS + DIFFUSION ZONE OF 1.6 MILS

TESTED IN HIGH VELOCITY (MACH 1) JET AT 2000 F IN CYCLES OF 1 HR AT TEMP +3 MIN COOLING IN AIR JET. SEE FIG 2.03111 FOR DETAILS

COMMERCIAL COATING SHOWN FOR COMPARISON IS WIDELY USED PROPRIETARY ALUMINIZED CONVERSION COATING

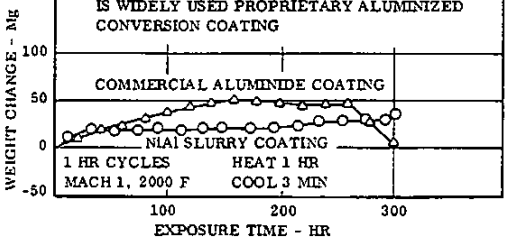

FIG. 2.0373 OXIDATION OF NiAl SLURRY COATING IN MACH 1 JET AT 2000F WITH COMPARISON TO COMMERCIAL ALUMINIDE COATING (41, pp. 3,4,20)

Ni-15Co-10Cr-5.5Al-4.7Ti-3Mo-0.95V
AS CAST WEDGE SPECIMEN AS SHOWN IN FIG. 2.03111 BARE OR COATED BY ELECTROLYTIC FUSED SALT(EFSP) PROCESS WHICH METALLIDES ALUMINUM DIRECTLY INTO SURFACE, PRODUCING AN ALUMINUM-RICH NiAl LAYER, OR COATED BY COMMERCIAL ALUMINIDE COATING.

TESTED IN MACH 1 JET AT 1900F USING CYCLE OF 1 HR FOLLOWED BY AIR COOLING TO RT IN 3 MINUTES
SEE FIG. 2.03111 FOR SKETCH OF SPECIMEN AND TEST DETAILS

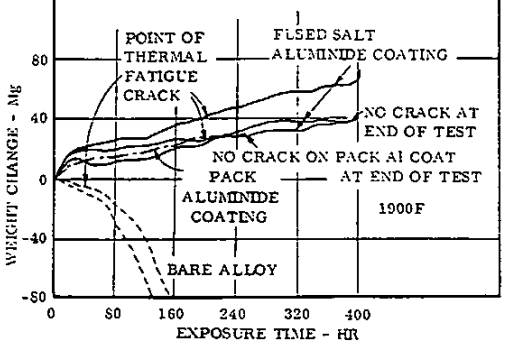

FIG. 2.0351 HIGH GAS VELOCITY OXIDATION AND THERMAL FATIGUE CRACKING AT 1900F OF ALLOY COATED BY AN ELECTROLYTIC FUSED SALT PROCESS (METALLIDED), AND COMPARISON WITH OXIDATION OF BARE ALLOY AND PACK ALUMINUM COATED ALLOY. (43, pp.2,3,20)

	Ni
15	Co
10	Cr
5.5	Al
4.7	Ti
3	Mo
0.95	V

IN-100

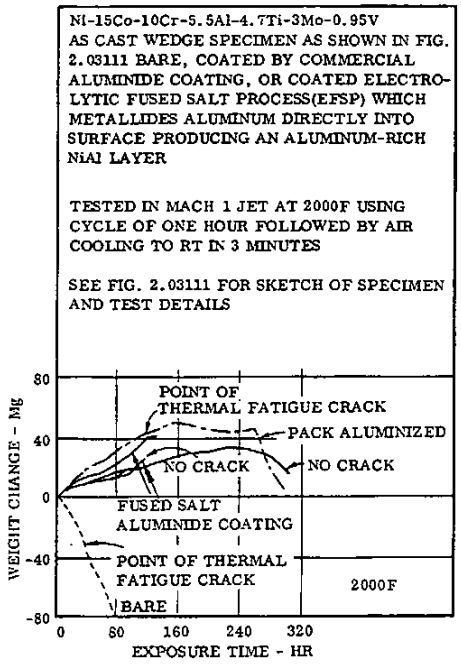

FIG. 2.0382 HIGH VELOCITY OXIDATION AND THERMAL FATIGUE CRACKING AT 2000F OF ALLOY COATED BY AN ELECTROLYTIC FUSED SALT PROCESS(METALLIDED), AND COMPARISON WITH BARE ALLOY AND PACK ALUMINUM COATED ALLOY. (43, pp.2,3,21)

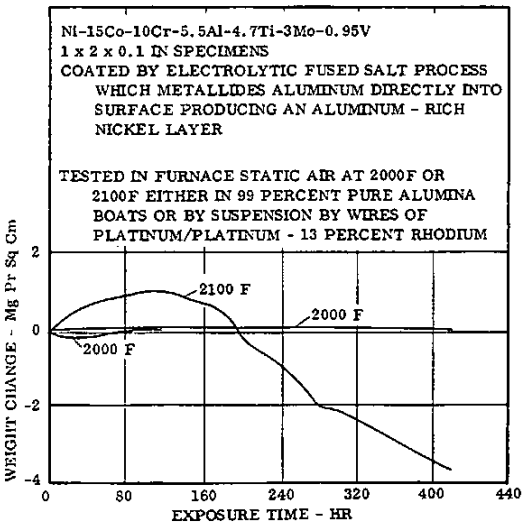

FIG 2.0383 STATIC OXIDATION AT 2000 AND 2100F OF ALLOY COATED BY ELECTROLYTIC FUSED SALT PROCESS (METALLIDING) (43, pp.2,22)

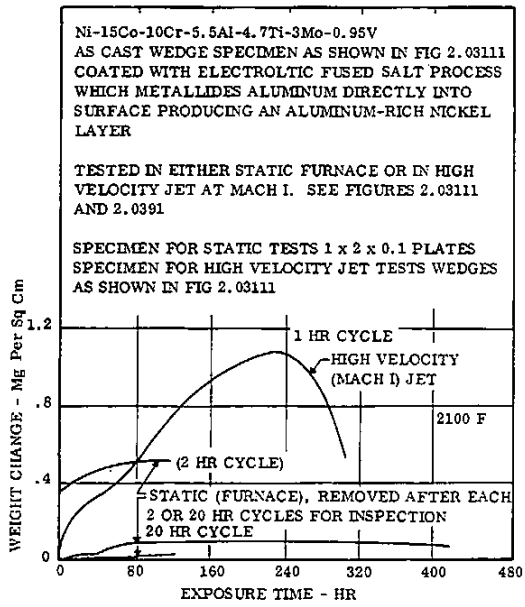

FIG. 2.0384 COMPARISON OF STATIC OXIDATION WITH OXIDATION IN HIGH VELOCITY JET (MACH I) AT 2100 F FOR METALLIDED COATING (43, pp.2,22)

	Ni
15	Co
10	Cr
5.5	Al
4.7	Ti
3	Mo
0.95	V

IN-100

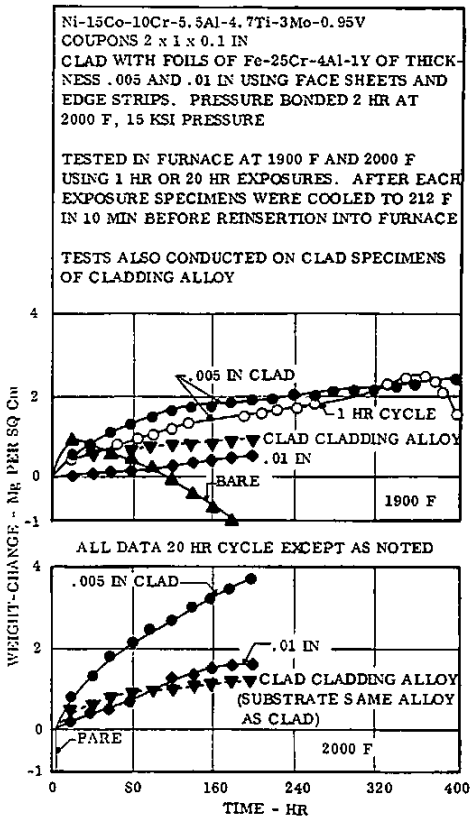

FIG. 2.0391 EFFECT OF CLADDING THICKNESS ON CYCLIC OXIDATION OF Fe-25Cr-4Al-1Y CLAD ALLOY AT 1900 AND 2000 F (42, pp. 2,3,29)

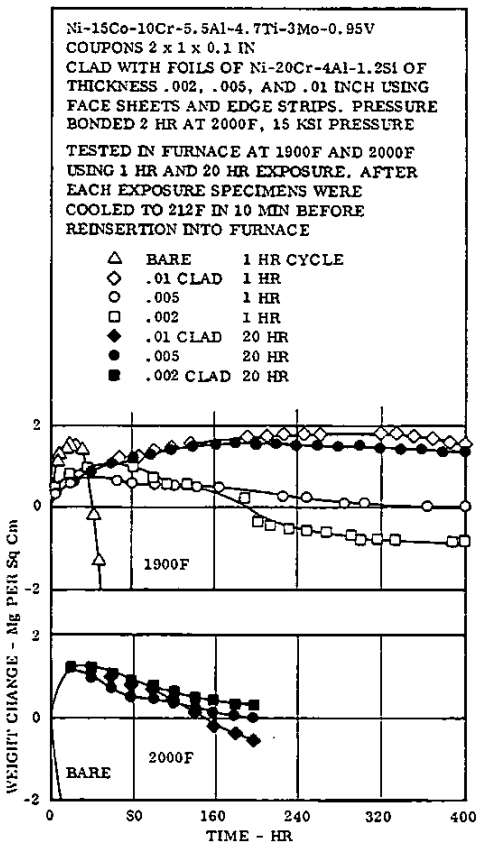

FIG. 2.0392 EFFECT OF CLADDING THICKNESS ON CYCLIC OXIDATION OF Ni-20Cr-4Al-1.2Si CLAD ALLOY AT 1900F AND 2000F (42,pp.2, 3, 25)

	Ni
15	Co
10	Cr
5.5	Al
4.7	Ti
3	Mo
0.95	V

IN-100

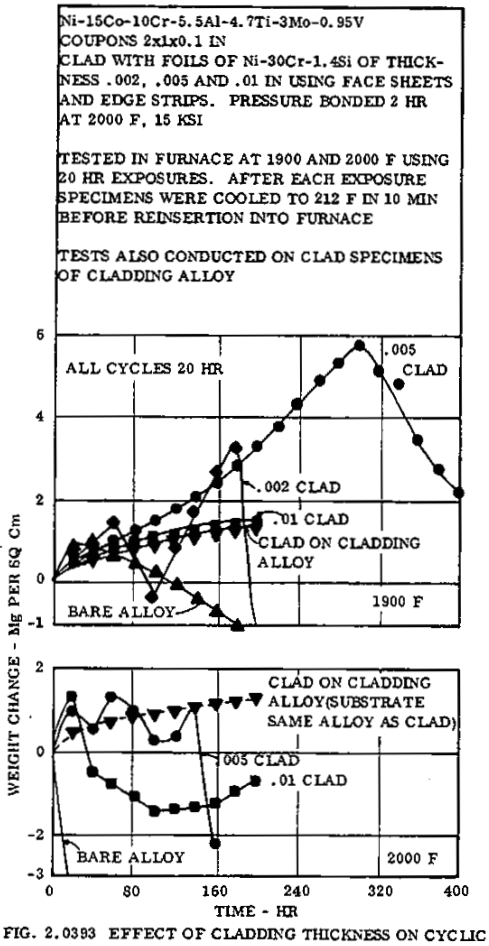

FIG. 2.0393 EFFECT OF CLADDING THICKNESS ON CYCLIC OXIDATION OF Ni-30Cr-1.4Si AT 1900 AND 2000F (42,pp.2,3,33)

	Ni
15	Co
10	Cr
5.5	Al
4.7	Ti
3	Mo
0.95	V

IN-100

Ni-15Co-10Cr-5.5Al-4.7Ti-3Mo-0.95V
AS CAST ALLOY MACHINED TO WEDGE BAR AS SHOWN IN FIG. 2.03111

COATED WITH CoCrAlY BY ELECTRON-BEAM-HEAT-SOURCE, PHYSICAL-VAPOR DEPOSITION PROCESS. NOMINAL COMPOSITION OF COATING Co-22Cr-14Al-0.1Y

TESTED IN MACH 1 JET AT 2000 F IN HEATING CYCLES OF 1 HR, FOLLOWED BY COOLING TO RT IN 3 MIN

TYPE OF COATING	TOTAL THICKNESS OF COATING IN	THICKNESS OF OUTER LAYER IN
□ CoCrAlY	.0045 TO .0055	.004 TO .0048
△ COMMERCIAL PACK ALUMINIDE	.0033	.0017
○ NO PARTICLE EMBEDMENT	.0017	.0012

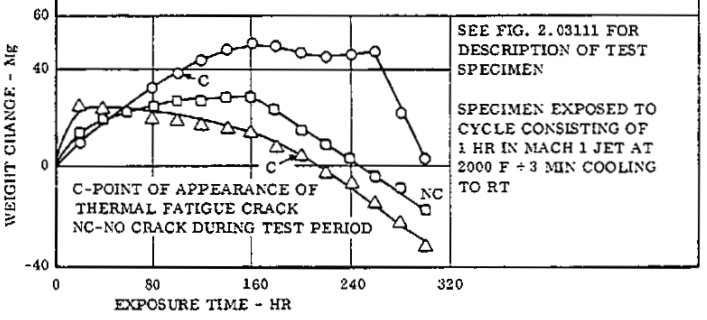

FIG. 2.03101 WEIGHT CHANGE AND THERMAL FATIGUE CRACKING TENDENCIES OF ALLOY WITH VAPOR DEPOSITED CoCrAlY COATING AND COMPARISON WITH PERFORMANCE OF ALLOY COATED BY COMMERCIAL PACK ALUMINIDE PROCESS (44, pp. 3, 18, 26)

	Ni
15	Co
10	Cr
5.5	Al
4.7	Ti
3	Mo
0.95	V

IN-100

Ni-15Co-10Cr-5.5Al-4.7Ti-3Mo-0.95V
AS CAST ALLOY MACHINED TO WEDGE BAR, AS SHOWN
EAPA(EMBEDDED ALUMINA-PARTICLE ALUMINIDE) COATING
APPLIED BY DUAL CYCLE, MODIFIED-PACK-CEMENTATION,
ALUMINIZING PROCESS. APPROX 15 V/O OF 2 MICROMETER
ALUMINA PARTICLES ENTRAPPED IN COATING
TESTED IN 2000F, MACH 1 JET, HEAT 1 HR, COOL 3 MIN

TYPE OF COATING	THICKNESS OF COATING - IN	THICKNESS OF OUTER NiAl LAYER - IN
○●■ NO COATING		
□ EMBEDDED ALUMINA-PARTICLE ALUMINIDE	.0005 TO .0015	.0002 TO .0007
◇ FUSED SALT, ALUMINIZED	.0025	.0015
△ COMMERCIAL PACK ALUMINIDE,	.0033	.0017
▽ NO PARTICLE EMBEDMENT	.0017	.0012

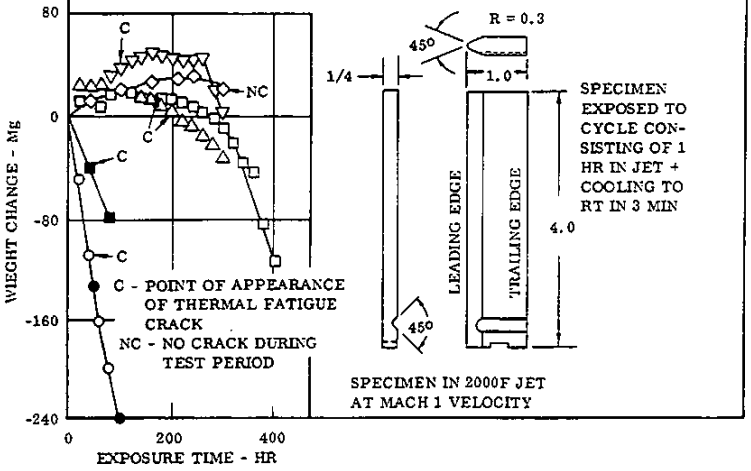

FIG. 2.03111 WEIGHT CHANGE AND THERMAL FATIGUE CRACKING TENDENCIES OF ALLOY WITH EAPA(EMBEDDED ALUMINA-PARTICLE ALUMINIDE) SUBJECTED TO 1 HR CYCLES AT 2000F IN MACH 1 JET BURNER, AND COMPARISON WITH PERFORMANCE OF BARE ALLOY AND OTHER TYPES OF COATINGS (44, pp. 2,18,22)

	Ni
15	Co
10	Cr
5.5	Al
4.7	Ti
3	Mo
0.95	V

IN-100

Ni-15 Co-10Cr-5.5Al-4.7Ti-3Mo-0.95V
AS CAST ALLOY MACHINED TO WEDGE BAR AS SHOWN IN FIG. 2.03111
COATED WITH Pt-Al BY APPLYING A .0003 LAYER OF Pt BY ELECTROPLATING AND ALUMINIZING BY PACK PROCESS.
FINAL COATING THICKNESS APPROX. .003 IN

CERMET (1) : Ni-Cr-Si ALLOY CONTAINING TiB_2 AND TiN PARTICLES
CERMET (2) : Ni-Cr-ALLOY CONTAINING $TiSi_2$ PARTICLES
CERMET (3) : CERMET (1) + ALUMINIZING PACK TREATMENT - (PACK: 2Al-2NaCl-96Al_2O_3, 2000F, 15 HR)
FeCrAlY: PLASMA SPRAYED Fe-25Cr-13Al-0.8Y, FOLLOWED BY OVERSPRAY WITH Al POWDER + (1100) F, 6 HR IN ARGON, THICKNESS (.018) IN
NiCrAl (1) : PROPRIETARY ALLOY CONTAINING NO ADDED OXIDES
NiCrAl (2) : PROPRIETARY ALLOY CONTAINING Y_2O_3 PARTICLES
CoCrAlY : PHYSICAL VAPOR DEPOSITED

SEE FIG. 2.03111 FOR SKETCH OF SPECIMEN

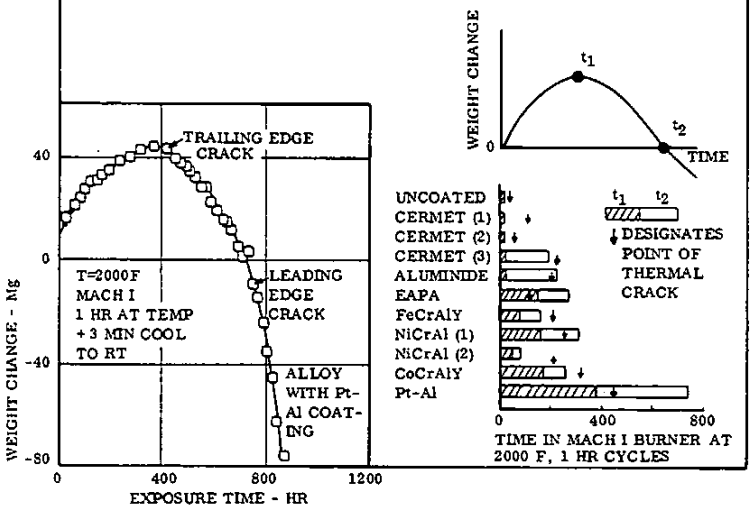

FIG. 2.03121 TYPICAL WEIGHT CHANGE PATTERN FOR COATED ALLOY CYCLED FOR ONE HR INTERVALS AT 2000 F, FOLLOWED BY COOLING TO RT IN 3 MIN FIGURE SHOWS DATA FOR Pt-Al ALLOY WITH SUMMARY OF RESULTS FOR SEVERAL OTHER ALLOYS (45, pp.2,3,13,14)

Alloy	Ni-15Co-10Cr-5.5Al-4.7Ti-3Mo-0.95V
Source	Haynes (10) p. 6
Condition	As Cast, Corrosion Tested (a)
	Wt. Change (a) Mg per Cm^2 (Loss)
Bare	71.3
Coating C - 3	9.5
Coating C - 9	9.4

(a) Exposed 1 hr in Na_2SO_4 + 0.5 percent. NaCl at 1652F.

TABLE 2.03131 EFFECT OF CORROSIVE ENVIRONMENT ON WEIGHT CHANGE IN BARE AND COATED CONDITION

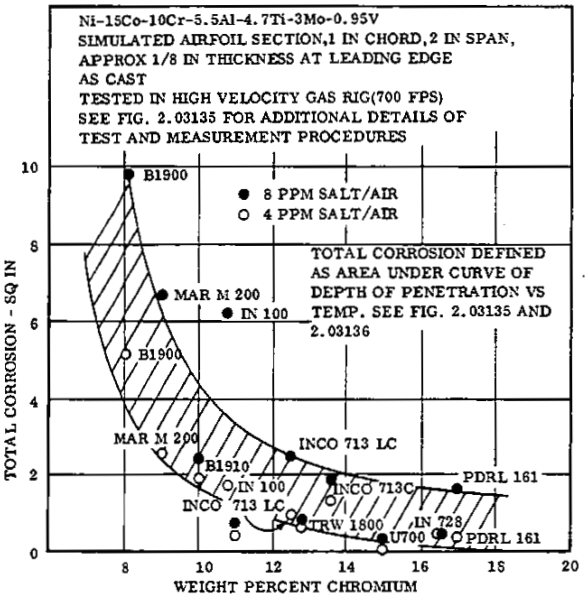

	Ni
15	Co
10	Cr
5.5	Al
4.7	Ti
3	Mo
0.95	V

IN-100

FIG. 2.03133 CORRELATION SHOWING THAT LOW CORROSION RESISTANCE OF ALLOY IS RELATED TO ITS LOW CHROMIUM CONTENT (27, p.132)

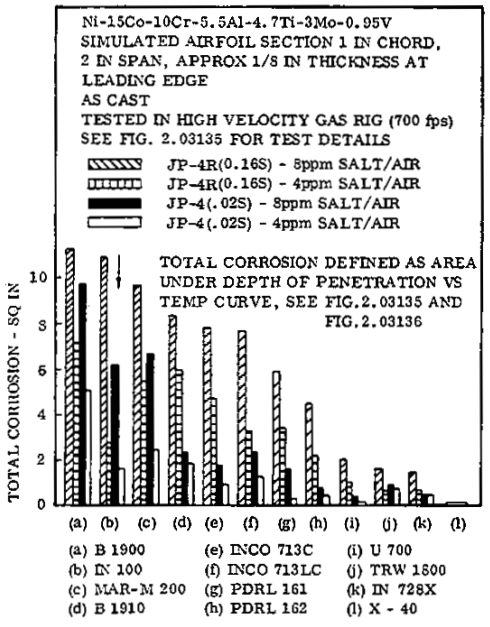

FIG. 2.03132 RELATIVE CORROSION OF VARIOUS SUPER-ALLOYS FOR TWO FUELS OF DIFFERENT SULFUR CONTENT AND TWO SALT/AIR RATIO CONTENTS (27, p.131)

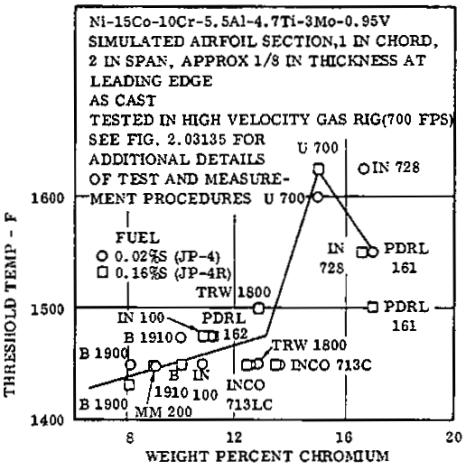

FIG. 2.03134 CORRELATION SHOWING THAT THE LOW THESHOLD TEMPERATURE FOR CORROSION IS PRINCIPALLY RELATED TO ITS LOW CHROMIUM CONTENT (27, p. 33)

	Ni
15	Co
10	Cr
5.5	Al
4.7	Ti
3	Mo
0.95	V

IN-100

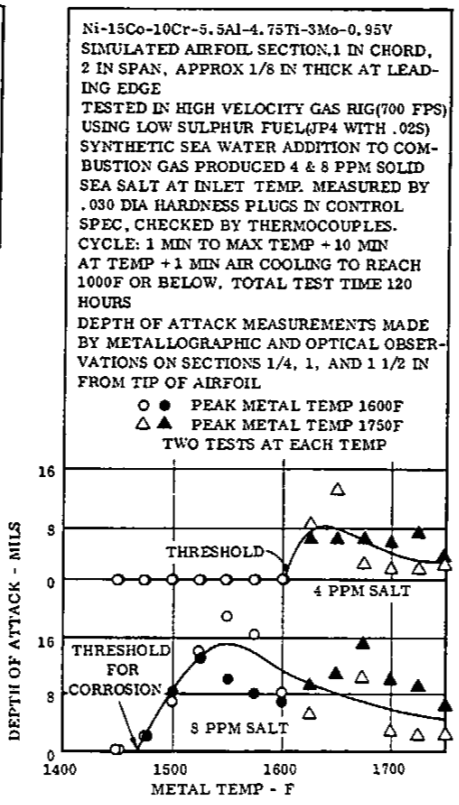

FIG. 2.03135 CORROSION (AS MEASURED BY DEPTH OF ATTACK) FOR ALLOY IN 700 FPS VELOCITY GAS JET USING LOW SULPHUR FUEL (JP4) WITH 4 PPM AND 8 PPM SEA SALT IN INLET AIR (27, pp. 1-6, 76, 88)

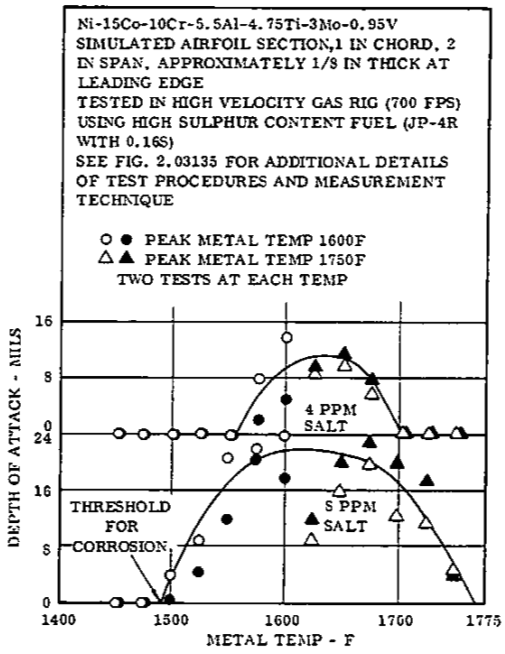

FIG. 2.03136 CORROSION (AS MEASURED BY DEPTH OF ATTACK) FOR ALLOY IN 700 FPS VELOCITY GAS JET USING HIGH SULPHUR FUEL (JP-4R) WITH 4 PPM AND 8PPM SEA SALT IN INLET AIR (27,pp.1-6,100,112)

Source	(46) pp 2, 3, 7, 16, 18
Alloy	Ni-15Co-10Cr-5.5Al-4.7Ti-3Mo-0.95
Condition	Coating Al-Cr-Mn: 1900F, 1.5 hr + 3 hr cool from pack + 1600F, 50 hr. Coating AEP No.32: RT application + 2080F, 2 hr + 1600F, 50 hr.
Specimen	Standard T56-A-9 solid turbine blades
Test Condition	Heat blades rotating at 1800 rpm in city gas-fired furnace to 1900F. Spray with aspirated solution of deionized water and 1.4 percent water soluble sodium sulfate. 1.5 min heat + 0.5 min spray, observe every 100 cycles. Remove when total corrosion area of .01 IN^2 (0.1 IN on each side)
	Av. No. cycles to hot corrosion failure (6 specimens) Coated with Al-Cr-Mn - 713 Coated with AEP No.32 - 541

TABLE 2.03137 HOT CORROSION RESISTANCE OF THINWALL ALLOY WITH TWO PROPRIETARY COATINGS IN 1900F CYCLIC TEMPERATURE TEST

	Ni
15	Co
10	Cr
5.5	Al
4.7	Ti
3	Mo
0.95	V

IN-100

Ni-15Co-10Cr-5.5Al-4.7Ti-3Mo-0.95V
1/4 DIA PINS, 1 1/8 IN LONG
AS CAST

TESTED IN A TURBINE SIMULATOR TYPICAL OF MARINE SERVICE USING COMPLEX TEMPERATURE AND VELOCITY PATTERN (SEE REF 29) TEMPERATURES INCLUDE PERIODS AT 1000, 1600, 1800 AND 2000 F VELOCITIES RANGE FROM 163 TO 275 FT PER SEC. SULFUR IN FUEL APPROX 400 PPM

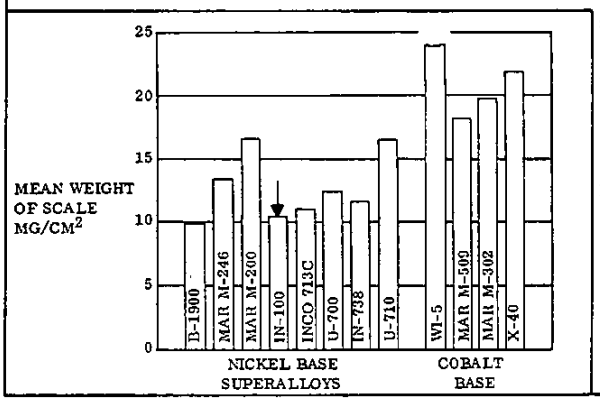

SURFACE SCALE REMOVED AFTER TEST. SCALE WEIGHTS CALCULATED FROM WEIGHT MEASUREMENTS BEFORE AND AFTER SCALE REMOVAL.

FIG. 2.03138 COMPARISON OF HOT-CORROSION BEHAVIOR IN A MARINE TURBINE SIMULATOR WITH OTHER NICKEL-AND COBALT-BASE ALLOYS (29, pp. 1-17)

Source	(23) p 9			
Alloy	Nominal: Ni-15Co-10Cr-5.5Al-4.7Ti-3Mo-0.95V For actual compositions see Fig. 3.024 (1)			
Condition	As Cast, Various Compositions and Grain Sizes Noted			
Test specimen & test condition	½ in. dia x 1¼ in. G.L. tested at RT(2)			
Level of electron vacancy concentration, $\bar{N}v$, and grain size	F_{tu} ksi	F_{ty} ksi	e(1¼ in.) Percent	RA Percent
Low $\bar{N}v$, Fine Grain Size	141.9	101.9	12	11
Medium $\bar{N}v$, Fine Grain Size	153.2	112.5	9.5	8.5
High $\bar{N}v$, Fine Grain Size	142.6	(3)96.7	9.0	9.0
Low $\bar{N}v$, Coarse Grain Size	142.2	102.6	9.0	9.0
Medium $\bar{N}v$, Coarse Grain Size	128.7	99.9	7.0	9.0
High $\bar{N}v$, Coarse Grain Size	128.3	106.2	3.5	6.0
Min required by AMS 5397	115.0	95.0	5.0	-

(1) Three alloys with minor variations in composition, achieved by additions of Al & Ti to same master heat. Several levels of electron vacancy concentration, $\bar{N}v$, designating tendency to form sigma precipitate, as defined in Figures.
(2) All values shown average of two tests except as designated.
(3) One test only.

TABLE 3.021 ROOM TEMPERATURE TENSILE PROPERTIES OF AS CAST ALLOY IN THREE LEVELS OF ELECTRON VACANCY CONCENTRATION, AND AT TWO LEVELS OF GRAIN SIZE

	Ni
15	Co
10	Cr
5.5	Al
4.7	Ti
3	Mo
0.95	V

IN-100

Source	(24) pp 3, 4, 6, 8								
Alloy	Ni-15Co-10Cr-5.5Al-4.7Ti-3Mo-0.95V (nominal), (3)								
Condition	Forged(1) and Heat Treated(2) as Indicated								
	Heat Treated			HT + 1350F, 1000 hr			HT + 1550F, 250 hr		
	Ti + Al Content (3)								
	Low	Med	High	Low	Med	High	Low	Med	High
F_{tu} - (ksi)	185.5	183.5	175	179	187	164	179.5	176.5	151.5
F_{ty} - (ksi)	139.5	140.5	141	144	142.5	140.5	124	123	120.5
e (1.25 IN) - percent	19	17.5	12.5	12.5	18	5	22.5	20.5	3.5
RA - percent	15	14.5	11.0	12.5	17.5	8	21	18.5	4.5

(1) 5 in dia casting extruded to 3.15dia @ 2050F. Flattened at 2050F to 1 3/4 thick pancake, then to 1 in thick pancake, then to 5/8 in thick pancake. Machined to 1/4 in dia specimens x 1.25 in gage length specimens.

(2) 2215F, 4 hrs + 2000F, 4 hrs + 1550F, 16 hrs + 1400F, 24 hrs.

(3) All three alloys from same master heat. Additions of Ti & Al to form alloys of varying degree of proneness to sigma phase precipitation, by controlling average electron vacancy concentration, $\bar{N}v$:

Low $\bar{N}v = 2.29$: Ni-13.73Co-10.26Cr-4.95Al-4.08Ti-3.66Mo-.96V
Med $\bar{N}v = 2.40$: Ni-13.41Co-10.15Cr-5.36Al-4.09Ti-3.58Mo-.96V
High $\bar{N}v = 2.59$: Ni-13.42Co-10.13Cr-5.46Al-4.63Ti-3.58Mo-1.01V

TABLE 3.022 MECHANICAL PROPERTIES AT ROOM TEMPERATURE OF FORGED ALLOY IN THREE CONDITIONS OF PRONENESS TO SIGMA PHASE PRECIPITATION. PROPERTIES SHOWN AFTER NORMAL HEAT TREATMENT AND AFTER HEAT TREATMENT FOLLOWED BY EXPOSURE TO ELEVATED TEMPERATURE.

Alloy	Ni-15Co-10Cr-5.5Al-4.7Ti-3Mo-0.95V				
Source	(24) p 8				
Condition	Forged + HT (2215F, 4 hrs + 2000F, 4 hrs + 1550F, 16 hrs + 1400F, 24 hrs + Exposure as indicated)				
Thermal Exposure	Al + Ti Content	F_{tu} (ksi)(4)	F_{ty} (ksi)(4)	e(1.25in)(4)	RA %(4)
As Heat Treated	Low(1)	185.5	139.5	19	15
	Medium(2)	183.5	140.5	17.5	14.5
	High(3)	175	141	12.5	11
Exposed 1000 hr @ 1350F	Low(1)	179	144	12.5	12.5
	Medium (2)	187	142.5	18	17.5
	High(3)	164	140.5	5	8
Exposed 250 hrs @ 1550F	Low(1)	179.5	124	22.5	21
	Medium(2)	176.5	123	20.5	18.5
	High(3)	151.5	120.5	3.5	4.5

(1) Sigma free
(2) Moderately sigma prone
(3) Very sigma prone, see Table 3.022 for actual compositions
(4) Average of 2 tests

TABLE 3.023 EFFECT OF THERMAL EXPOSURE SUBSEQUENT TO HEAT TREATMENT ON ROOM TEMPERATURE TENSILE PROPERTIES FOR FORGED ALLOY WITH THREE LEVELS OF Al + Ti CONTENT (ELECTRON VACANCY CONCENTRATION, $\bar{N}v$, RELATING TO PROPENSITY TOWARD SIGMA FORMATION)

	Ni
15	Co
10	Cr
5.5	Al
4.7	Ti
3	Mo
0.95	V

IN-100

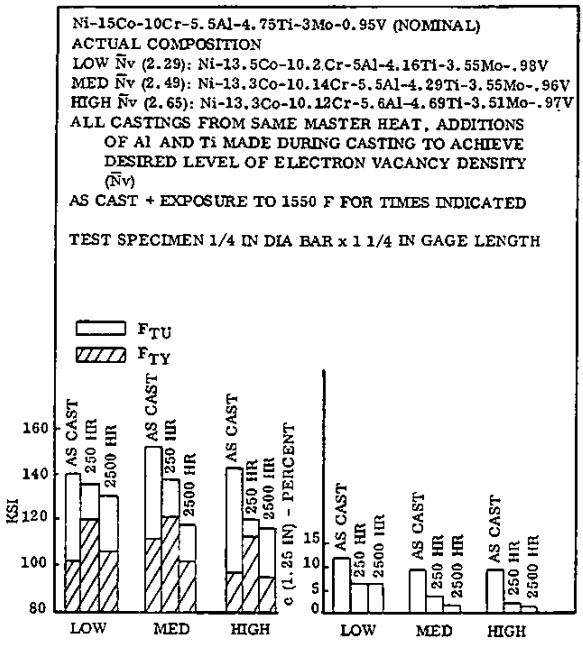

FIG. 3.024 EFFECT OF EXPOSURE AT 1550 F FOR 250 HR AND FOR 2500 HR ON ROOM TEMPERATURE TENSILE PROPERTIES OF ALLOY WITH Al-Ti COMPOSITION VARIED TO ACHIEVE THREE LEVELS OF ELECTRON VACANCY CONCENTRATION, $\bar{N}v$ (22, pp. 1-3, 10)

Source	(28) pp Z 4.5.7					
Alloy	Ni-15Co-10Cr-5.5Al-4.75Ti-3Mo-0.95V (Nominal, see actual below)					
Composition	As Cast: Ni-15.4Co-10.5Cr-5.55Al-4.72Ti-3.02Mo-1.05V FM Powder: Ni-13.97Co-9.54Cr-5.65Al-4.82Ti-3.70Mo-158 ppm O_2 HM Powder: Ni-15.4Co-10.5Cr-5.55Al-4.72Ti-3.02Mo-1.05V-53 ppm O_2 NM Powder: Ni-15.18Co-9.4Cr-5.81Al-4.82Ti-3.08Mo-.99V-79 ppm O_2					
Powder Size	FM Powder -250 to 44 microns HM Powder -707 to 74 microns NM Powder -500 to 44 microns					
Powder Consolidation	HIP FM Powder; Pressed at 2320F, 25,000 psi for 1 hr to strip 1 x 1.5 x 20 IN HIP HM Powder; Extruded to 3/4 IN Dia Rod, Pressed at 2300F, 15,000 psi 1 hr, Extruded at 2000F with 12:1 Reduction Direct Extruded FM & NM Powders; Extruded at 2150F with 20:1 Reduction to 1/2 IN Dia Bar x 7 Ft					
Specimen Size	3/8 IN Dia Threaded Tensile Bar					
	As Cast	HM Powder As HIP + Extr	FM As HIP	FM As Extr	NM As Extr	NM(1) As Grain Coarsened
F_{tu} ksi	143	-	163	244	238	188
F_{ty} ksi	136	-	137	175	171	137
e(1 IN)	4	-	8	20	21	14
RA, PERCENT	8	-	10	16	17	7
Hardness RC	32	41	49	43	43	33

(1) Exposed 2270F, 24 hours. Average grain size 100 μ m, some grains as large as 200 μ m

TABLE 3.025 ROOM TEMPERATURE TENSILE PROPERTIES AND HARDNESS OF POWDER METALLURGY PRODUCT PREPARED FROM POWDERS OF VARIOUS COMPOSITIONS AND GRAIN SIZE AND CONSOLIDATED BY SEVERAL PROCESSES

	Ni
15	Co
10	Cr
5.5	Al
4.7	Ti
3	Mo
0.95	V

IN-100

Alloy	Ni-15Co-10Cr-5.5Al-4.7Ti-3Mo-0.95V(1)			
Source	(19) pp 6, 7, 10			
Condition	Superplastically Forged(2), ASTM Grain Size 12-14			
Heat Treatment	Solutionized at 2050F, Stabilized at 1600F and 1800F + Precipitation Hardened at 1200F and 1400F			
	Disk 1 (499 - A2A)		Disk 2 (499 - A2B)	
	RT	1300F	RT	1300F
F_{tu} (ksi)	232.4	177.0	232.0	179.1
F_{ty} (ksi)	164.5	152.7	164.9	156.0
e percent	22.0	14.0	22.0	14.7
RA percent	22.2	22.3	21.5	16.4

(1) Typical composition: Ni-18.5Co-12.4Cr-4.98Al-4.32Ti-3.2Mo-0.78V-.07C-.06Zr-.02B

(2) By patented Gatorizing™ Process

TABLE 3.026 TENSILE PROPERTIES OF SUPERPLASTICALLY FORMED PANCAKE FORGING USED IN FATIGUE CRACK GROWTH STUDIES

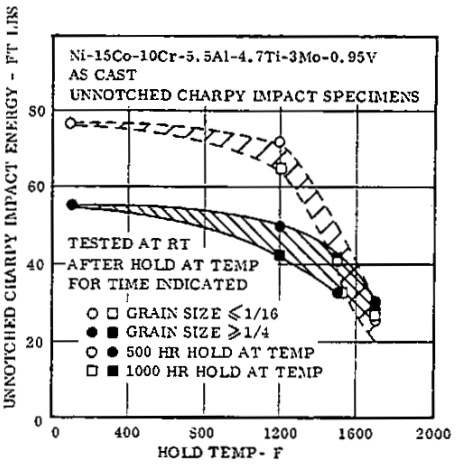

FIG. 3.0291 UNNOTCHED CHARPY IMPACT STRENGTH AT ROOM TEMPERATURE AFTER HOLD FOR 500 OR 1000 HR AT ELEVATED TEMPERATURE (4, p. 11)

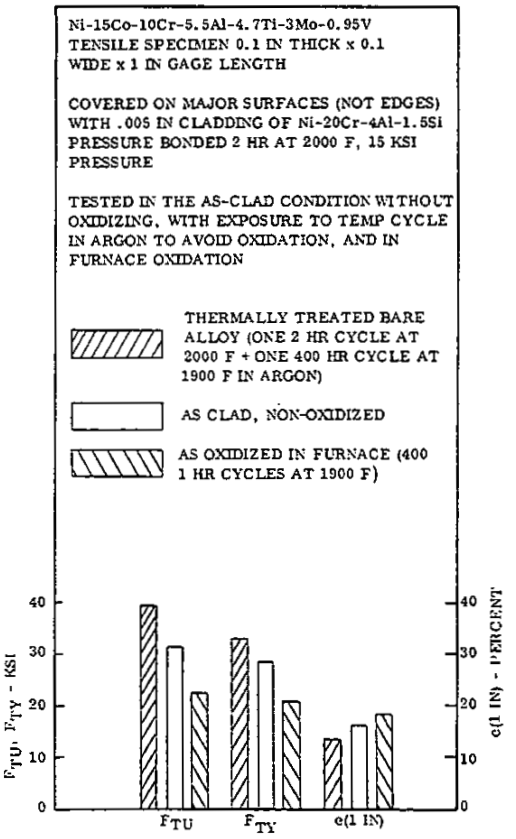

FIG. 3.027 COMPARISON OF TENSILE PROPERTIES OF ALLOY WITH Ni-20Cr-4Al-1.2Si CLADDING ALLOY BEFORE AND AFTER OXIDATION (42, pp. 2, 3, 20, 29)

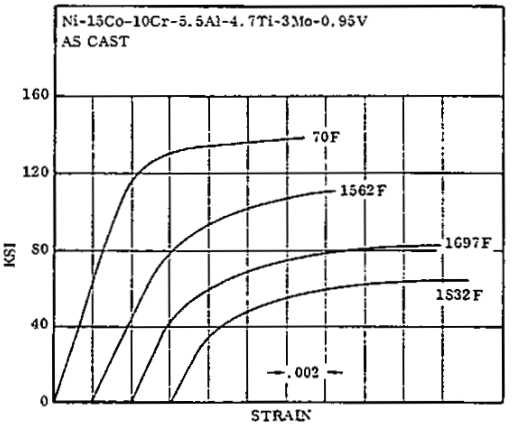

FIG. 3.03111 STRESS-STRAIN CURVES FOR AS-CAST ALLOY AT ROOM AND ELEVATED TEMPERATURES (16 pp. 7, 10, 115 REVISED BY PERSONAL COMMUNICATION, METCUT TO MPDC 6-13-78)

	Ni
15	Co
10	Cr
5.5	Al
4.7	Ti
3	Mo
0.95	V

IN-100

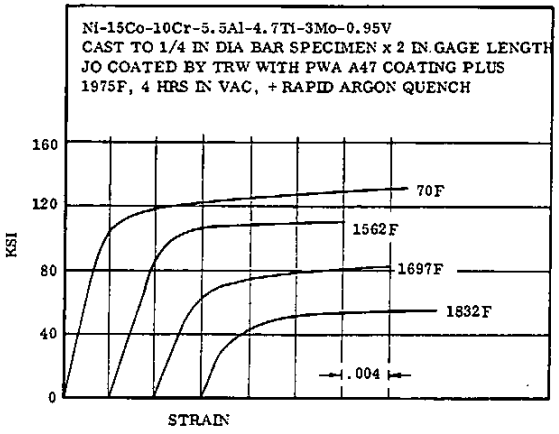

FIG. 3.03112 STRESS-STRAIN CURVES FOR JO COATED ALLOY AT ROOM AND ELEVATED TEMPERATURES (16, pp. 7, 10, 123)

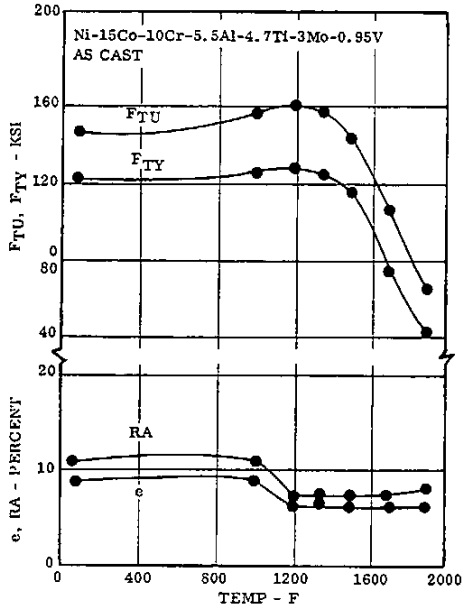

FIG. 3.03121 EFFECT OF TEST TEMPERATURE ON MECHANICAL PROPERTIES AS CITED BY ALLOY DEVELOPER (4, p. 5)

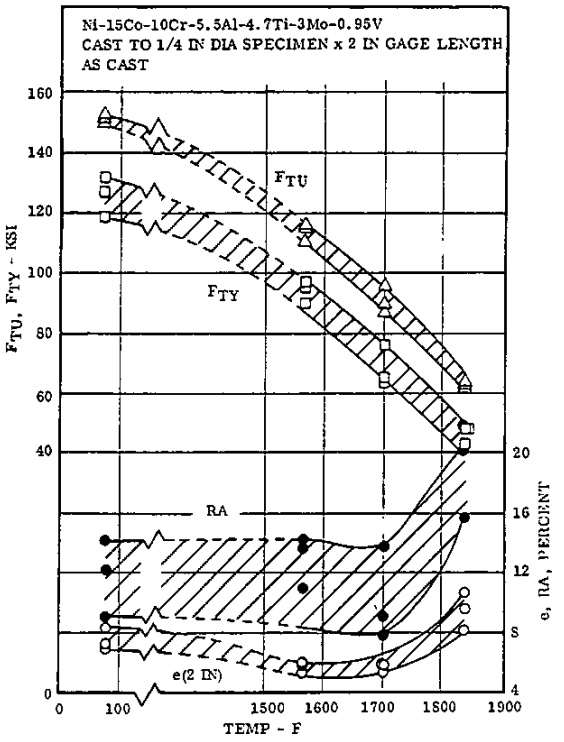

FIG. 3.03122 TENSILE PROPERTIES OF AS CAST BAR AT ROOM AND ELEVATED TEMPERATURES (16, pp. 13, 112, 114)

	Ni
15	Co
10	Cr
5.5	Al
4.7	Ti
3	Mo
0.95	V

IN-100

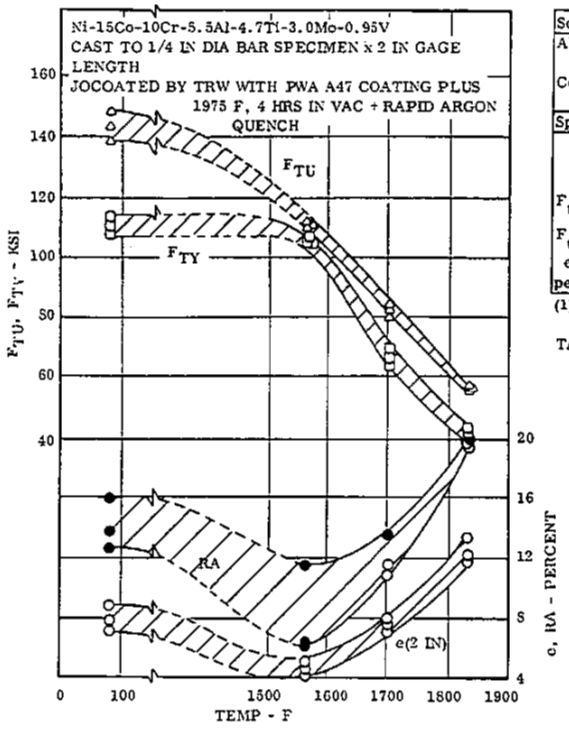

FIG. 3.03123 TENSILE PROPERTIES OF JOCOATED BAR AT ROOM AND ELEVATED TEMPERATURES (16 pp.13,121,122)

Source	(46) pp 2, 3, 7, 68, 69					
Alloy	Ni-15Co-10Cr-5.5Al-4.7Ti-3Mo-0.95V					
Condition	As Cast + Coated with Two Proprietary Coatings: Al-Cr-Mn or AEP No. 32 See Fig. 3.0515 for Coating Conditions					
Specimen Type	Simulated Airfoil, See Fig. 3.0515					
	AEP No. 32 Coating			Al-Cr-Mn Coating		
	RT	1400F	1800F	RT	1400F	1800F
	(1)			(1)		
F_{tu} (ksi)	114	125.8	67.8	101.0	110.3	68.4
F_{ty} (ksi)	108.9	101.9	55.3	96.7	108.4	49.9
e (in) percent	3.7	3.7	3.2	1.7	-	5.3

(1) Average of two tests

TABLE 3.03141 TENSILE PROPERTIES AT ROOM AND ELEVATED TEMPERATURES OF THINWALL ALLOY COATED WITH TWO PROPRIETARY COATINGS

Source	(3S) p 95			
Alloy	Ni-15Co-10Cr-5.5Al-4.7Ti-3Mo-0.95V			
Condition	As Cast	2150F 2 hr Rapid Air Cool	2050F 24 hr Rapid Air Cool	1900F 24 hr Rapid Air Cool
(1) Tested at 1300F				
F_{tu} (ksi)	156	138	129.3	135.7
F_{ty} (ksi)	124.3	119	114.7	119.3
e percent	8.8	6.0	4.5	3.7
RA percent	14.3	7.0	5.1	5.8

(1) All values average of 3 tests.

TABLE 3.03131 EFFECT OF SEVERAL SOLUTION HEAT TREATMENTS ON THE TENSILE PROPERTIES AT 1300F

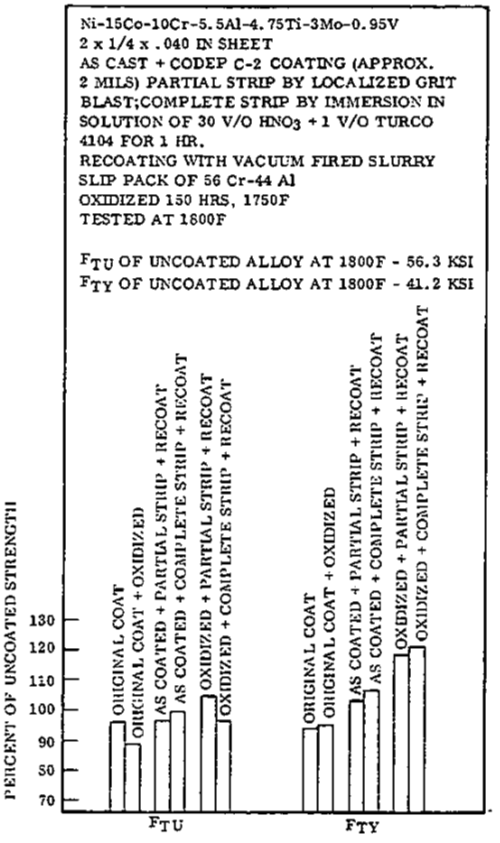

FIG. 3.03142 EFFECT OF COATING, HIGH TEMPERATURE EXPOSURE, AND SEVERAL REPAIR PROCESSES ON TENSILE AND YIELD STRENGTH AT 1800F COMPARED TO AS CAST UNCOATED BASE MATERIAL (25, pp.36,115,116)

	Ni
15	Co
10	Cr
5.5	Al
4.7	Ti
3	Mo
0.95	V

IN-100

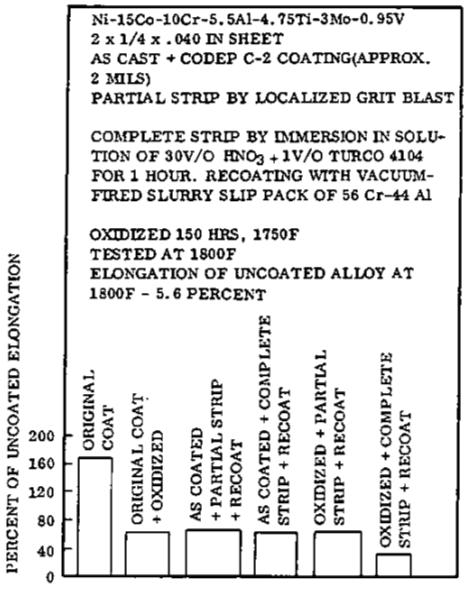

FIG. 3.03143 EFFECT OF COATING, HIGH TEMPERATURE EXPOSURE, AND SEVERAL REPAIR PROCESSES ON ELONGATION AT 1800F COMPARED TO AS CAST UNCOATED BASE MATERIAL(25, pp.36,115,118)

Source	(39) p 339		
Alloy	Ni-15Co-10Cr-5.5Al-4.7Ti-3Mo-0.95V		
Condition	Powder Metallurgy product, deformed and heat treated as shown		
	Extruded 10.6 to 1 at 2000F, Rolled 3 to 1 at 2000F	Extruded 10.6 to 1 at 2000F, Rolled 3 to 1 at 2000F + 2150F, 4 hr, oil quench + 1200F, 22 hr, air cool + 1400F, 8 hr air cool	Extruded 10.6 to 1 at 2000F + Superplastically deformed 100% in tension at 2000F + 2275F, 56 hr, air cool
RT			
F_{tu} (ksi)	310	254.6	170.7
F_{ty} (ksi)	295.8	177.8	129.4
e percent	12	27	10
RA percent	8	25	15
1200F			
F_{tu} (ksi)	257.4	204.8	163.6
F_{ty} (ksi)	241.8	180.6	125.2
e percent	10	15	8
RA percent	16	12	10

TABLE 3.03151 EFFECT OF REDUCTION PRACTICE AND HEAT TREATMENT ON THE TENSILE PROPERTIES AT RT AND 1200F OF POWDER METALLURGY ALLOY

	Ni
15	Co
10	Cr
5.5	Al
4.7	Ti
3	Mo
0.95	V

IN-100

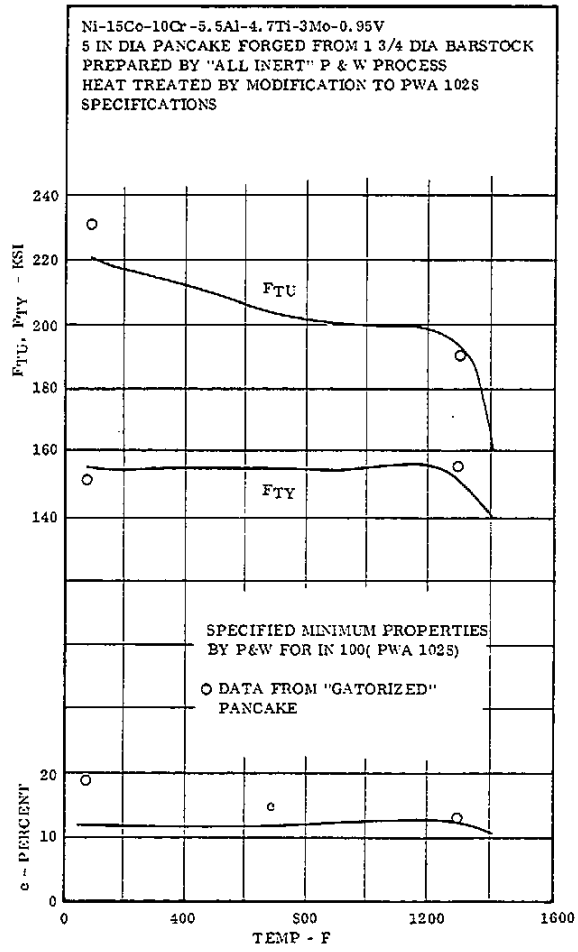

FIG. 3.03152 TENSILE PROPERTIES OF SPECIMEN FROM POWDER ALLOY PANCAKE AT RT AND 1300F, WITH COMPARISON TO PRATT & WHITNEY SPECIFICATIONS FOR ALLOY (35, FIGS. 1,2)

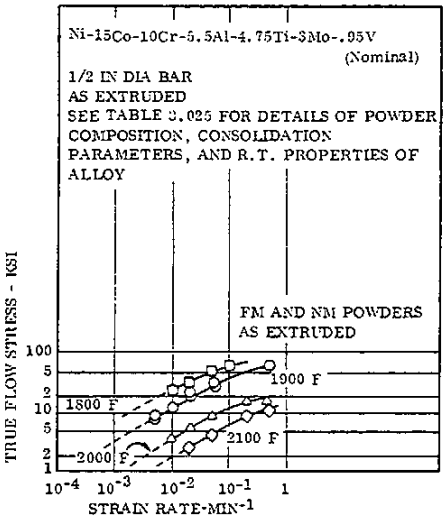

FIG. 3.03153 FLOW CHARACTERISTICS IN THE RANGE AT LOW STRAIN RATES AND TEMPERATURES WHERE SUPERPLASTICITY CAN BE ACHIEVED (28 p.Z-24)

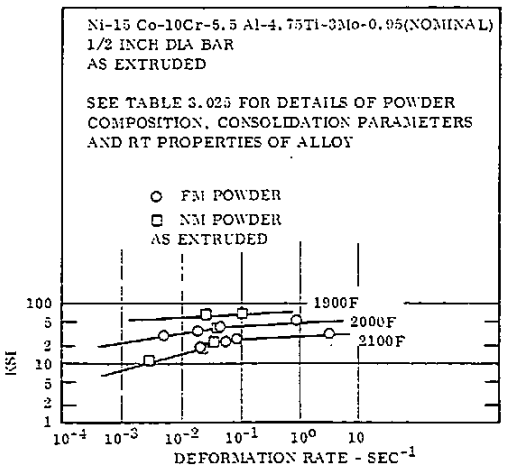

FIG. 3.03154 RELATION BETWEEN STRESS AND HIGH DEFORMATION RATE AT 1900 TO 2100F FOR ALLOY EXTRUDED DIRECTLY FROM POWDER. (28, p.Z-22)

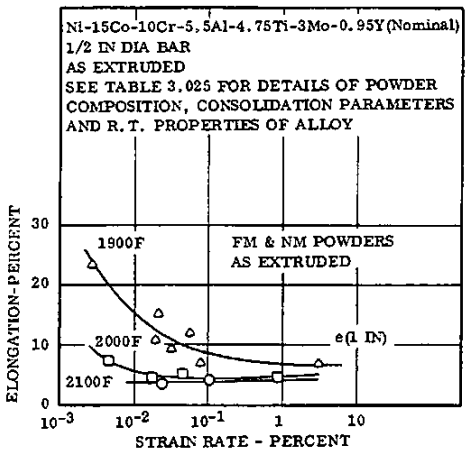

FIG. 3.3155 HIGH STRAIN RATE EFFECT ON ELONGATION AT FRACTURE AT 1900 TO 2100F FOR ALLOY DIRECTLY EXTRUDED FROM POWDER (28, p. Z-22)

Source	(26) p VIII - 10			
Alloy	Ni-15Co-10Cr-5.5Al-4.75Ti-3Mo-0.95V			
Condition	As Cast + 1600F, 4 hrs, AC			
Test Condition	5000 psig			
	Helium		Hydrogen	
	RT	1250F	RT	1250F
F_{tu} (ksi)	118.5	103.2	107.5, 87.5	99.0, 114.0
F_{ty} (ksi)	99.8	101.8	106.5, 87.5	99.0, 106.1
e(1 in), percent	9.5	2.0	3.0, 2.5	1.5, 2.0
RA percent	14.7	6.7	3.3, 5.5	2.0, 7.1

TABLE 3.03171 TENSILE PROPERTIES AT RT AND 1250F IN 5000 psig HELIUM AND HYDROGEN

	Ni
15	Co
10	Cr
5.5	Al
4.7	Ti
3	Mo
0.95	V

IN-100

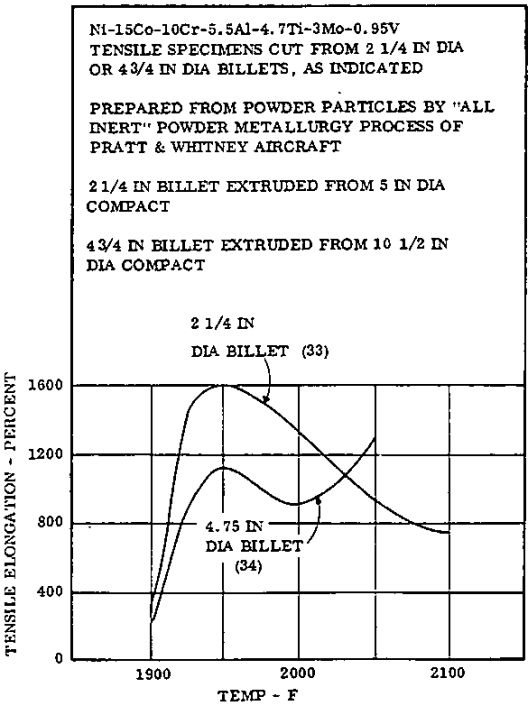

FIG. 3.03156 SUPERPLASTICITY EXHIBITED BY POWDER METALLURGY ALLOY (33, FIG. 3), (34, FIG. 3)

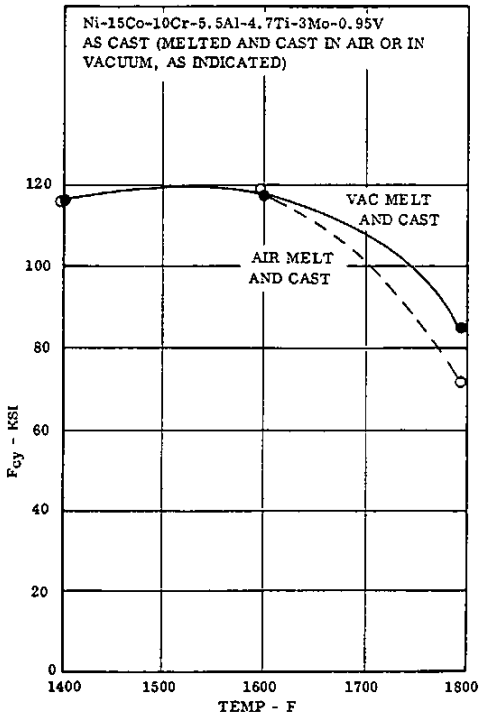

FIG. 3.0321 EFFECT OF TEST TEMPERATURE ON COMPRESSION YIELD STRENGTH FOR AIR MELTED AND CAST ALLOY AND FOR VACUUM MELTED AND CAST ALLOY (32, FIG 4, 5)

	Ni
15	Co
10	Cr
5.5	Al
4.7	Ti
3	Mo
0.95	V

IN-100

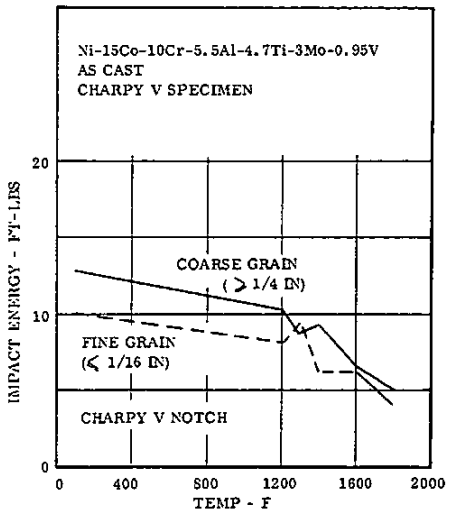

FIG. 3.0331 EFFECT OF TEMPERATURE ON CHARPY V IMPACT ENERGY (4, p.12)

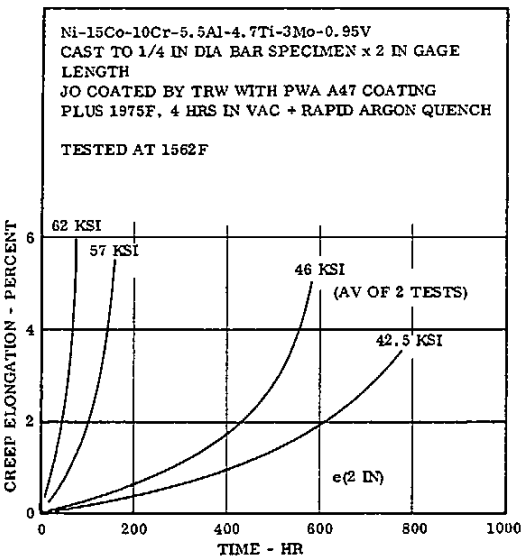

FIG. 3.0412 CREEP CURVES FOR JO COATED ALLOY AT 1562F. (16, pp. 13, 121, 124, 125,)

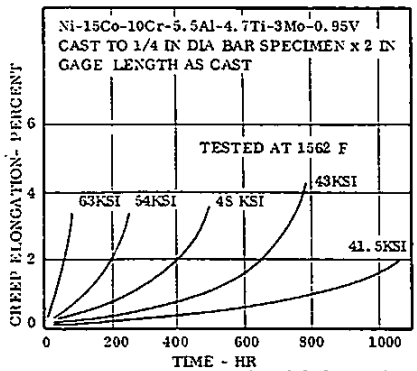

FIG. 3.0411 CREEP CURVES OF AS CAST ALLOY AT 1562F (16, pp.13, 112, 114, 117)

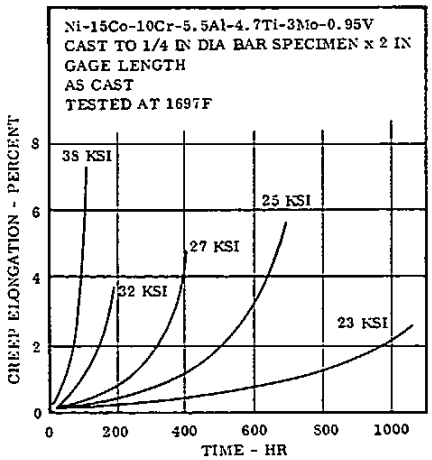

FIG. 3.0413 CREEP CURVES OF AS CAST ALLOY AT 1697F (16, pp. 13, 112, 114, 118)

	Ni
15	Co
10	Cr
5.5	Al
4.7	Ti
3	Mo
0.95	V

IN-100

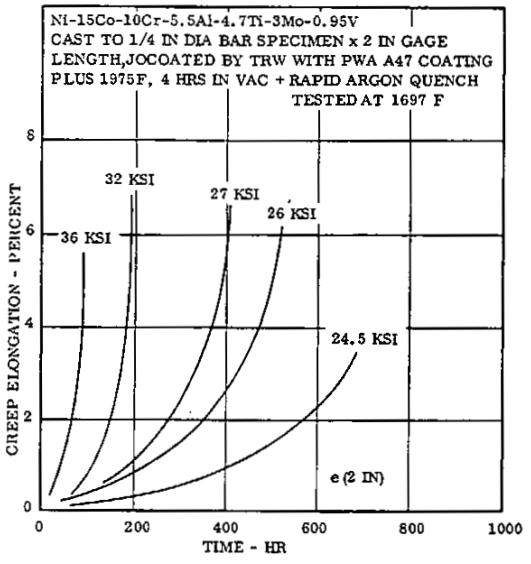

FIG. 3.0414 CREEP CURVES FOR JOCOATED ALLOY AT 1697F
(16 pp.13,121,124,126)

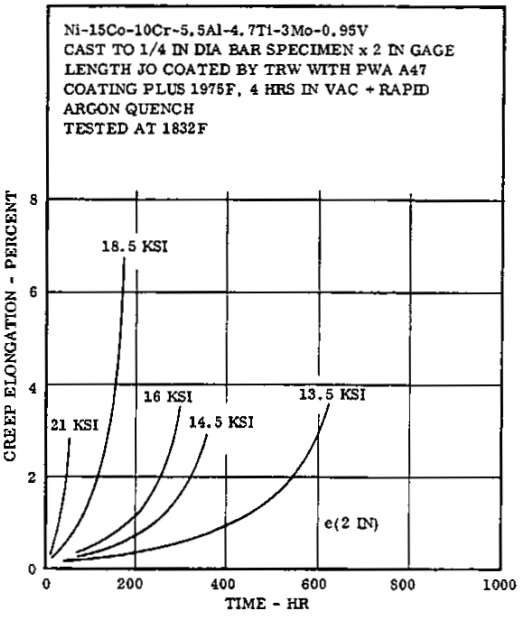

FIG. 3.0416 CREEP CURVES FOR JO COATED ALLOY AT 1832F
(16,pp. 13, 121, 124,127)

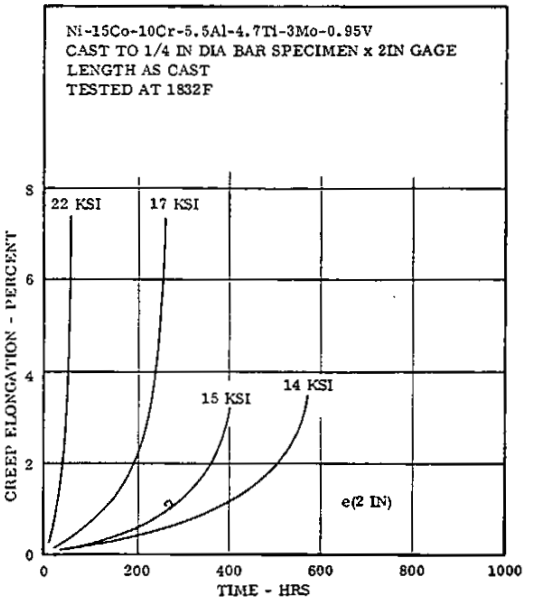

FIG. 3.0415 CREEP CURVES OF AS CAST ALLOY AT 1832F.
(16,pp. 13, 112,114,119)

	Ni
15	Co
10	Cr
5.5	Al
4.7	Ti
3	Mo
0.95	V

IN-100

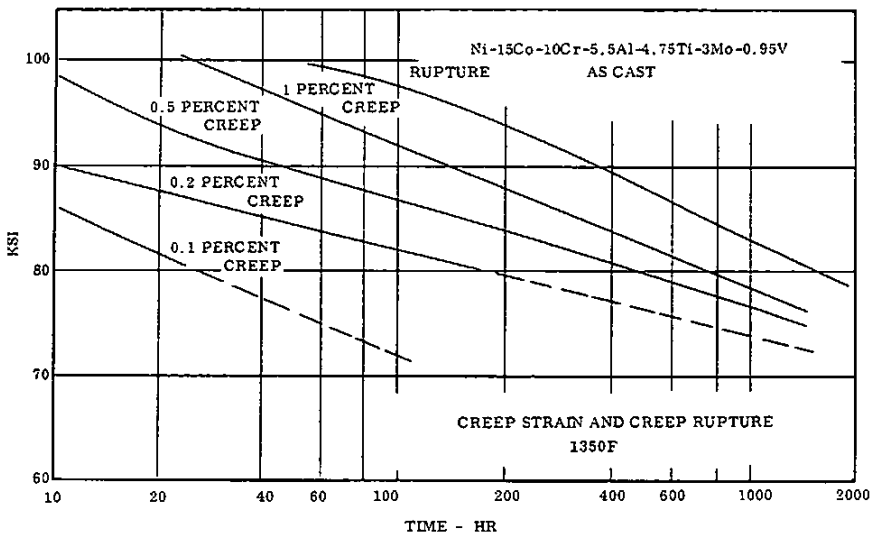

FIG. 3.0417 ALLOY DEVELOPER'S SUGGESTED DESIGN CURVES FOR CREEP STRAIN AND CREEP RUPTURE AT 1350F (4)

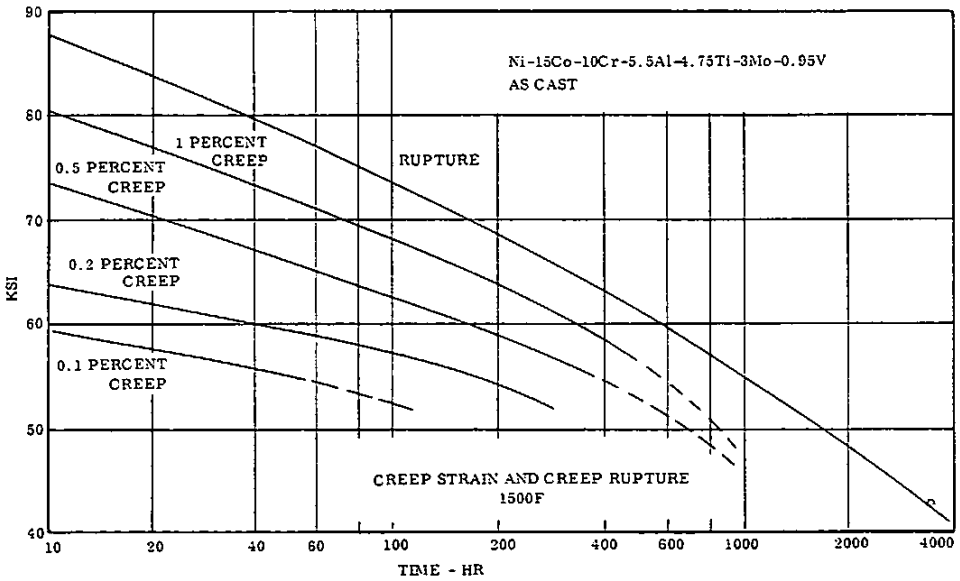

FIG. 3.0418 ALLOY DEVELOPER'S SUGGESTED DESIGN CURVES FOR CREEP STRAIN AND CREEP RUPTURE AT 1500F (4)

	Ni
15	Co
10	Cr
5.5	Al
4.7	Ti
3	Mo
0.95	V

IN-100

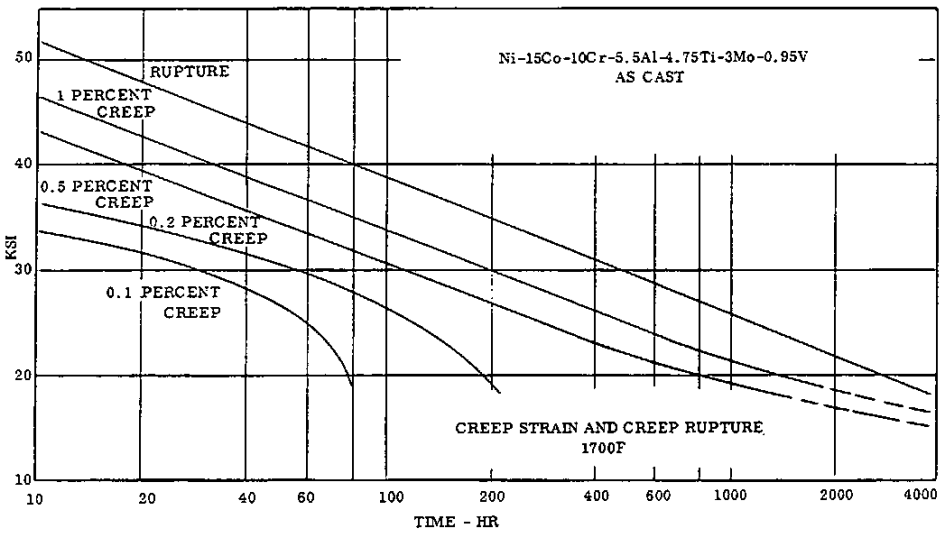

FIG. 3.0419 ALLOY DEVELOPER'S SUGGESTED DESIGN CURVES FOR CREEP STRAIN AND CREEP RUPTURE AT 1700F (4)

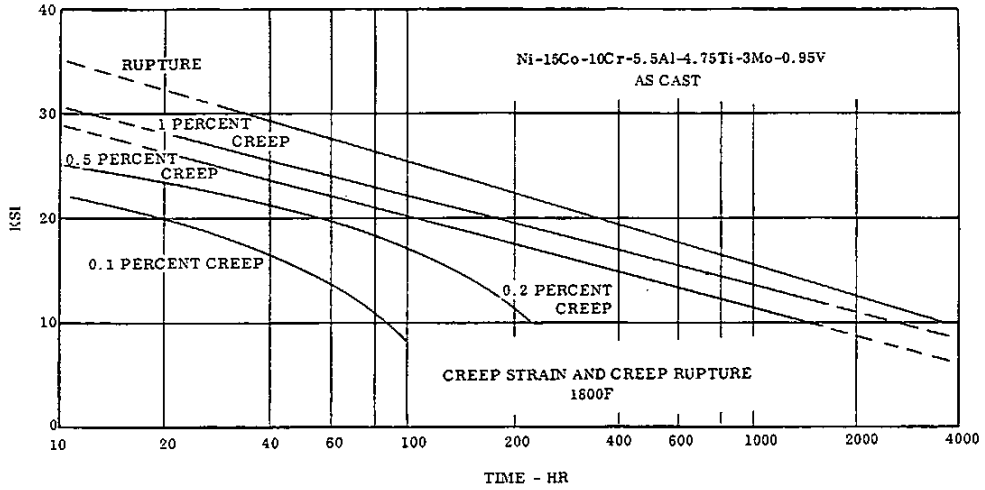

FIG. 3.04110 ALLOY DEVELOPER'S SUGGESTED DESIGN CURVES FOR CREEP STRAIN AND CREEP RUPTURE AT 1800F (4)

	Ni
15	Co
10	Cr
5.5	Al
4.7	Ti
3	Mo
0.95	V

IN-100

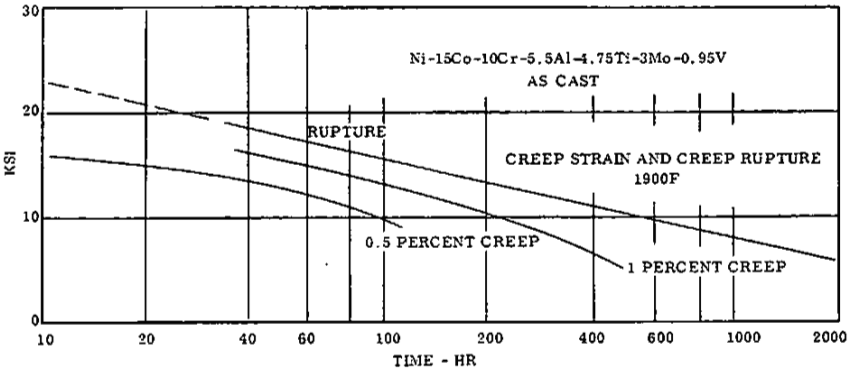

FIG. 3.04111 ALLOY DEVELOPER'S SUGGESTED DESIGN CURVES FOR CREEP STRAIN AND CREEP RUPTURE AT 1900F (4)

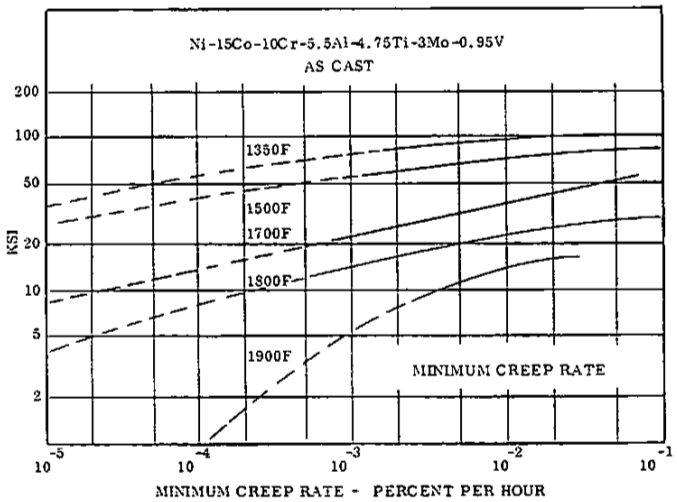

FIG. 3.04112 MINIMUM CREEP RATE CURVES FOR TEMPERATURES FROM 1350 TO 1900F (5)

Alloy	Ni-15Co-10Cr-5.5Al-4.7Ti-3Mo-0.95V[a]			
Source	(19) pp 6, 7, 10			
Condition	Superplastically Forged [b] ASTM Grain Size 12-14			
Heat Treatment:	Solutionized at 2050F, Stabilized at 1600F and 1800F, + Precipitation Hardened at 1200F and 1400F			
	Disk 1 (499-A2A)		Disk 2 (499-A2B)	
	1300F 80 ksi	1350F 95 ksi	1300F 80 ksi	1350F 95 ksi
Time to 0.1 Percent Creep, hr	-	-	114.5	-
Time to 0.2 Percent Creep, hr	175.5	-	142.5	-
Time to Rupture, hr	> 233.2	28.0	>143.2	18.9
e at Fracture, Percent	-	10.6	-	7.6
RA at Fracture, Percent	-	15.9	-	12.2

(a) Typical composition: Ni-18.5Co-12.4Cr-4.98Al-4.32Ti-3.2Mo-0.78V-.07C-.06Zr-.02B

(b) By patented GATORIZING PROCESS

TABLE 3.0421 CREEP AND CREEP RUPTURE PROPERTIES OF SUPERPLASTICALLY FORMED PANCAKE FORGING USED IN FATIGUE CRACK GROWTH STUDIES

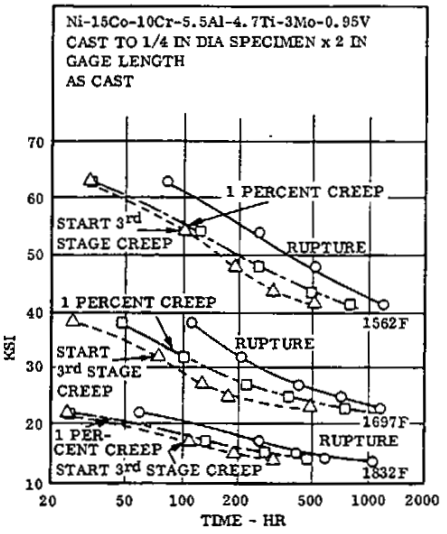

	Ni
15	Co
10	Cr
5.5	Al
4.7	Ti
3	Mo
0.95	V

IN-100

FIG. 3.0431 RELATION AMONG START OF THIRD STAGE CREEP, TIME TO 1 PERCENT CREEP, AND RUPTURE TIME FOR AS CAST ALLOY (16,p.116)

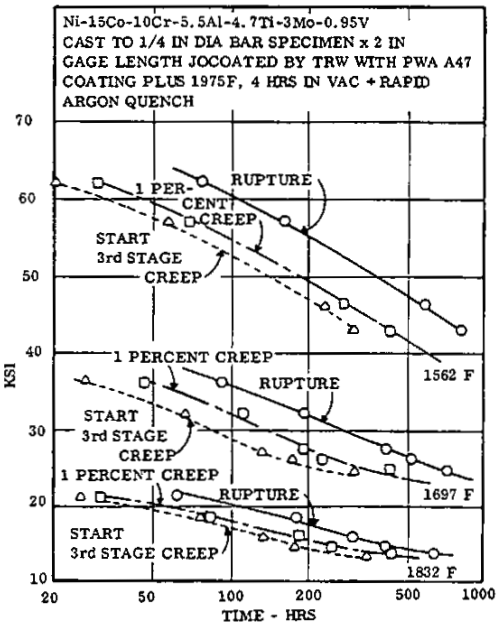

FIG. 3.0432 RELATION AMONG TIME OF THIRD STAGE CREEP, TIME TO 1 PERCENT CREEP AND RUPTURE TIME FOR JOCOATED ALLOY (16,p.124)

	Ni
15	Co
10	Cr
5.5	Al
4.7	Ti
3	Mo
0.95	V

IN-100

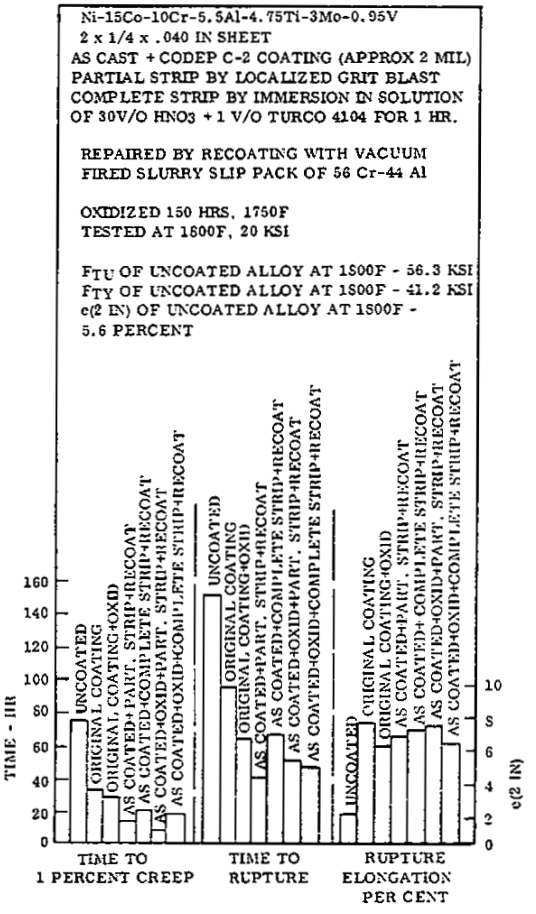

FIG. 3.0441 CREEP AND RUPTURE PROPERTIES OF ALLOY AFTER REPAIR OF OXIDATION DAMAGE AND MECHANICAL DAMAGE EFFECTS (25, pp. 36, 130)

	Ni
15	Co
10	Cr
5.5	Al
4.7	Ti
3	Mo
0.95	V

IN-100

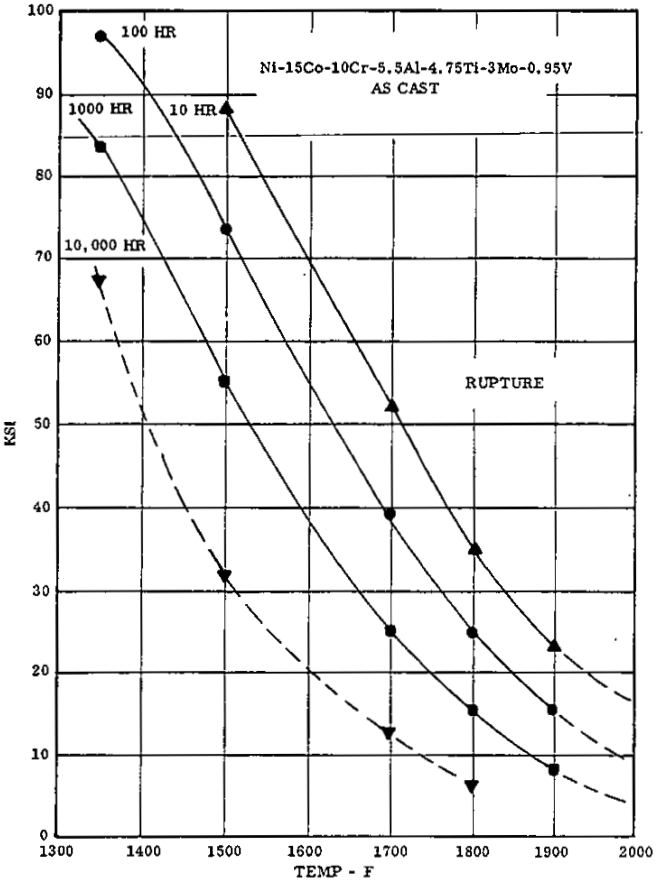

FIG. 3.0451 TYPICAL CREEP RUPTURE PROPERTIES IN LIFE RANGE FROM 10 TO 10,000 HRS AT TEMPERATURES FROM 1300 TO 2000 F (4)

	Ni
15	Co
10	Cr
5.5	Al
4.7	Ti
3	Mo
0.95	V

IN-100

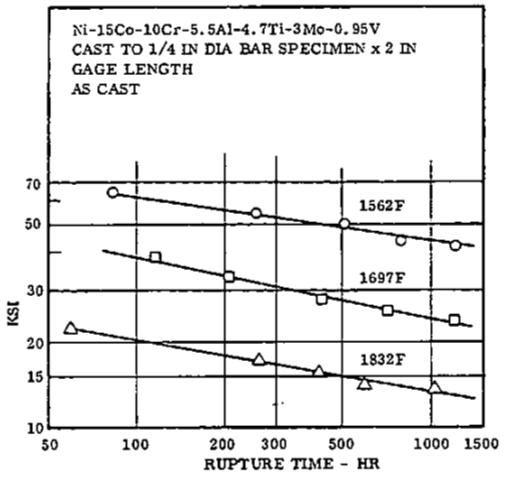

FIG. 3.0452 CREEP RUPTURE CURVES FOR AS CAST ALLOY AT 1562F, 1697F, AND 1832F (16, pp.13, 116 120)

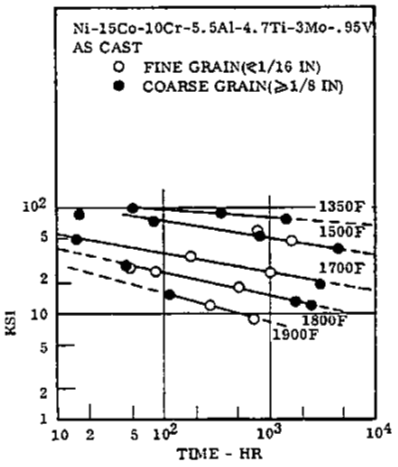

FIG. 3.0453 CREEP RUPTURE DATA FOR AS CAST ALLOY AS DETERMINED BY DEVELOPER (4, p.6)

Source	(38) p 95			
Alloy	Ni-15Co-10Cr-5.5Al-4.7Ti-3Mo-0.95V			
Condition	As Cast	2150F, 2 Hr Rapid Air Cool	1900F, 24 Hr Rapid Air Cool	2050F, 24 Hr Rapid Air Cool
Tested at[1] 1800F, 29 ksi				
Life, hrs	31.8	32	25.3	25.9
e, percent	6.9	6.8	8.5	7.13
RA, percent	8.8	10.7	11.5	9.3

(1) All values average of 3 tests

TABLE 3.0461 EFFECT OF SEVERAL SOLUTION HEAT TREATMENTS ON THE CREEP-RUPTURE LIFE AT 1800F, 29 KSI

Alloy	Ni-15Co-10Cr-5.5Al-4.7Ti-3Mo-0.95V							
Source	Haynes (10 p 13)							
Condition	As Cast (Bare or Coated As Indicated)							
	34 ksi 1700F		22 ksi 1800F		17 ksi 1850F		13 ksi 1900F	
	Bare	Coated[a]	Bare	Coated[a]	Bare	Coated[a]	Bare	Coated[a]
Creep Rupture Life, Hours	68.4	53.7	122	129	224	170	180	210
e(2in), percent	5.2	5.8	8.4	6.2	6.5	10	5.1	9.0

(a) Haynes C-9 coating

TABLE 3.0471 EFFECT OF COATING ON CREEP RUPTURE PROPERTIES AT STRESSES AND TEMPERATURES YIELDING CREEP RUPTURE LIVES IN THE RANGE OF 50 TO 200 HOURS

	Ni
15	Co
10	Cr
5.5	Al
4.7	Ti
3	Mo
0.95	V

IN-100

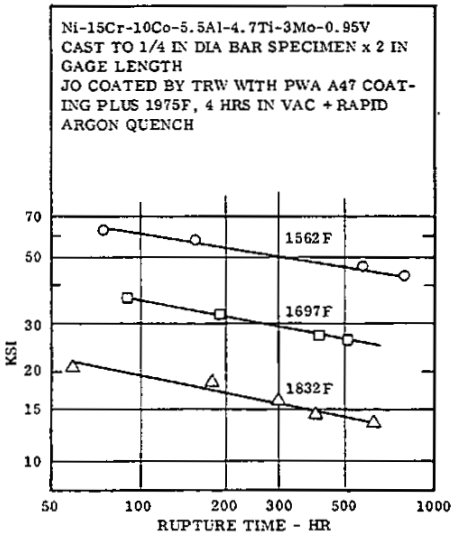

FIG. 3.0472 CREEP RUPTURE CURVES FOR JO COATED ALLOY AT 1562F, 1697F, AND 1832F (16, pp. 13, 121, 128)

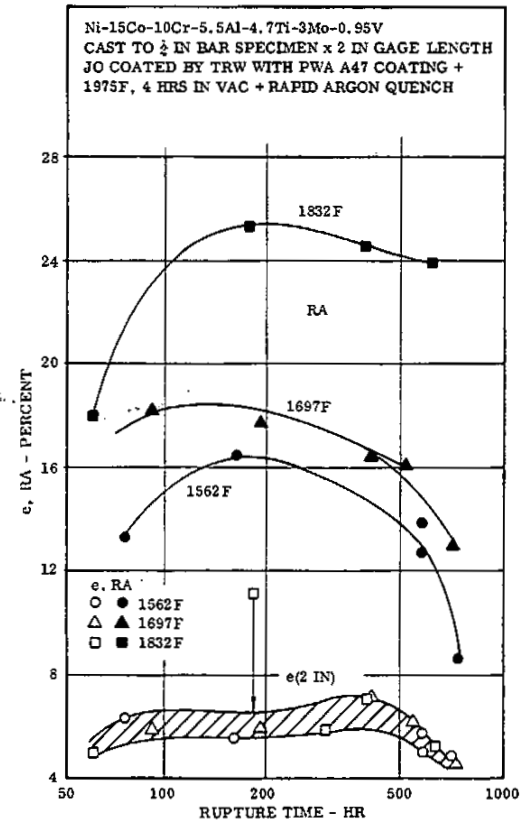

FIG. 3.0473 CORRELATION BETWEEN DUCTILITY AND RUPTURE TIME AT 1562F, 1697F, AND 1832F FOR JO COATED ALLOY (16, pp. 13, 124)

	Ni
15	Co
10	Cr
5.5	Al
4.7	Ti
3	Mo
0.95	V

IN-100

Source	(46) pp 2, 3, 7, 64				
Alloy	Ni-15Co-10Cr-5.5Al-4.7Ti-3Mo-0.95V				
Condition	As Cast + Coated With Two Proprietary Coatings Al-Cr-Mn and AEP No. 32 (see Fig. 3.0515)				
Specimen Type	Simulated Airfoil, (see Fig. 3.0515)				
	AEP No. 32 Coating		Al-Cr-Mn Coating		
	1800F, 20 ksi	1450F, 65 ksi	1800F, 20 ksi	1450F, 65 ksi	1450F, 50 ksi
Creep Rupture Life, Hrs. Spec No.					
1	61.6	166.9	27.9	27.9	401.7
2	53.4	141.3	19.6		401.6
3	21.0	31.5	7.1		
4	17.9				
5	13.7				
6	10.0				
Average (1)	23.5	90.6	15.8	27.9	401.7
e(1in) Percent Spec No.					
1	3.8	5.2	3.6	5.9	3.0
2	3.2	3.3	4.2		3.7
3	1.2	1.3	7.1		
4	3.3				
5	3.2				
6	3.0				
Average	3.0	3.3	5.0	5.9	3.4

(1) Based on Log_{10} of Life (Averages of Log Life)

TABLE 3.0474 CREEP RUPTURE LIVES AND ELONGATIONS AT 1450F AND 1800F FOR THINWALL ALLOY COATED WITH TWO PROPRIETARY COATINGS

Alloy	Ni-15Co-10Cr-5.5Al-4.7Ti-3Mo-0.95V	
Source	General Electric, (12)	
Condition	As Cast	
	1500F	
	40 ksi	50 ksi
Life with sigma formation, hrs.	967	469
Estimated life, no sigma formation, hrs.	8000	2000

TABLE 3.0481 BENEFICIAL EFFECTS ON CREEP RUPTURE BEHAVIOR ACHIEVED BY AVOIDING SIGMA PHASE PRECIPITATION

Source	(24) pp 3, 4, 6, 14								
Alloy	Ni-15Co-10Cr-5.5Al-4.7Ti-3Mo-0.95V (Nominal)(1)								
Condition	Forged and Heat Treated (1)								
	Low $\bar{N}v$ = 2.29			Medium $\bar{N}v$ = 2.40			High $\bar{N}v$ = 2.59		
Test Temp & Stress (2)	Time to Rupture Hrs	e(1.25IN) Percent	RA Percent	Time to Rupture Hrs	e(1.25IN) Percent	RA Percent	Time to Rupture Hrs	e(1.25IN) Percent	RA Percent
1200F, 150 ksi	27	15	13	-	-	-	-	-	-
1200F, 95 ksi	14,005	2	2.5	12,027	3	2.5	3,303	1	0
1300F, 95 ksi	705	2.5	1.5	877.5	5	5	639	5.5	7
1425F, 95 ksi	19.1	3.5	2.5	30.1	7	6	19.4	9.5	11
1550F, 40 ksi	1,337	5	4	1,307	5.5	5	310.6	11	12.5
1625F, 40 ksi	203	-	4	234	6	4.5	145	8	6.5
1800F, 20 ksi	129	-	10.5	122	5	5	122	9	9.5

(1) See Table 3.022 for actual compositions, forging parameters and heat treatment
(2) Average of 2 tests in most cases

TABLE 3.0482 CREEP RUPTURE PROPERTIES OF FORGED ALLOY IN THREE CONDITIONS OF PRONENESS TO SIGMA PHASE PRECIPITATION

	Ni
15	Co
10	Cr
5.5	Al
4.7	Ti
3	Mo
0.95	V

IN-100

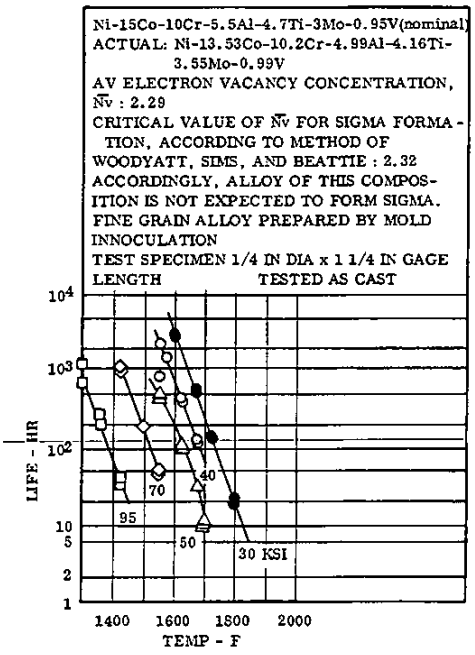

FIG. 3.0483 CREEP RUPTURE CURVES FOR FINE GRAIN ALLOY OF COMPOSITION SUFFICIENTLY LOW IN Al AND Ti TO AVOID SIGMA PRECIPITATION (23, pp. 3, 5, 12)

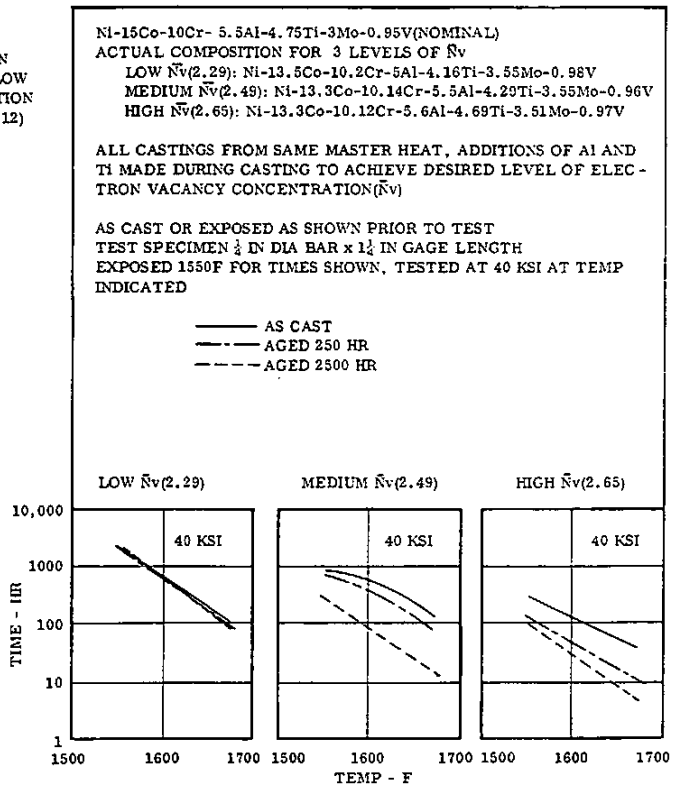

FIG. 3.0484 CREEP RUPTURE CURVES AT 40 KSI FOR ALLOY IN THREE LEVELS OF ELECTRON VACANCY CONCENTRATION ACHIEVED BY ADDITIONS OF Al-Ti TO A SINGLE HEAT. TESTED IN AS CAST CONDITION OR AFTER EXPOSURE AT 1550F FOR 250 AND 2500 HRS. (22, pp. 1-3, 15)

	Ni
15	Co
10	Cr
5.5	Al
4.7	Ti
3	Mo
0.95	V

IN-100

Ni-15Co-10Cr-5.5Al-4.7Ti-3Mo-0.95V (NOMINAL)
SEE FIGURE 3.0484 FOR ACTUAL COMPOSITIONS OF ALLOYS OF LOW, MEDIUM, AND HIGH ELECTRON VACANCY CONCENTRATION, ACHIEVED BY VARIATIONS OF Al AND Ti.

SEE ALSO TABLE 3.021 FOR OTHER DETAILS OF ALLOY PREPARATION, AND SPECIMEN DIMENSIONS. RESULTS SHOWN HERE REFER TO FINE GRAIN ALLOY STRUCTURES.

DATA POINTS SHOWN ARE FOR ALLOYS OF MEDIUM AND HIGH ELECTRON VACANCY CONCENTRATION. DOTTED CURVES ARE FOR REFERENCE FROM THE LOW $\bar{N}v$ ALLOY WHEREIN NO SIGMA FORMS IN THE TIMES SHOWN. ACTUAL DATA ARE SHOWN IN FIGURE 3.0483

CURVES FOR ONSET OF SIGMA PRECIPITATION ARE BASED ON FIG 2.0123 BUT CORRECTED BY ESTIMATION TO ACCOUNT FOR EFFECT OF STRESS

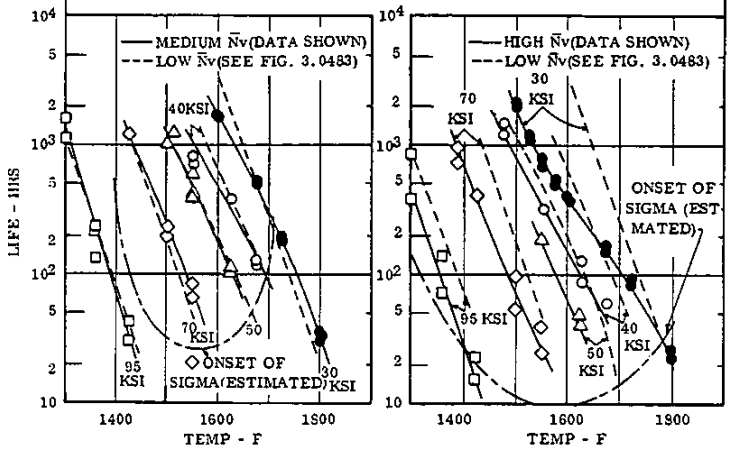

FIG. 3.0485 CREEP RUPTURE CURVES FOR FINE GRAIN ALLOYS OF LOW, MEDIUM, AND HIGH ELECTRON VACANCY CONCENTRATION(Nv), REPRESENTING PROGRESSIVELY INCREASING TENDENCY TOWARD SIGMA PHASE PRECIPITATION. CURVES SHOW THAT STRONG TENDENCY FOR SIGMA PRECIPITATION RESULTS IN REDUCTION OF CREEP RUPTURE STRENGTHS.
(23, pp. 3,7,8,12,13)

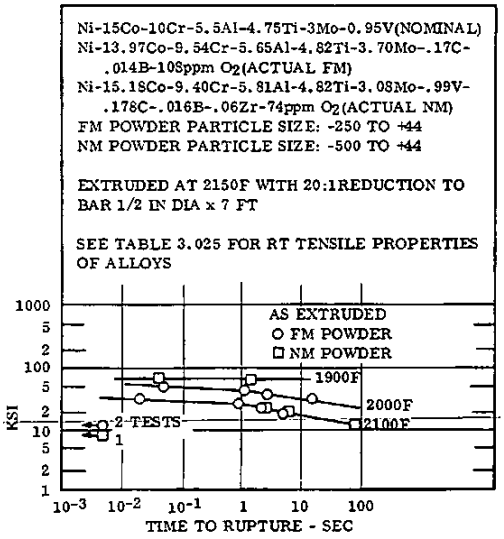

FIG. 3.0491 CREEP RUPTURE PROPERTIES IN VERY SHORT TIME RANGE AT 1900 TO 2100F FOR EXTRUDED ALLOY PREPARED FROM TWO LOTS OF POWDER (28, pp. Z-4 TO Z-7, Z-21)

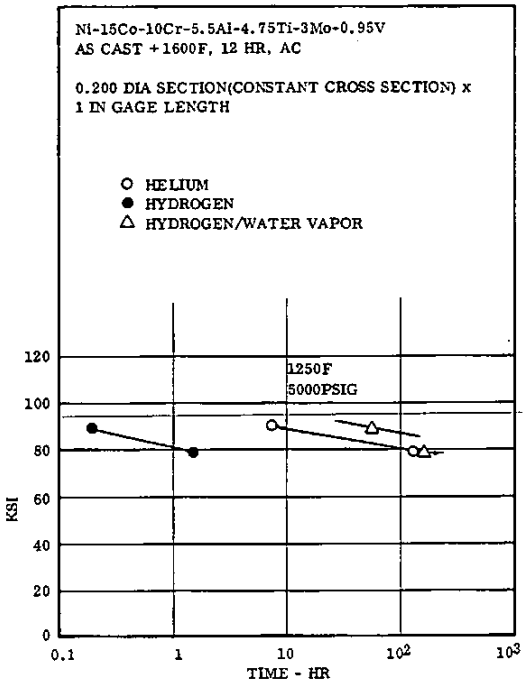

	Ni
15	Co
10	Cr
5.5	Al
4.7	Ti
3	Mo
0.95	V

IN-100

FIG. 3.04101 CREEP RUPTURE OF ALLOY IN HELIUM, HYDROGEN, AND HYDROGEN/WATER VAPOR AT 1250F AND 5000 PSIG PRESSURE (26, pp. III-13, VII-13)

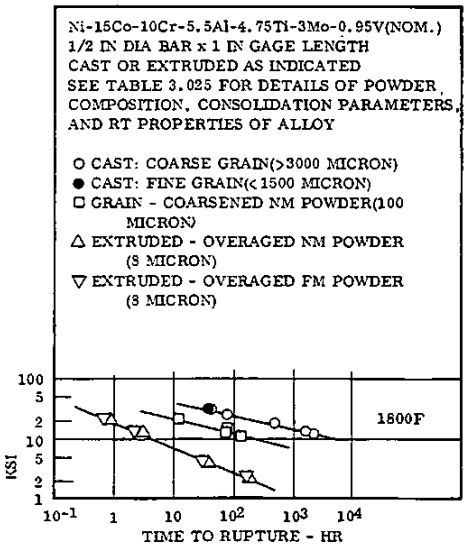

FIG. 3.0492 CREEP RUPTURE CURVES AT 1800F FOR CAST ALLOY OF VARIOUS GRAIN SIZE, AND FOR ALLOY EXTRUDED FROM POWDERS(28, p. Z-25)

Alloy	Ni-15Co-10Cr-5.5Al-4.7Ti-3Mo-0.95V
Source	Haynes
Condition	As Cast, Tested at RT. R.R. Moore*
	Number of Cycles To Failure at ± 25 ksi, 70F
Bare	19.2×10^6
C - 9 Coating	31.8×10^6 (av of 5 tests)
* Bending, R = 1	

TABLE 3.0511 EFFECT OF ALUMINUM BASE COATING ON ROTATING BENDING FATIGUE PROPERTIES AT ROOM TEMPERATURE

	Ni
15	Co
10	Cr
5.5	Al
4.7	Ti
3	Mo
0.95	V

IN-100

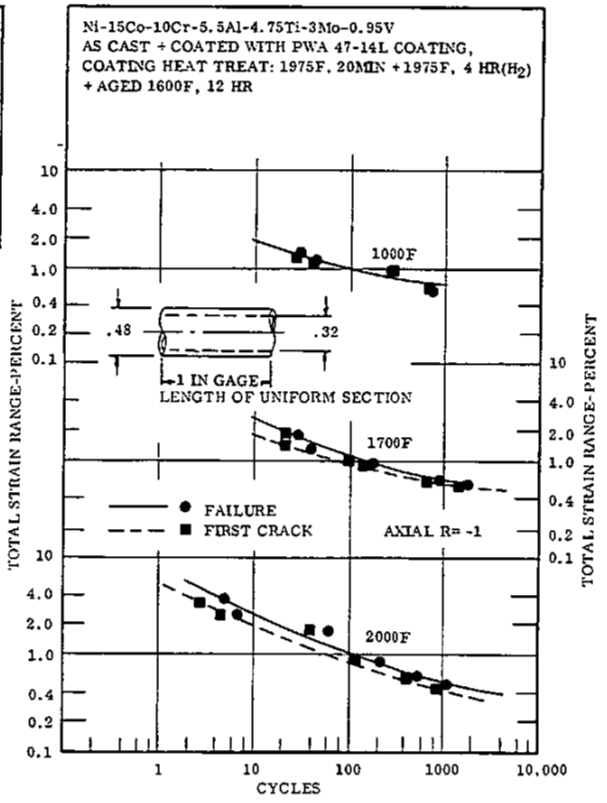

FIG. 3.0512 LOW CYCLE FATIGUE CHARACTERISTICS OF SMOOTH HOLLOW SPECIMEN WITH ONE INCH GAGE LENGTH OF UNIFORM CROSS SECTION AT TEMPERATURES FROM 1000 TO 2000F IN STRAIN-CONTROLLED CYCLING (1, p. C-8, C-12)

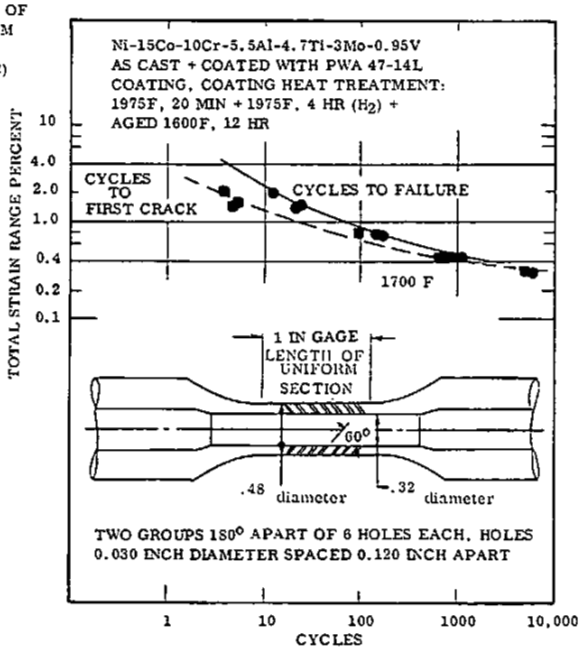

FIG. 3.0513 LOW CYCLE FATIGUE CHARACTERISTICS AT 1700F OF HOLLOW SPECIMEN WITH TWO SETS OF DIAGONAL HOLES (1,p.C8,C12)

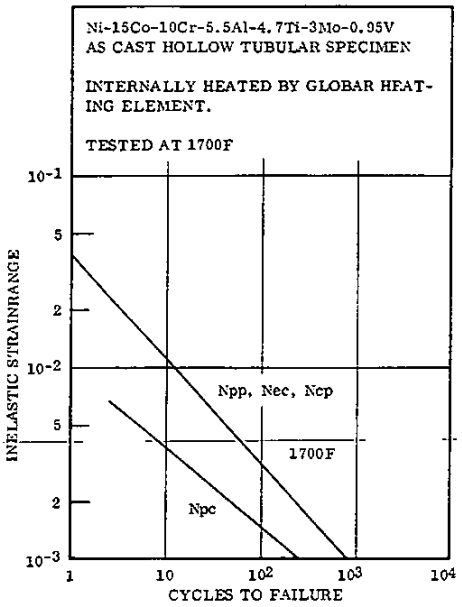

FIG. 3.0514 STRAINRANGE PARTITIONING LIFE RELATIONSHIPS FOR CAST ALLOY AT 1700F (49, p.23)

Alloy	Ni-15Co-10Cr-5.5Al-4.7Ti-3Mo.0.95V	
Source	Haynes (10) p. 10	
Condition	As Cast. Tested in Thermal Shock (b)	
	Number of Cycles to Cracking	
	1850F	2100F
Bare	500	
	400	
Coating C - 9	> 500 (a)	200
Coating C-3	-	200

(a) Two tests, stopped at 500 cycles, no cracking
(b) Airfoil shape alternated for 60 seconds in furnace at test temperature, then 90 seconds in water spray

TABLE 3.0521 THERMAL SHOCK FATIGUE CHARACTERISTICS OF AIRFOIL SHAPE WITH AND WITHOUT ALUMINUM BASE COATING

	Ni
15	Co
10	Cr
5.5	Al
4.7	Ti
3	Mo
0.95	V

IN-100

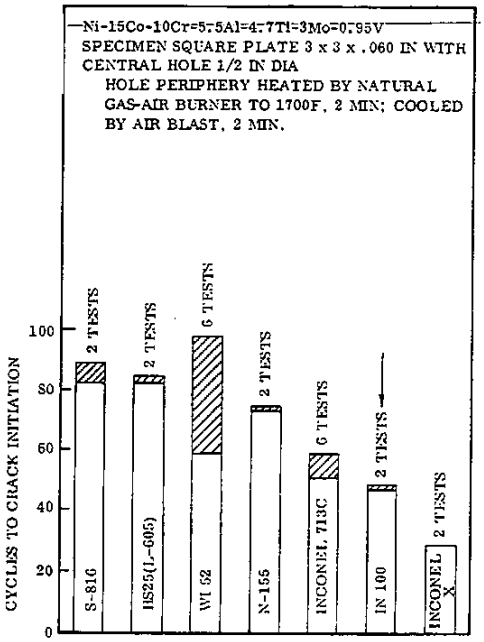

FIG. 3.0522 THERMAL FATIGUE RESISTANCE OF SQUARE PLATE RAPIDLY HEATED AND COOLED AT PERIPHERY OF CENTRAL HOLE, AND COMPARISON WITH THERMAL FATIGUE RESISTANCE OF OTHER COMMONLY USED CAST ALLOYS (30, p. 15)

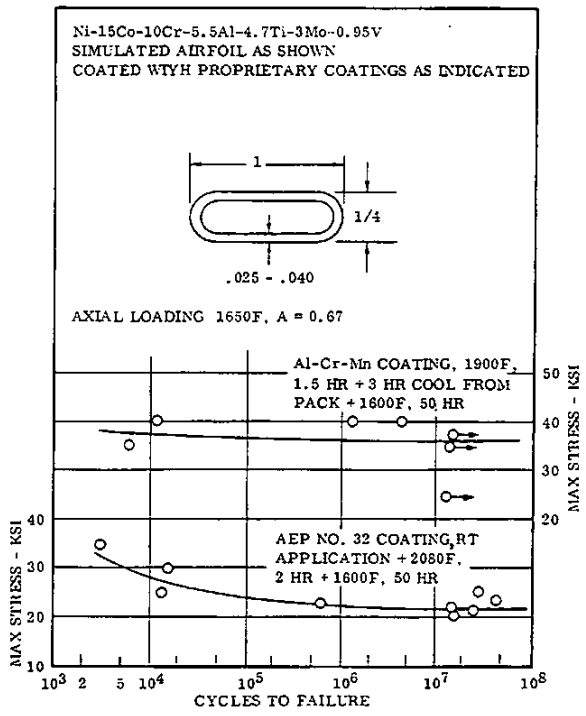

FIG. 3.0515 AXIAL FATIGUE AT 1650F OF SIMULATED HOLLOW AIRFOILS COATED WITH PROPRIETARY COATINGS (46, pp. 7, 83, 84)

	Ni
15	Co
10	Cr
5.5	Al
4.7	Ti
3	Mo
0.95	V

IN-100

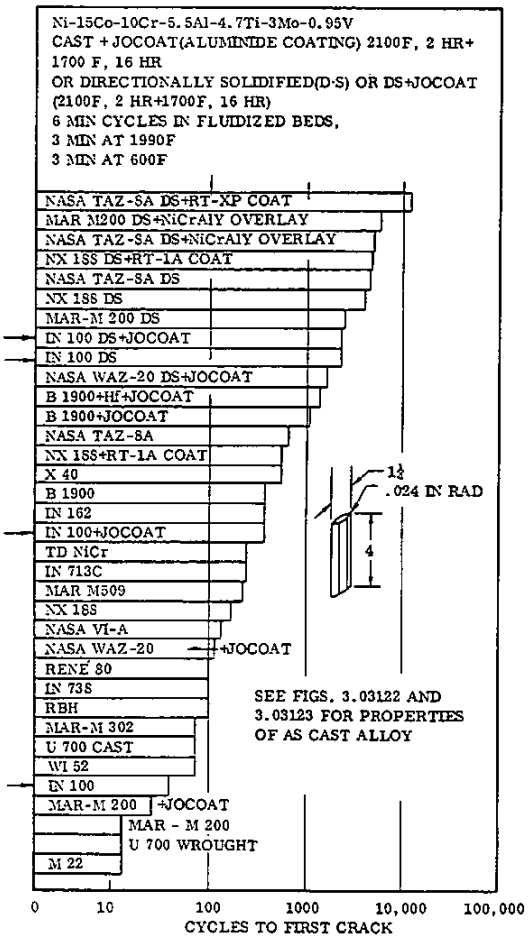

FIG. 3.0523 THERMAL FATIGUE CRACK INITIATION OF AS CAST OR DIRECTIONALLY SOLIDIFIED ALLOY WITH AND WITHOUT JOCOAT TESTED IN ALTERNATE FLUIDIZED BEDS AT 1990 AND 600F. (31, pp. 17,19,24)

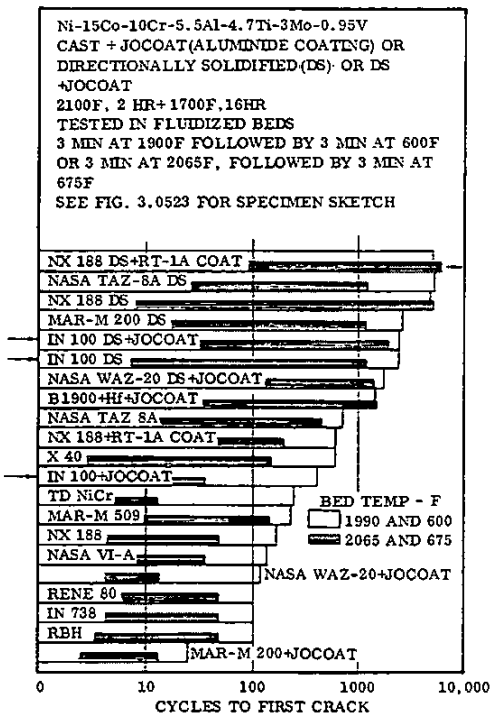

FIG. 3.0524 THERMAL FATIGUE CRACK INITIATION OF AS CAST OR DIRECTIONALLY SOLIDIFIED ALLOY WITH AND WITHOUT JOCOAT TESTED IN ALTERNATE FLUIDIZED BEDS AT TWO SETS OF TEMPERATURES(31, pp. 17-19,25)

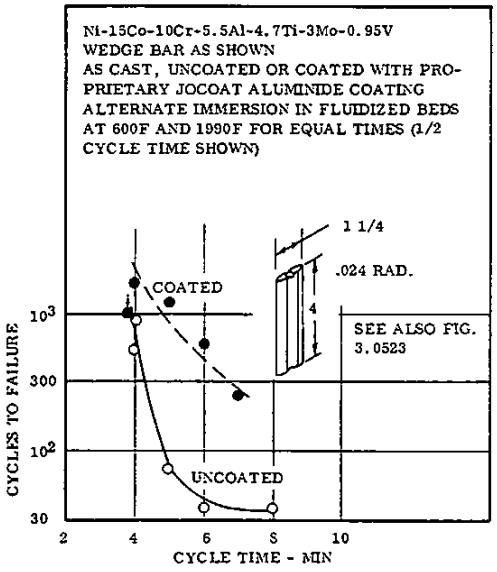

FIG. 3.0525 EFFECT OF CYCLE TIME ON THERMAL FATIGUE CRACKING OF COATED AND UNCOATED WEDGES ALTERNATELY IMMERSED IN FLUIDIZED BEDS AT 600F AND 1990F (48, p. 654)

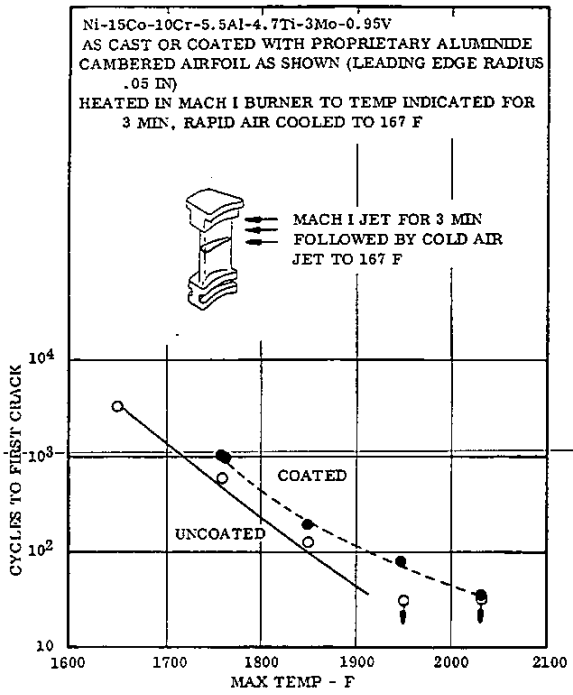

FIG. 3.0526 EFFECT OF MAXIMUM CYCLE TEMPERATURE ON THERMAL FATIGUE CRACKING OF COATED AND UNCOATED AIRFOILS SIMULATING TURBINE BLADES SUBJECTED TO MACH I GAS FLOW FOLLOWED BY RAPID AIR JET COOLING (48, p. 655)

Source	(46) pp 2, 3, 42, 44			
Alloy	Ni-15Co-10Cr-5.5Al-4.7Ti-3Mo-0.95V			
Condition	Coated with Al-Cr-Mn or AEP No. 32, see Fig. 3.0515 for Coating Treatment			
Specimen Type	Cast simulated hollow airfoil, see Fig. 3.0515			
Test Conditions	Mean tensile stress of 10.5 ksi. 40 sec. at 2050F + 40 sec. cooling with RT air. Specimen inspected with Fluorescent Penetrant after every 100 cycles			
Specimen	Cycles to Fatigue Crack			
	Coating		Comparison with best and worst alloys tested	
Number	Al-Cr-Mn	AEP No. 32	Best AEP No. 32 on NASA VI-A	Worst JoCoat on U-700
1	4808	4090	9556	628
2	3080	3545	8130	440
3	1930	1979	8130	340
4	1640	1977	7918	260
5	1547	1360	7048	230
6	1405	983	6250	210
7	685	831	2010	170
Av. based on Log.-cycles-to-failure	1834	1807	6406	296

Ni
15 Co
10 Cr
5.5 Al
4.7 Ti
3 Mo
0.95 V
IN-100

TABLE 3.0528 THERMAL FATIGUE OF THINWALL ALLOY WITH TWO PROPRIETARY COATINGS SUBJECTED TO 10.5 KSI TENSILE MEAN STRESS AND TO TEMPERATURE CYCLING FROM 2050F.

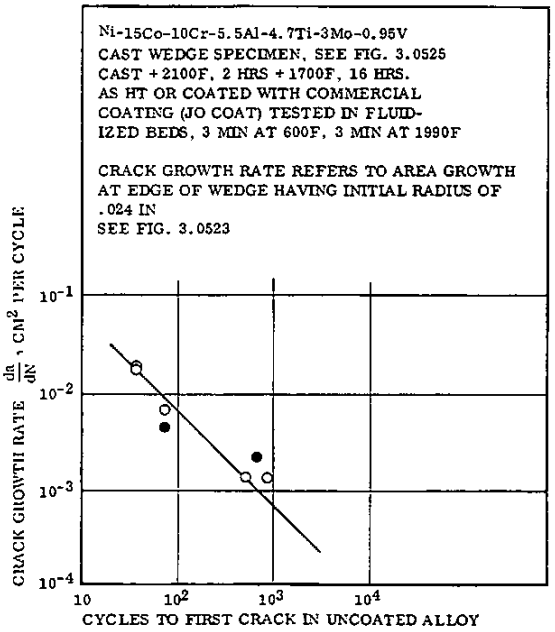

FIG. 3.0527 RELATION BETWEEN CRACK GROWTH RATE AND RESISTANCE TO INITIAL CRACKING IN THERMAL CYCLING (50, TABLE II, FIG. 9)

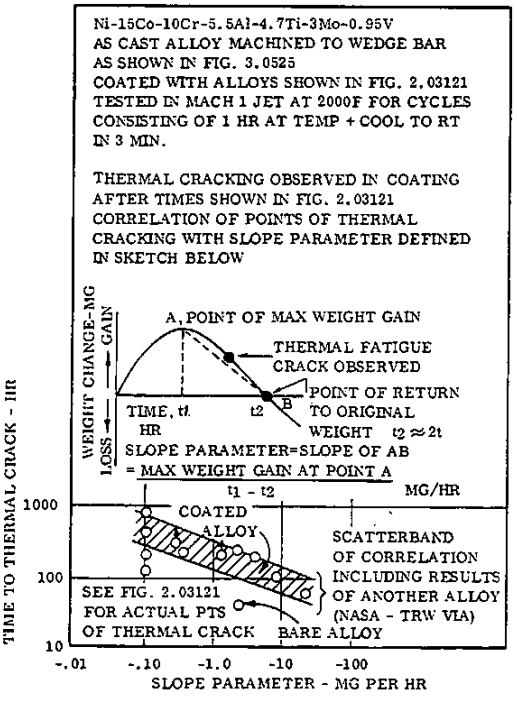

FIG. 3.0529 CORRELATION OF TIME TO INITIATE THERMAL CRACKING WITH WEIGHT GAIN SLOPE PARAMETER FOR ALLOY COATED IN VARIOUS WAYS(45,pp. 14,15)

	Ni
15	Co
10	Cr
5.5	Al
4.7	Ti
3	Mo
0.95	V

IN-100

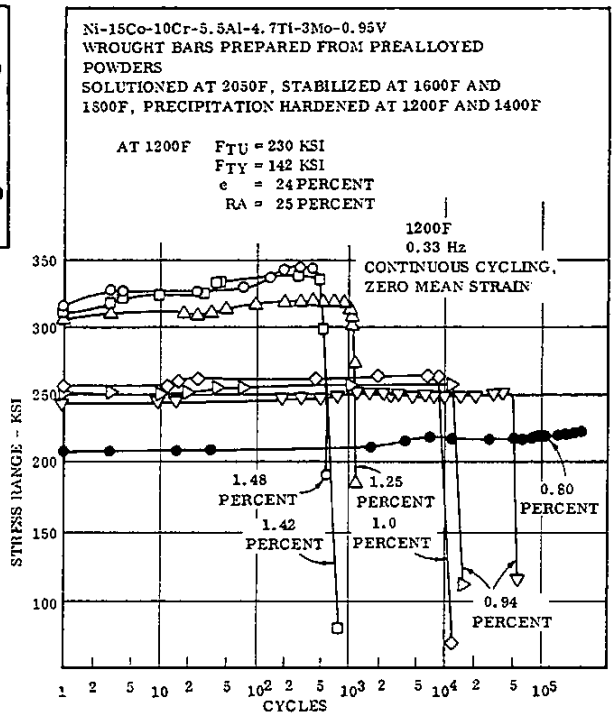

FIG. 3.0531 STRESS RANGE VARIATION DURING LOW CYCLE FATIGUE TESTS AT 1200F OF POWDER METALLURGY BARS PREPARED BY PRATT AND WHITNEY GATORIZING PROCESS (37, FIG. 6)

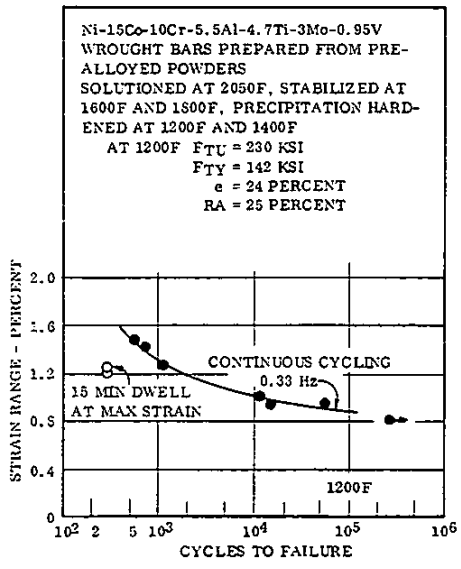

FIG. 3.0532 LOW CYCLE FATIGUE AT 1200F OF POWDER METALLURGY BARS PREPARED BY PRATT AND WHITNEY GATORIZING PROCESS, DATA POINTS REPRESENT CYCLES TO COMPLETE FRACTURE (37, FIG. 15)

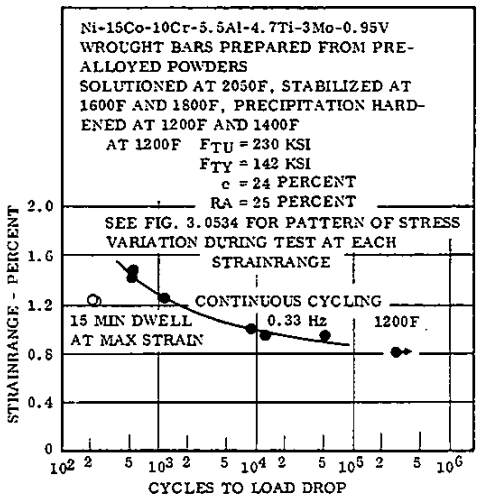

FIG. 3.0533 LOW CYCLE FATIGUE AT 1200F OF POWDER METALLURGY BARS PREPARED BY PRATT AND WHITNEY AIRCRAFT GATORIZING PROCESS DATA POINTS REPRESENT CYCLES TO 5 PERCENT LOAD DROP (37, FIG. 14)

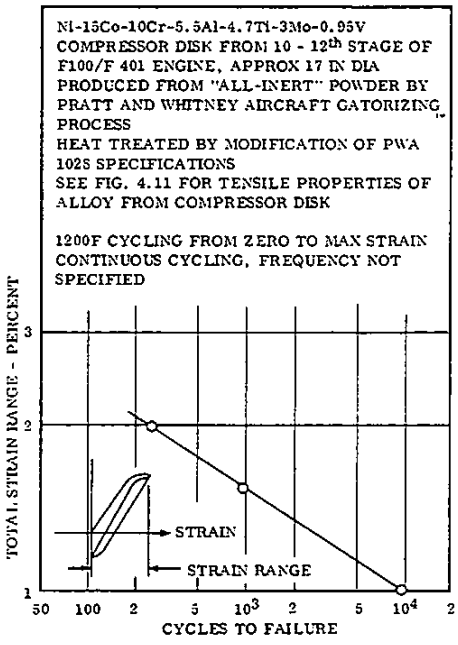

FIG. 3.0534 LOW CYCLE FATIGUE AT 1200F OF SPECIMEN FROM POWDER METALLURGY COMPRESSOR DISK (36, FIG. 3)

15	Ni
10	Co
5.5	Cr
4.7	Al
3	Ti
0.95	Mo
	V

IN-100

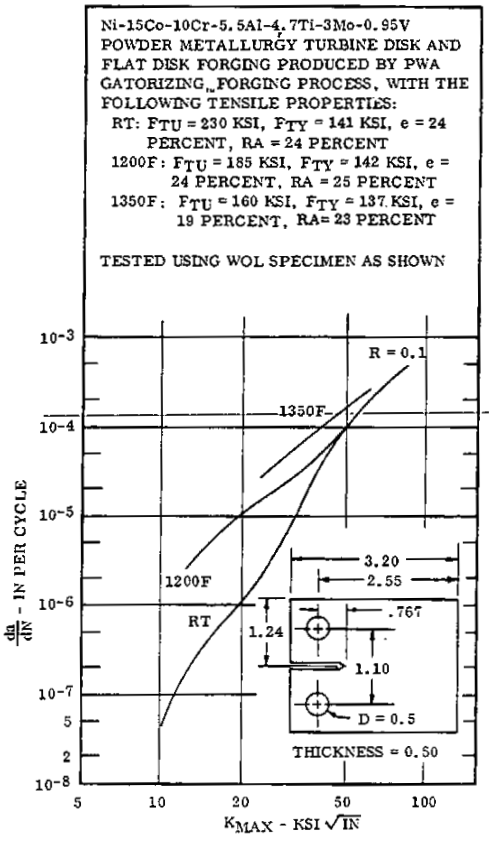

FIG. 3.0541 BASIC CRACK GROWTH CURVES AT RT, 1200F, 1350F, FOR CONSTANT AMPLITUDE LOADING OF WOL SPECIMEN (40, TABLE 1, FIGS.1 3)

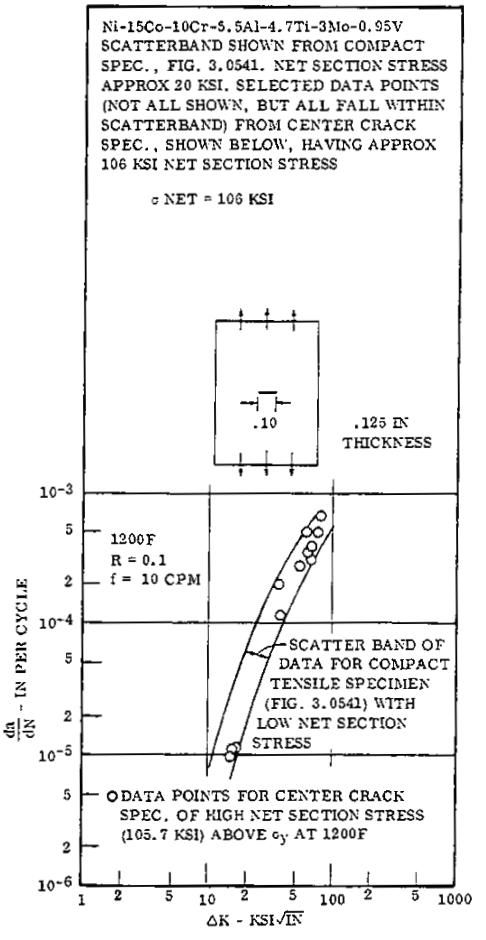

FIG. 3.0542 EFFECT OF NET SECTION STRESS ON CRACK GROWTH RATE AT 1200F (20, pp.4,5,6,8,17)

	Ni
15	Co
10	Cr
5.5	Al
4.7	Ti
3	Mo
0.95	V

IN-100

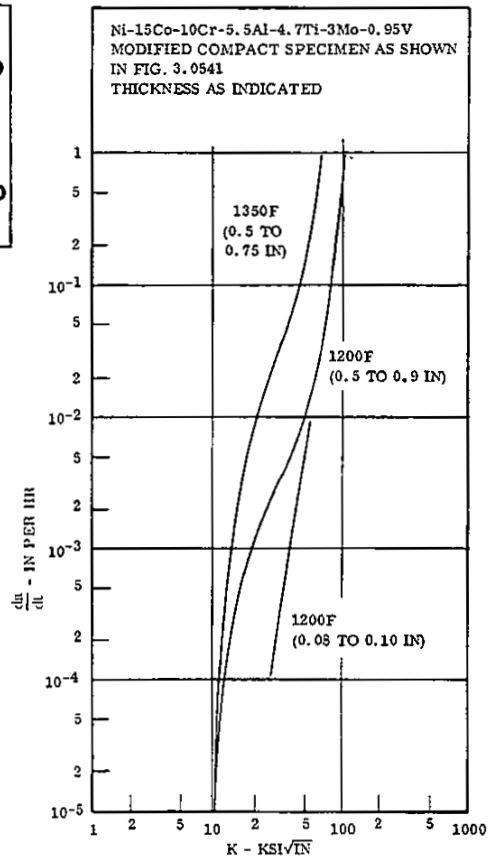

FIG. 3.0543 EFFECT OF TEMPERATURE AND SPECIMEN THICKNESS ON SUSTAINED LOAD CRACK PROPAGATION RATE. (20, pp. 4, 8, 13)

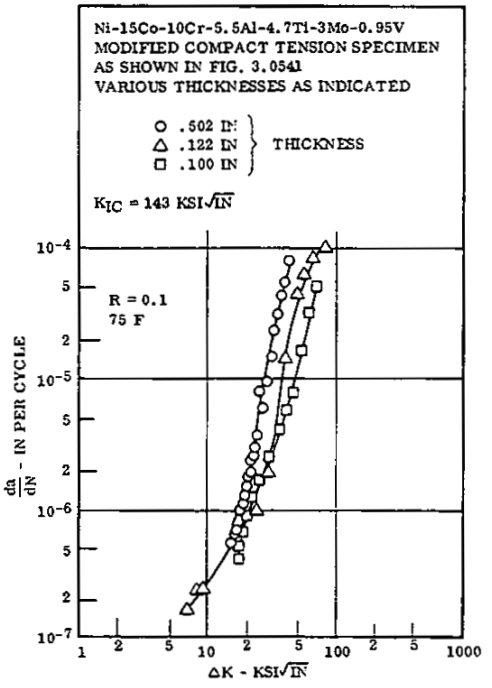

FIG. 3.0544 EFFECT OF SPECIMEN THICKNESS ON CRACK GROWTH RATE AT RT. (20, pp. 4, 8, 9)

	Ni
15	Co
10	Cr
5.5	Al
4.7	Ti
3	Mo
0.95	V

IN-100

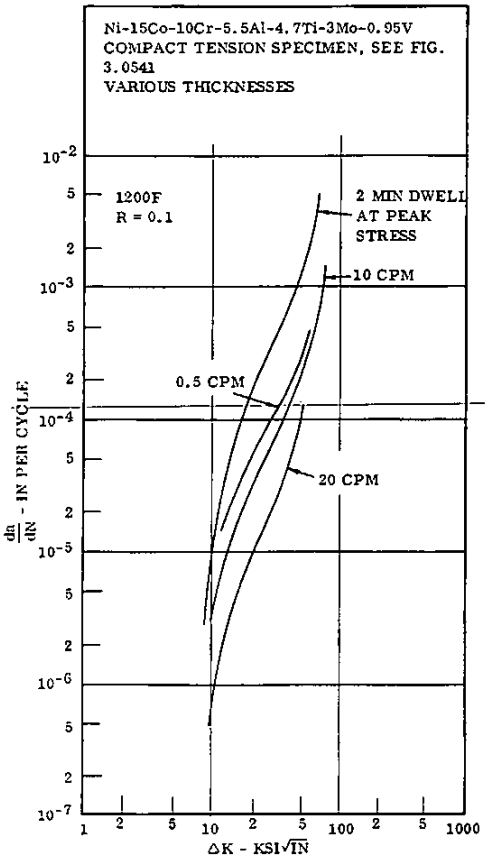

FIG. 3.0545 EFFECT OF FREQUENCY ON CRACK GROWTH RATE IN CONTINUOUS CYCLING AT 1200F
(20, pp. 4, 5, 6, 8, 25)

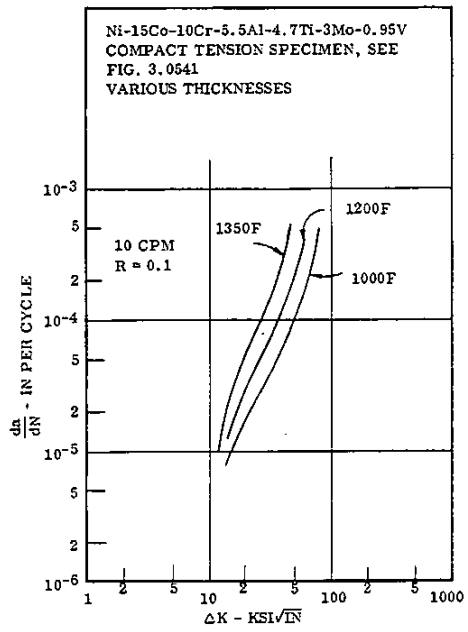

FIG. 3.0546 EFFECT OF TEMPERATURE ON CRACK GROWTH RATE AT 10 CPM, R = 0.1
(20, pp. 4, 5, 6, 8, 28)

	Ni
15	Co
10	Cr
5.5	Al
4.7	Ti
3	Mo
0.95	V

IN-100

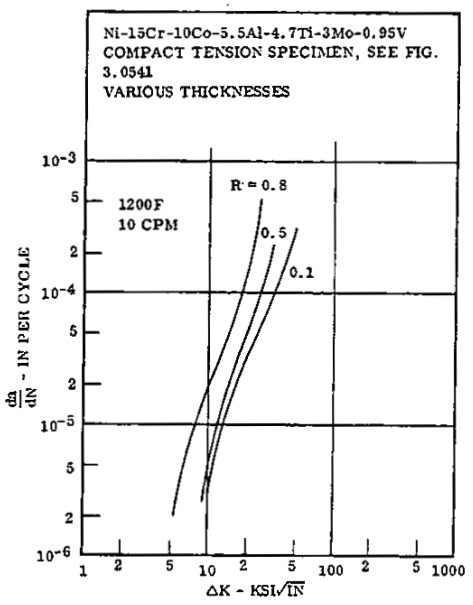

FIG. 3.0547 EFFECT OF STRESS RATIO ON CRACK GROWTH RATE AT 1200F, 10 CPM (20, pp. 4,5,6,8,26)

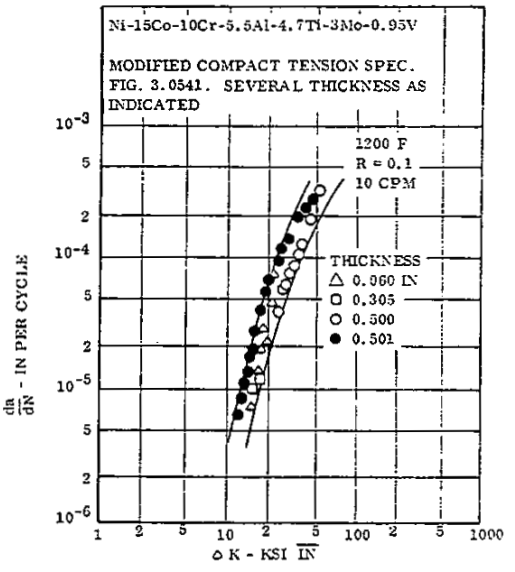

FIG. 3.0549 EFFECT OF SPECIMEN THICKNESS ON CRACK GROWTH RATE AT 1200 F. CONTINUOUS CYCLING AT 10 CPM (20, pp.4,8,11)

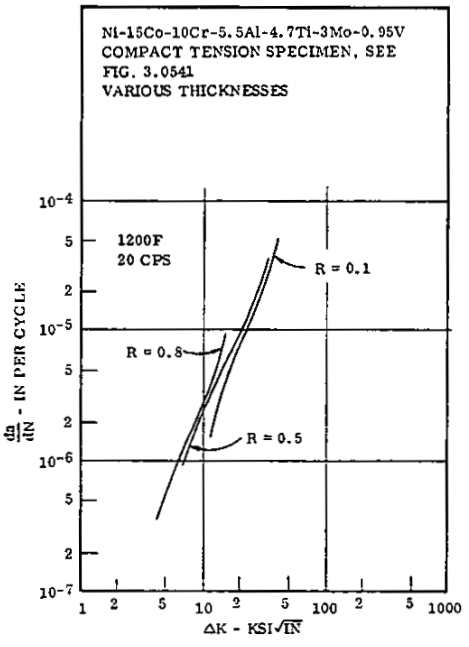

FIG. 3.0548 EFFECT OF STRESS RATIO ON CRACK GROWTH RATE AT 1200F, 20 CPS. (20, pp.4,5,6,8,27)

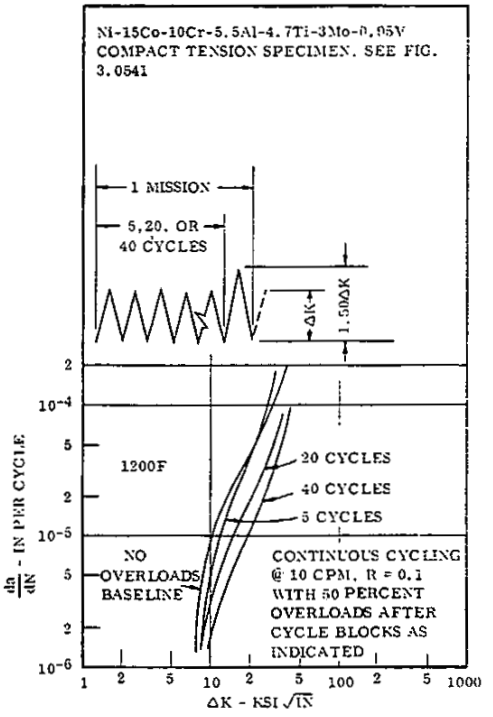

FIG. 3.0551 CRACK GROWTH AT 1200F UNDER CONTINUOUS CYCLING AND WITH 50 PERCENT OVERLOAD EVERY 5, 20, OR 40 CYCLES (20, pp.4,5, 45)

	Ni
15	Co
10	Cr
5.5	Al
4.7	Ti
3	Mo
0.95	V

IN-100

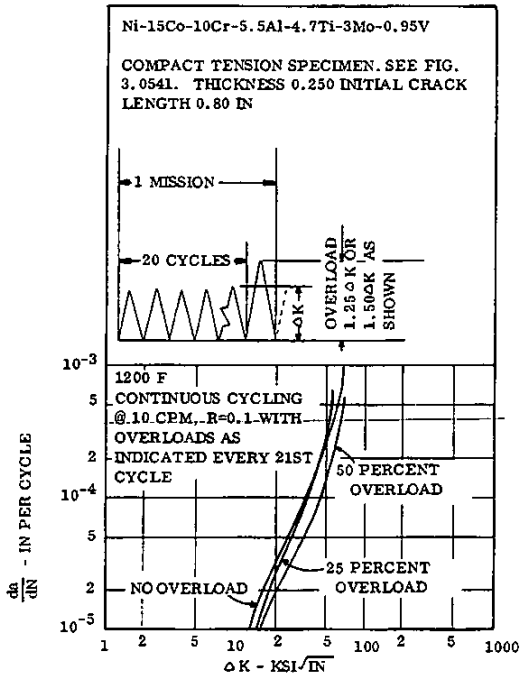

FIG. 3.0552 CRACK GROWTH AT 1200F UNDER CONTINUOUS CYCLING AND WITH 25 PERCENT OR 50 PERCENT OVERLOADS EVERY 21 CYCLES (20, pp. 4, 5, 6, 47)

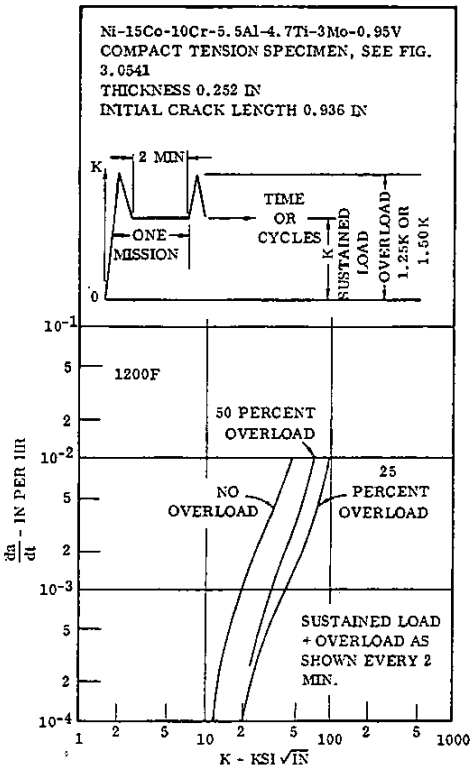

FIG. 3.0553 CRACK GROWTH AT 1200F UNDER SUSTAINED LOAD AND WITH 25 PERCENT OR 50 PERCENT OVERLOADS EVERY 2 MINUTES (20, pp. 4, 5, 41, 43)

	Ni
15	Co
10	Cr
5.5	Al
4.7	Ti
3	Mo
0.95	V

IN-100

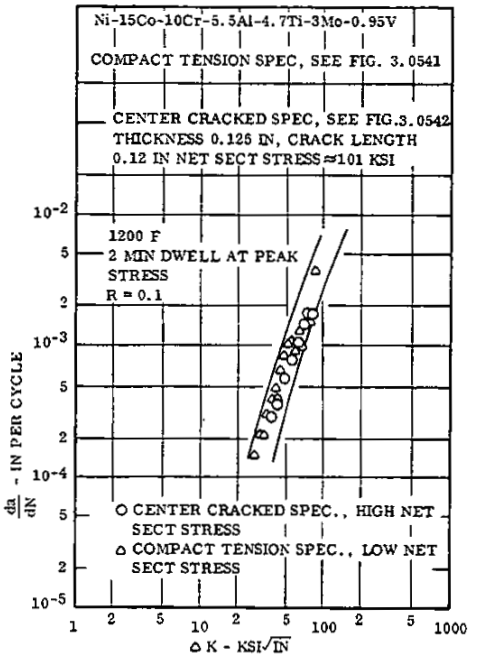

FIG. 3.0561 EFFECT OF NET SECTION STRESS ON CRACK GROWTH RATE FOR 2 MINUTE DWELL AT PEAK STRESS AT 1200 F (20, pp. 4, 5, 6, 8, 18)

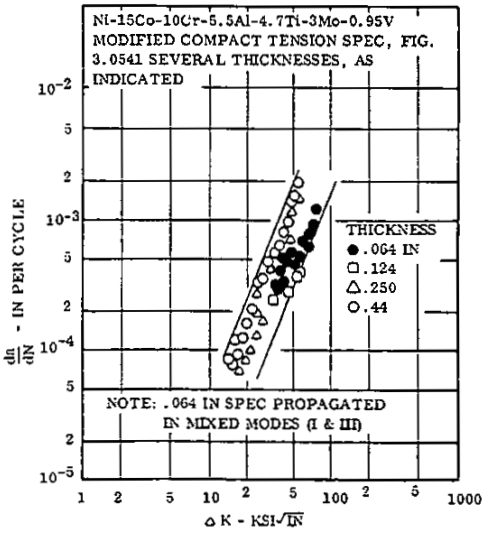

FIG. 3.0562 EFFECT OF SPECIMEN THICKNESS ON CRACK GROWTH RATE AT 1200 F, 2 MIN DWELL AT MAX LOAD, 10 CPM DURING VARIABLE STRESS PERIOD (20, pp. 4, 8, 12)

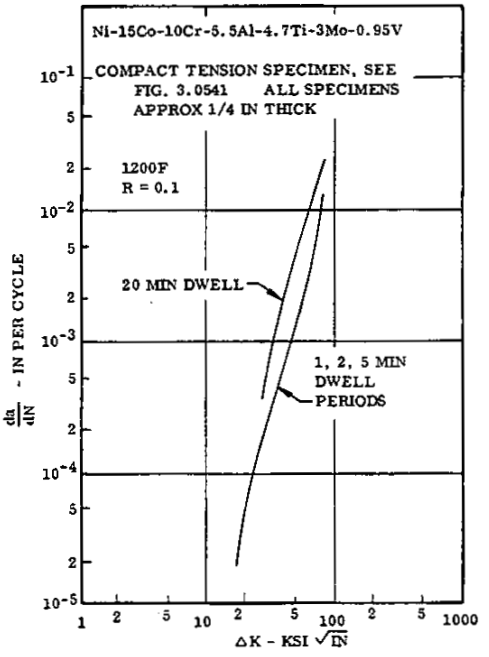

FIG. 3.0563 EFFECT OF DWELL TIME AT PEAK STRESS ON CRACK GROWTH RATE AT 1200F, R = 0.1.
(20, pp. 4, 5, 6, 8, 32)

	Ni
15	Co
10	Cr
5.5	Al
4.7	Ti
3	Mo
0.95	V

IN-100

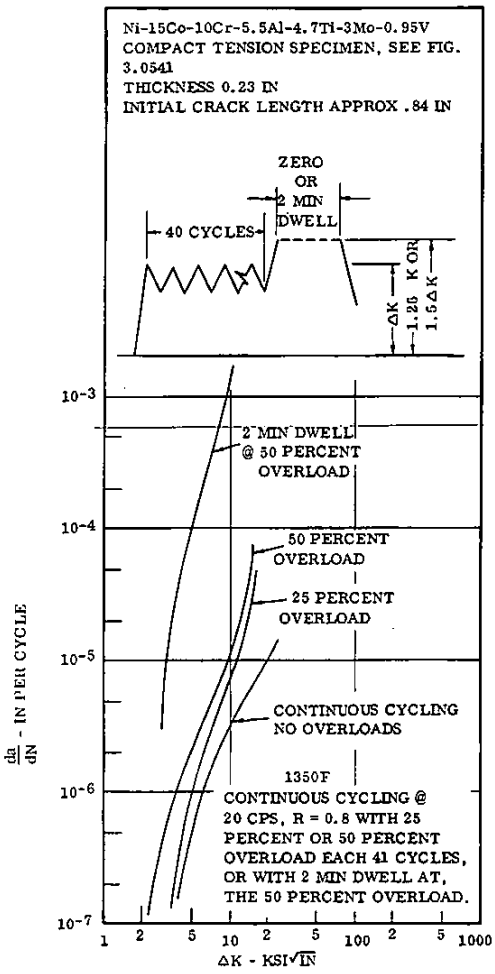

FIG. 3.0564 CRACK GROWTH AT 1350F AT CONTINUOUS CYCLING, OR WITH 25 AND 50 PERCENT OVERLOAD, OR WITH 2 MIN DWELL AT THE 50 PERCENT OVERLOAD CONDITION
(20, pp.4,5,54,55)

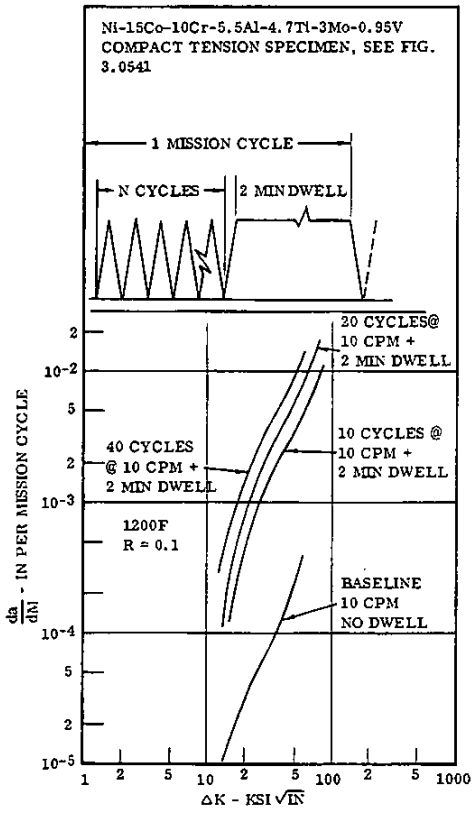

FIG. 3.0565 INTERACTION OF LOW CYCLE FATIGUE WITH DWELL PERIODS AT MAX LOAD FOR TESTS AT 1200F, R = 0.1 (20,pp. 4,6,7,33,34)

	Ni
15	Co
10	Cr
5.5	Al
4.7	Ti
3	Mo
0.95	V

IN-100

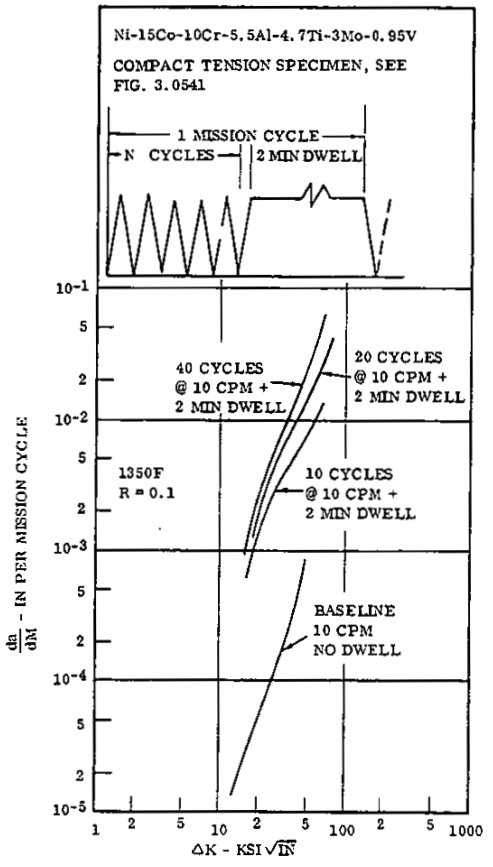

FIG. 3.0566 INTERACTION OF LOW CYCLE FATIGUE WITH DWELL PERIODS AT MAX LOAD FOR TESTS AT 1350F, R = 0.1(20, pp. 4, 6, 7, 33, 35)

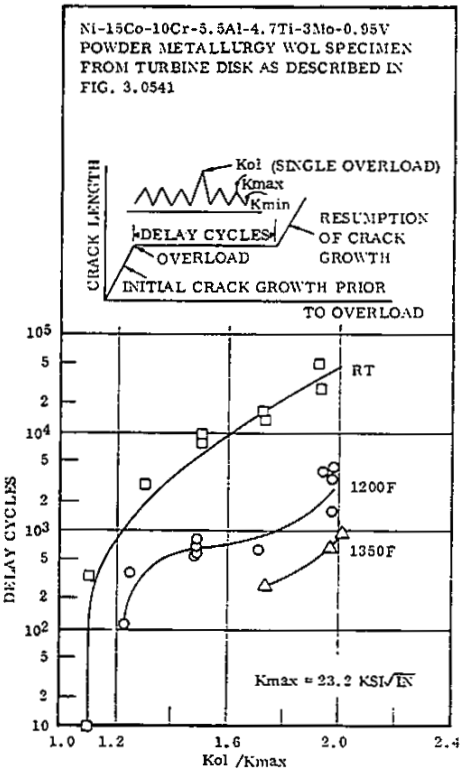

FIG. 3.0571 DELAY CYCLES PRIOR TO RESUMPTION OF BASIC CRACK GROWTH AFTER SINGLE CYCLE OF OVERLOAD. BASELINE Kmax = 23.2 KSI√IN (40, FIGS. 2.4)

	Ni
15	Co
10	Cr
5.5	Al
4.7	Ti
3	Mo
0.95	V

IN-100

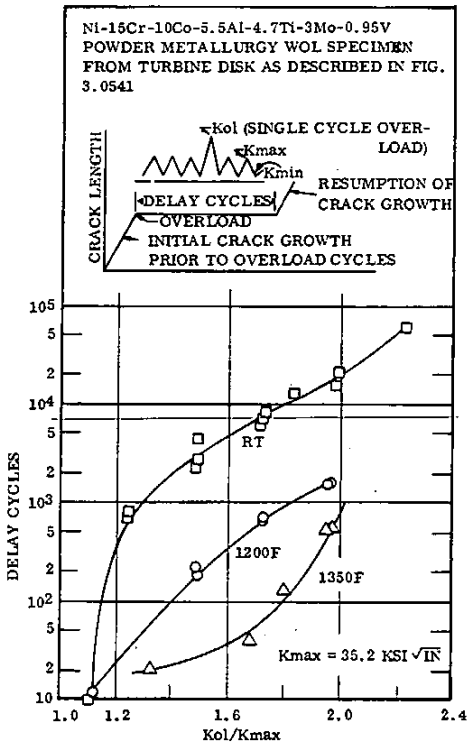

FIG. 3.0572 DELAY CYCLES PRIOR TO RESUMPTION OF BASIC CRACK GROWTH AFTER SINGLE CYCLE OVERLOAD, BASELINE Kmax = 35.2 KSI √IN (40, FIGS. 2, 3)

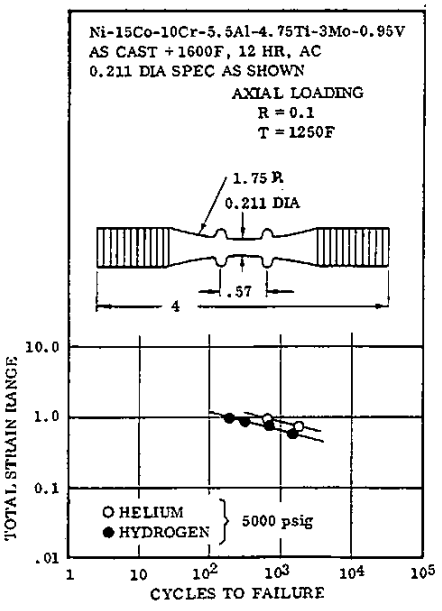

FIG. 3.0582 HIGH CYCLE AXIAL FATIGUE IN HIGH PRESSURE HYDROGEN AND HELIUM AT 1250F (26, pp. III-10, IV-4, 9)

FIG. 3.0581 LOW CYCLE FATIGUE AT 1250F IN HIGH PRESSURE HYDROGEN AND HELIUM (26, pp. III-9, V-9, 17)

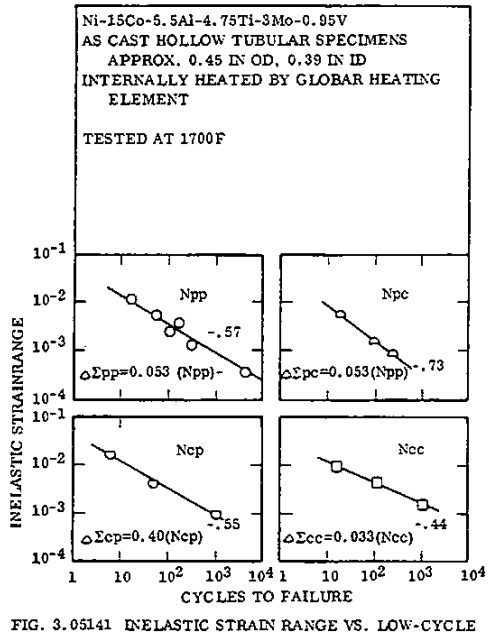

FIG. 3.05141 INELASTIC STRAIN RANGE VS. LOW-CYCLE FATIGUE LIFE FOR EACH PARTIONED STRAIN RANGE COMPONENT FOR AS-CAST THINWALL TUBING AT 1700F (49, p. 23), (53, p. 4 & FIG. 6)

	Ni
15	Co
10	Cr
5.5	Al
4.7	Ti
3	Mo
0.95	V

IN-100

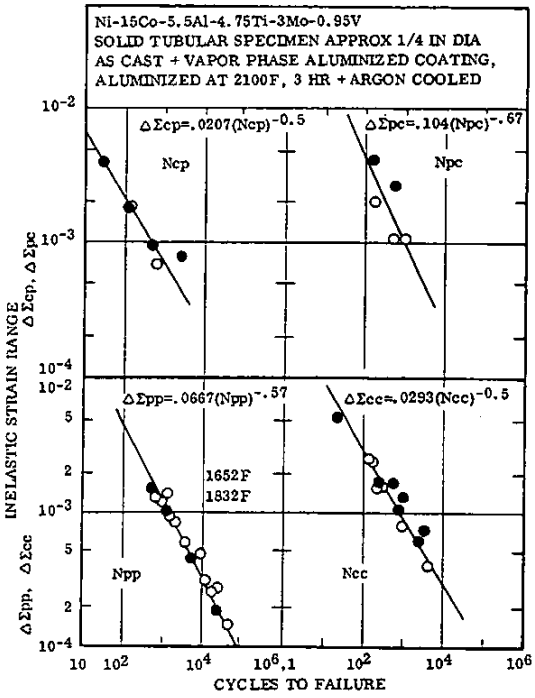

FIG. 3.05142 STRAINRANGE PARTIONING LIFE RELATIONSHIPS AT 1652F AND 1832F FOR AS-CAST ALUMINUM-COATED ALLOY (54, pp. 4-10)

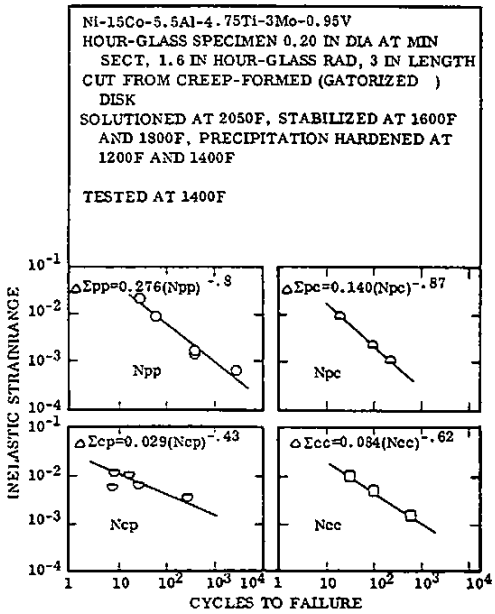

FIG. 3.05143 INELASTIC STRAINRANGE VS LOW-CYCLE FATIGUE LIFE FOR EACH PARTITIONED STRAINRANGE COMPONENT AT 1400F. SPECIMENS FROM CREEP-FORMED (GATORIZED$_{TM}$) TURBINE DISK (53, p. 4 & FIG. 5)

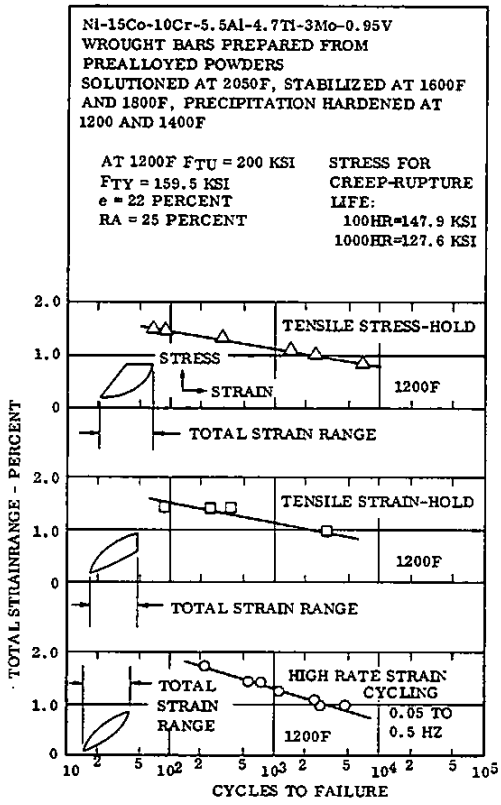

FIG. 3.05144 TOTAL STRAIN RANGE VS LOW-CYCLE FATIGUE LIFE AT 1200F OF POWDER METALLURGY BARS PREPARED BY PRATT & WHITNEY GATORIZING$_{TM}$ PROCESS AND TESTED UNDER RAPID STRAIN CYCLING, TENSILE STRESS-HOLD, AND TENSILE STRAIN-HOLD. (52)

	Ni
15	Co
10	Cr
5.5	Al
4.7	Ti
3	Mo
0.95	V

IN-100

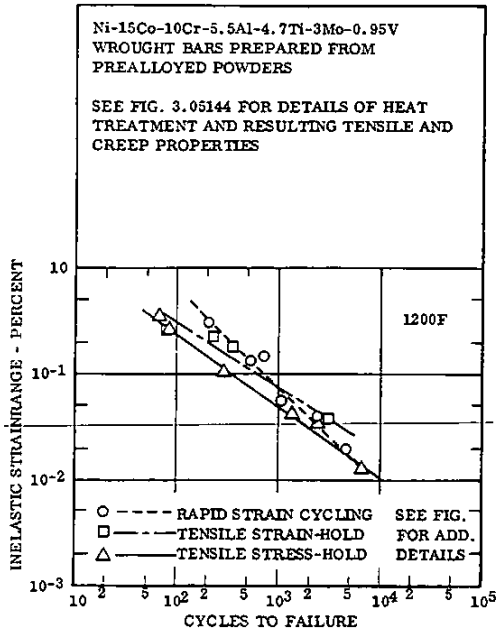

FIG. 3.05145 INELASTIC STRAINRANGE VS LOW CYCLE FATIGUE LIFE AT 1200F OF POWDER METALLURGY BARS PREPARED BY PRATT AND WHITNEY GATORIZING$_{TM}$ PROCESS AND TESTED UNDER RAPID STRAIN CYCLING, TENSILE STRESS-HOLD, AND TENSILE STRAIN-HOLD. (52)

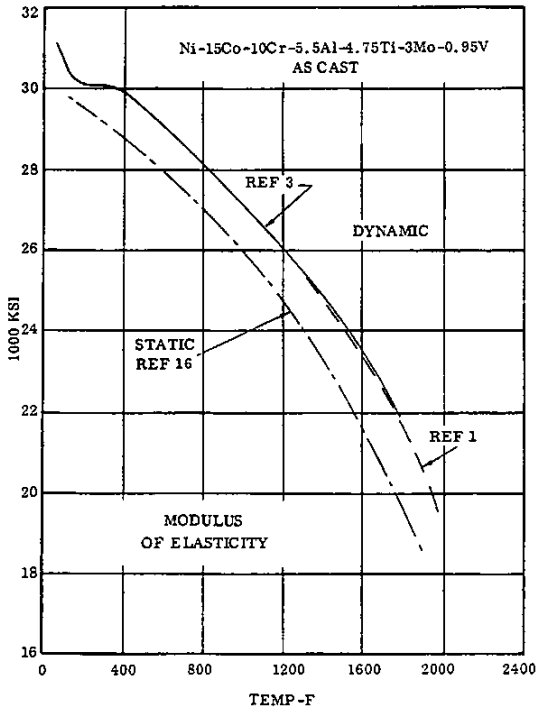

FIG. 3.062 DYNAMIC MODULUS OF ELASTICITY (3,p.8,1,p.C-7) (16,p.114)

	Ni
15	Co
10	Cr
5.5	Al
4.7	Ti
3	Mo
0.95	V

IN-100

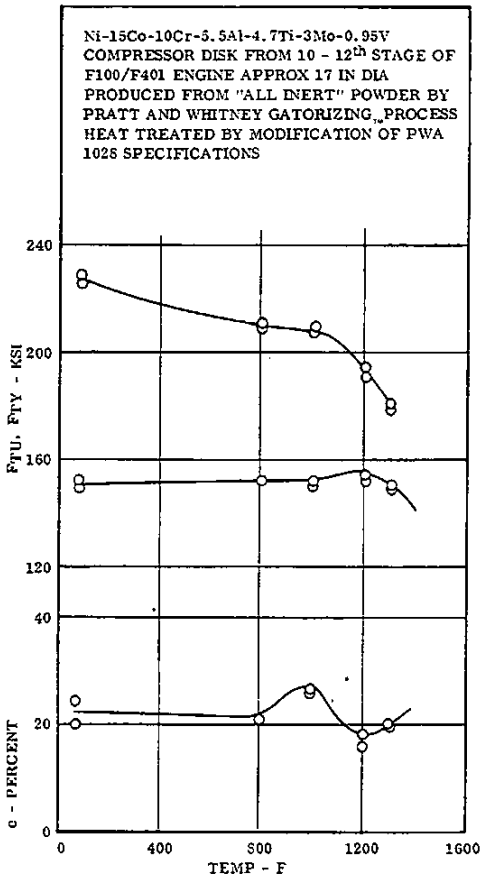

FIG. 4.11 MECHANICAL PROPERTIES FROM RT TO 1300F OF SPECIMENS FROM THE 10 - 12th STAGE COMPRESSOR OF F100/F401 ENGINE

(36, Fig. 2)

Source	(47) pp 30, 83
Alloy	Ni-15Co-10Cr-5.5Al-4.7Ti-3Mo-0.95V
Condition	As Cast and Machined To Fir Tree Specimen As Shown
Test Temperature	RT

Specimen

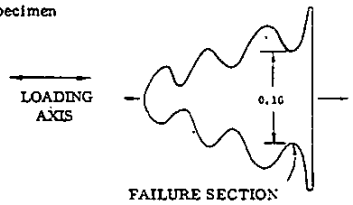

Fir Tree Attachment Loaded with Mating Waspalloy Female Fixture. Failure in IN 100 Across 0.16 IN Dimension As Shown. Depth 0.61 IN
F_{tu} of Alloy 115 KSI

Specimen No.	Nominal Stress At Failure, KSI
1	138.5
2	130.9

TABLE 4.12 ROOM TEMPERATURE TENSILE STRENGTH OF FIR TREE SIMULATING TURBINE BLADE ATTACHMENT

	Ni
15	Co
10	Cr
5.5	Al
4.7	Ti
3	Mo
0.95	V

IN-100

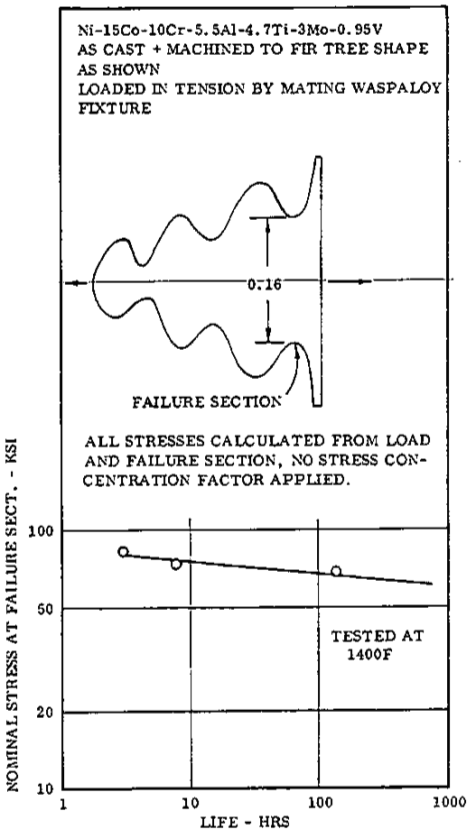

FIG. 4.13 CREEP RUPTURE AT 1400F OF FIR TREE SIMULATING TURBINE BLADE ATTACHMENT (47, pp. 31, 107)

	Ni
15	Co
10	Cr
5.5	Al
4.7	Ti
3	Mo
0.95	V

IN-100

Source	(47) pp 32, 83
Alloy	Ni-15Co-10Cr-5.5Al-4.7Ti-3Mo-0.95V
Condition	As Cast and Machined To Fir Tree Specimen As Shown
Test Temperature	RT

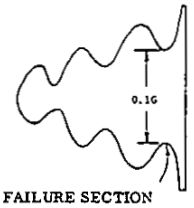

FAILURE SECTION

Specimen Loaded In Tension + Vibratory Bending Moment. Stresses shown are nominal stresses across failure section (no correction for stress concentration) + bending stress at outer fibers of failure section.

Static Stress, ksi	Alternating Stress, ksi	Cycles to Failure(1)
20	15	3.1×10^6
20	30	8.7×10^5
20	5 for 10^6 cycles + 10 for 10^6 cycles + 15 to failure	3.6×10^6
25	5 for 10^6 cycles + 10 for 10^6 cycles + 15 to failure	2.04×10^6
15	15	9.6×10^6

(1) If failure did not occur in 10^6 cycles, alternating stress was increased for an additional 10^6 cycles, if necessary. If failure still did not occur in 10^6, alternating stress was again increased. Failure cycles shown are at the last alternating stress shown.

TABLE 4.14 FATIGUE AT RT UNDER COMBINED STATIC AND VIBRATORY STRESS OF TURBINE BLADE FIR TREE FASTENING

Source	(47) pp 25, 26, 33, 87, 94		
Alloy	Ni-15Co-10Cr-5.5Al-4.7Ti-3Mo-0.95V		
Test Specimen	4 x 1.5 x 0.5 Bar Electron Beam Welded to Similar Waspaloy Bar. After Heat Treat, Machined to Specimen Described Below		
Condition	As Cast + Welded + Heat Treat (to restrengthen Waspaloy): 1850F, 1 Hour + 1550F, 4 Hour + 1400F, 16 Hour + Machined to Approximately 0.3 x 0.3 At Test Section		
Test Temperature	RT		
Basic Strength of Welded Alloys	Min F_{tu}, IN 100	115 KSI	At RT
	Min F_{tu}, Waspaloy	180 KSI	
Condition Determined by X-Ray Prior to Test	Failure Strength KSI	Location of Failure	
Good	112	Weld	
Weld Cracks(1)	89.2	Weld	
(1) Caused by loss of ductility in IN 100 as result of change in microstructure during welding.			

TABLE 4.211 ROOM TEMPERATURE TENSILE STRENGTH OF WELDMENT TO WASPALOY

	Ni
15	Co
10	Cr
5.5	Al
4.7	Ti
3	Mo
0.95	V

IN-100

Source	(47) pp 25, 26, 34, 87, 94		
Alloy	Ni-15Co-10Cr-5.5Al-4.7Ti-3Mo-0.95V		
Test Specimens	4 x 1.5 x 0.5 Bar, Electron Beam Welded to Similar Waspaloy Bar. After Heat Treat, Machined to Specimens described below.		
Condition	As Cast + Welded + Heat Treat (to restrengthen Waspaloy): 1850F, 1 Hr + 1550F, 4 Hr + 1400F, 16 Hr + Machine To Approximately 0.3 x 0.3 at Test Section		
Test Temperature	1400F		
Condition Determined by X-Ray Prior to Test	Stress at Failure Location, (Ksi)	Life (Hr)	Location of Failure
Weld Cracks(1)	91	0.1	Weld
Weld Cracks(1)	56.5	31	Weld
Good	54.6	>224.6(2)	Waspaloy
Weld Cracks	45.5	76.5	Weld
Weld Cracks	60.2	1.8	Weld

(1) Caused by loss of ductility in IN 100 as result of change in microstructure during welding.
(2) Failure in Waspaloy, weld still intact.

TABLE 4.212 CREEP RUPTURE AT 1400F OF ELECTRON BEAM WELDMENT TO WASPALOY

Source	(47) pp 25, 26, 35, 87		
Alloy	Ni-15Co-10Cr-5.5Al-4.7Ti-3Mo-0.95V		
Test Specimen	4 x 1.5 x 0.5 Bar Electron Beam Welded to Similar Waspaloy Bar + Heat Treatment as Shown Below + Machined to Specimen Shape Shown		
	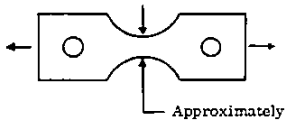 Steady Load Applied Axially, Vibratory Load Applied Normal To Plane of Specimen Approximately 0.12 x .095 Thick At Minimum Section		
Condition	As Cast + Welded + Heat Treat (to restrengthen Waspaloy): 1850F, 1 Hr + 1550F, 4 Hr + 1400F, 16 Hr Min F_{tu} IN 100 - 115 KSI Min F_{tu} Waspaloy - 180 KSI At RT		
Test Temperature	RT		
Condition as Determined by X-Ray Prior to Test	Static Stress KSI	Vibratory Stress ± KSI	Cycles(1) To Failure
Weld Cracks(2)	62.2	9.8	2.3×10^6
Weld Cracks(2)	62.2	4.9	1.75×10^6
Good	62.2	4.9	$>10^7$
Good	62.2	9.8	3.67×10^6

(1) All failures in weld
(2) Caused by loss of ductility in IN 100 as result of change in microstructure during welding

TABLE 4.213 FATIGUE AT RT UNDER COMBINED STATIC AND VIBRATORY STRESS OF ELECTRON BEAM WELDMENT TO WASPALOY

	Ni
15	Co
10	Cr
5.5	Al
4.7	Ti
3	Mo
0.95	V

IN-100

Source	(47) pp 27, 28, 38, 91, 110
Alloy	Ni-15Co-10Cr-5.5Al-4.7Ti-3Mo-0.95V

Test Specimen and Brazing

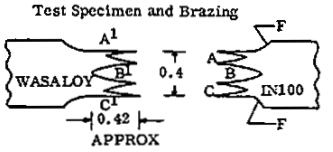

Faces A and A^1 and C and C^1 Mate. Double Fingers B Fit Into Hollow B^1. Prior to Brazing .0005 Ni Plate Deposited on Tines + 900F, 30 Min To Bond. For Brazing Clearances .002 to .004 In Maintained.

Brazed In H_2 At 2000F, 20 Min. Diffusion of Braze 1800F, 8 Hr + 1900F, 8 Hr + 1950F, 56 Hr.

Following Braze HT to Restrengthen Waspaloy: Fast Cool From 1950F to 1000F At 40F Per Min + 1550F, 4 Hr + Cool to 1000F + 1400F, 16 Hr

Test Temperature	RT	Min F_{tu} IN100 115 KSI Min F_{tu} Waspaloy 150 KSI
Braze Area Percent	Stress KSI	Location of Failure
90	112	Blade Radius
90	100	IN 100
		Point F in Sketch Above

TABLE 4.221 ROOM TEMPERATURE TENSILE STRENGTH OF BRAZED ATTACHMENT TO WASPALOY

Source	(47) pp 28, 28, 39, 91, 110
Alloy	Ni-15Co-10Cr-5.5Al-4.7Ti-3Mo-0.95V

Depth At Test Section Approximately 0.35 IN

Test Specimen

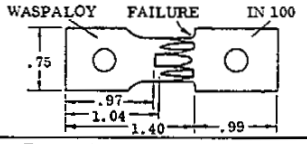

See Table 4.221 For Details of Geometry of Braze Surfaces and Brazing Procedure
Axial Load Applied For Steady Stress
Alternating Stress Applied By Resonant Vibration

Test Temperature	RT	
Static Stress KSI	Alternating Stress KSI (2)	Cycles To Failure(1)
29.8	20.4	5×10^5
14.9	10.2 for 10^6 cycles + 13.6 for 10^6 cycles + 17 to failure	6.2×10^6
29.8	6.9 for 10^6 cycles + 10.2 for 10^6 cycles + 13.6 for 10^6 cycles + 17 for 10^6 cycles + 20.4 to failure	1.9×10^6
37.3	6.9 for 10^6 cycles + 10.2 for 10^6 cycles + 13.6 to failure	9.2×10^6
22.4	13.6	10^7

(1) All failures at base cross section of IN 100
(2) If failure did not occur in 10^6 cycles, alternating stress was increased for an additional 10^6 cycles if necessary at the next higher stress level shown. Failure cycles shown are for last value of alternating stress listed.

TABLE 4.222 FATIGUE AT RT UNDER COMBINED STATIC AND VIBRATORY STRESS OF BRAZED JOINT SIMULATING TURBINE BLADE FASTENING TO WASPALOY

	Ni
15	Co
10	Cr
5.5	Al
4.7	Ti
3	Mo
0.95	V

IN-100

Source	(51) p 208				
Alloy	Ni-15Co-10Cr-5.5Al-4.7Ti-3Mo-0.95V				
Condition	Cast and Bonded To U700 by TLP Process (1)				
Test Temperature	1400F				
Base Metal Requirements at 1400F	IN 100, Min KSI F_{tu} 115, F_{ty} 95 U-700 Min KSI F_{tu} 135, F_{ty} 105				
Bonding Condition	F_{tu} (KSI)	F_{ty} (KSI)	e (%)	RA (%)	Failure Location
2000F, 4 Hrs	137.3	128.1	2.3	0.6	IN 100
2000F, 4 Hrs	141.5	127	5.2	10.3	IN 100
2000F, 4 Hrs	140.4	127	4.0	6.4	Bond Region
2100F, 4 Hrs	136.1	124.4	4.2	10.3	IN 100
2100F, 4 Hrs	134.2	128.1	1.7	2.3	IN 100
2100F, 4 Hrs	142.0	129.4	8.6	9.5	IN 100
2100F, 4 Hrs	134.8	121.8	3.8	10.3	IN 100

(1) TLP is Pratt and Whitney Aircraft Trade Name for Transition-Liquid-Phase Bond by adding thin layer between surfaces to be bonded and exposing to temperature near melting point in vacuum. Melting temperature depressant (Boron) is added to bonding alloy. Some alloying elements of base composition (i.e. Al, Ti, C) are restricted to prevent formation of stable interface phases.

TABLE 4.231 TENSILE PROPERTIES AT 1400F FOR TLP BOND BETWEEN CAST ALLOY AND WROUGHT UDIMET 700

REFERENCES

1. Stewart, O.L. and Vogel, W.H., "Methods for Predicting Thermal Stress Cracking in Turbine Stator and Rotor Blades." NASA CR-54636. PWA-3142. (July 10, 1967)
2. Collins, H.E. and Quigg, R.J., "Carbide and Intermetallic Instability in Advanced Nickel-Base Superalloys." Paper presented at ASM National Meeting, Cleveland, Ohio, (October 1967)
3. International Nickel Co., "High Temperature, High Strength Nickel Base Alloys" (1964)
4. International Nickel Co., Engineering Properties of IN-100 Alloy.
5. Personal Communication, DMIC, to Materials Properties Data Center, November 1967, based on compilation under preparation for ASTM-ASME Joint Committee on the Effects of Temperature on the Properties of Metals.
6. Wasielewski, G.E., "Nickel-Base Superalloy Oxidation", AFML-TR-67-30, (Jan 1967)
7. Jackson, C.M. and Hall, A.M. "Surface Treatments for Nickel and Nickel Base Alloys", NASA TM-X-53448, (April 20, 1966)
8. General Telephone and Electronics Laboratories and Sylcor Division, Sylvania Electric Products, RSIC 1553
9. Sama, Lawrence, Sylcor Division, Sylvania Electric Products Company, Personal Communication cited as Ref. 47 of Jackson and Hall report (ref 7, above)
10. Union Carbide Corp., Stellite Division, "Haynes Diffusion Coatings", (November 1963)
11. Wlodek, S.T., "The Structure on IN 100", Trans Met Sec. AIME, 1964, Vol. 230, No. 8, pp. 1078-1090.
12. Ross, E.W., "Rene 100 - A Sigma-Free Blade Alloy," Preprint of paper submitted to ASM, (1967)
13. Boesch, W.J., Cremisio, R.S., and Richmond, F.M. "Progress in Superalloys for S.S.T. Engines," Journal of Metals (June 1967)
14. Jensen, D.E. Pinkowish, and Donachie, M.J., Jr. "Effects of Elevated Temperature Exposure on Three Cast Nickel Base Alloys", Paper presented at ASM National Meeting, Cleveland, Ohio (Oct. 1967)
15. Woodyatt, L.R. Sims, C.T., and Beattie, H.J., "Prediction of Sigma-Type Phase Occurrence from Compositions in Austenitic Superalloys", Trans, AIME, Vol. 236, No. 4 (April 1966)
16. Fritz, L.J. and Koster, W.P. "Tensile and Creep Rupture Properties of (16) Uncoated and (2) Coated Engineering Alloys at Elevated Temperatures." NASA CR-135138 (Jan. 15, 1977)
16. Simmons, W.F., and Gunia, R.B., "Compilation of Trade Names, Specifications, and Producers of Stainless Alloys and Superalloys", ASTM Data Series DS 45 (1969)
18. Simmons, W.F. and Gunia, R.B., "Compilation and Index of Trade Names, Specifications, and Producers of Stainless Alloys and Superalloys", ASTM DS45A (1972)
19. Annis, C.G., Wallace, R.M. and Sims, D.L., "An Interpolative Model for Elevated Temperature Fatigue Crack Propagation", AFML-TR-76-176 (Nov. 1976)
20. Wallace, R.M., Annis, G.G. and Sims, D.L., "Application of Fracture Mechanics at Elevated Temperatures", AFML TR-76-176 Part II (April 1977)
21. Collins, H.E., "Relative Long Time Stability of Carbide and Intermetallic Phases in Nickel-Base Superalloys" Trans ASM, Vol. 62, No. 1 (March 1969)
22. Dreshfield, Robert L. and Ashbrook, Richard, L, "Further Observations on the Formation of Sigma Phase In a Nickel Base Superalloy (IN-100)" NASA TN D-6015 (Sept. 1970)
23. Dreshfield, Robert L. and Ashbrook, Richard L. "Sigma Phase Formation and Its Effect on Stress-Rupture Properties of IN-100", NASA TN D-5185 (April 1969)
24. Dreshfield, Robert L. and Ashbrook, Richard L. "Effects of Sigma-Phase Formation on Some Mechanical Properties of A Wrought Nickel-Base Superalloy (IN-100)", NASA TN D-7654 (May 1974)
25. Jones, E.E. and Peck, J.V., "Development of Repair and Reprocess Coatings For Air-Cooled Nickel Alloy Turbine Blades", AFML-TR-71-278 (Dec. 1971)
26. Harris, J.A., Jr. and Van Wanderham, M.C., "Properties of Materials in High Pressure Hydrogen at Cryogenic, Room and Elevated Temperature", Pratt & Whitney Aircraft Report FR5768 (July 1973) Final Report to NASA under Contract NAS8-26191.
27. Walters, J.J., "Study of The Hot Corrosion of Superalloys", AFML-TR-67-297 (Sept. 1967)
28. Moskowitz, L.N., Pelloux, R.M. and Grant, N.J., "Properties of IN-100 Processed by Powder Metallurgy" in Superalloys-Processing: Proceedings of the Second International Conference, MCIC Report 72-10 (Sept. 1972) pp Z-1 to Z-25.
29. Schirmer, R.M. and Quigg, H.T., "Effect of Very Low Sulfur in JP-5 Fuel on Hot Corrosion", Proceedings of Tenth National Conference on Environmental Effects on Aircraft Propulsion Systems, Naval Air Propulsion Test Center (Trenton, NJ) (May 1971)

30. Stetson, A.R. "Thermal Fatigue Testing of Gas Turbine Engine Materials", Solar Research Newsletter, Vol. 3 No. 1 (1966)
31. Bizon, P.T. and Spera, D.A., "Comparative Thermal Fatigue Resistance of Twenty-Six Nickel and Cobalt-Base Alloys", NASA TN D-8071 (Oct. 1975)
32. Prasad, J.S., Fortunato, D.E. and Watmough, T., "Development of Cast Superalloy Dies for Hot Die Forging Systems", IIT Research Institute Interim Progress Report IR-161-7 (III) to Air Force Materials Lab (Feb. 1968)
33. Anon. "Superplastic IN 100 Barstock Produced From "All Inert" Powder Billet , Pratt and Whitney Aircraft F100/F401 Technical Bulletin B690812-1 (Aug. 1969)
34. Anon. "10-12th Stage F100/F401 Compressor Disk of IN 100 Forged From "All Inert" Powder Billet , Pratt & Whitney Aircraft, F100/F401 Bulletin B700122-1 (Jan. 1970)
35. Anon. "Heat Treatment Studies Performed on GATORIZED IN100 Pancakes Forged From "All-Inert" Powder ™ Barstock Show Excellent Potential for Meeting Mechanical Property Design Requirements of F100/F401 Engine" Pratt & Whitney Aircraft F100/F401 Bulletin B700122-2 (Jan. 1970)
36. Anon. "10-12th Stage F100/F401 Compressor Disk of IN 100 Forged From "All-Inert" Powder Billet Meets Mechanical Design Requirements", Pratt & Whitney Aircraft Technical Bulletin B-700122-4 (Jan. 1970)
37. Warren, J.R., and Sims, D.L., "Evaluation of Cyclic Behavior of Turbine Disk Alloys", Quarterly Technical Progress Narrative No. 5 Under Contract PWA to NASA No. NAS3-20367 PWA FR-9208, Period July 1 to Sept. 30, 1977, (Oct. 1977)
38. Hall, A.M., Beuhring, V.F., "Thermal and Mechanical Treatments for Nickel and Some Nickel-Base Alloys: Effects on Mechanical Properties", NASA SP 5106 (1972)
39. Dunn, R.G., Sponseller, D.C. and Dahl, J.M., "Ductility Improvements in Superalloys", Proc. of Conference Toward Improved Ductility and Toughness, Kyoto, The Iron and Steel Institute of Japan and the Japan Institute of Metals (Oct. 1971)
40. Macha, D.E., "Fatigue-Crack-Growth Retardation Behavior of IN-100 at Elevated Temperatures", Paper presented at 1977 Spring Meeting, Dallas, TX of Society for Experimental Stress Analysis.
41. Smialek, J.L., "Exploratory Study of Oxidation-Resistant Aluminized Slurry Coatings for IN 100 and WI-52 Superalloys", NASA TN D-6329 (May 1971)
42. Gedwill, M.A., "Cyclic Oxidation Resistance of Clad IN 100 at 1040 and 1090°C: Time, Cycle Frequency, and Clad Thickness Effects", NASA TN D-6276 (June 1971)
43. Sanders, W.A., Barrett, C.A. and Probst, H.B., "Evaluation of High-Gas-Velocity and Static Oxidation Behavior of Fused-Salt-Aluminided IN 100 Between 1038° and 1149°C", NASA TN D-6400 (July 1971)
44. Deadmore, D.L., "Cyclic Oxidation of Cobalt-Chromium-Aluminum-Yttrium and Aluminide Coatings on IN 100 and VIA Alloys in High Velocity Gases", NASA TN D-6842 (July 1972)
45. Deadmore, D.L., "High-Velocity-Oxidation Performance of Metal-Chromium-Aluminum (MCrAl), Cermet, and Modified Aluminide Coatings on IN 100 and Type VIA Alloys at 1093C", NASA TN D-7530 (Feb. 1974)
46. Ryan, K.H., "Comparative Evaluation of Coated Alloys For Turbine Components of Advanced Aircraft Gas Turbine Engines, Vol. II - Test Results", AFML-TR-71-173 Vol. II (Jan. 1972)
47. Kelch, G.W. and Nelson, R.W., "Turbine Blade/Disk Fabrication Investigation", USAAV Labs Report No. 70-53 (Sept. 1970)
48. Spera, D.A., "Comparison of Experimental and Theoretical Thermal Fatigue Lives of Five Nickel Base Alloys", in ASTM STP 520, pp 648 to 657 (1973)
49. Hirschberg, M.H. and Halford, G.R., "Use of Strain-range Partitioning to Predict High Temperature Low Cycle Fatigue". NASA TN D-8072 (Jan. 1976)
50. Spera, D.A., Howes, M.A. and Bizon, P.T., "Thermal Fatigue Resistance of 15 High Temperature Alloys Determined by the Fluidized Bed Technique", NASA TM X-5295 (Mar. 1971)
51. Duvall, D.S., Owczarski, W.A. and Paulanis, D.F., "TLP* Bonding: A New Method For Joining Heat Resistant Alloys", Welding Journal (April 1974) pp 203-214.
52. Van Wanderham, M.C., Wallace, R.M., and Annis, C.G., Pratt and Whitney Aircraft, Mechanics of Materials and Structures, West Palm Beach, Fla., paper presented at AGARD Meeting, Salbarg, Denmark, April 1978.

	Ni
15	Co
10	Cr
5.5	Al
4.7	Ti
3	Mo
0.95	V

IN-100